# The Canadian Journal of Chemical Engineering

*formerly*

**CANADIAN JOURNAL OF TECHNOLOGY**

UNIV OF MICHIGAN
AUG 3 1959
ENGINEERING

CONTENTS


| | | |
|---|---|---|
| *Fundamental Aspects of Solids-Gas Flow. Part I: Introductory Concepts and Idealized Motion in Viscous Regime* | *L. B. Torobin*<br>*W. H. Gauvin* | **129** |
| *Thermodynamic Properties of Some Organic Compounds. I. PVT Relationships and Calculated Thermodynamic Properties for Normal Butanol* | *L. W. Shemilt*<br>*R. W. Esplen*<br>*R. Singh Mann* | **142** |
| *Rate Control in the Hydrometallurgical Preparation of Uranium Dioxide* | *D. R. Wiles* | **153** |
| *Aeration in Tower-Type Fermenters* | *D. Murphy*<br>*D. S. Clark*<br>*C. P. Lentz* | **157** |
| *The Effect of Pressure on the Enthalpy of Gases* | *Reza Kordbacheh*<br>*Chi Tien* | **162** |


*Published by*
THE CHEMICAL INSTITUTE OF CANADA
OTTAWA CANADA

*Photograph taken at C-I-L Central Research Laboratory, Beloeil, P.Q.*

# EXPOSURE: 1μ second

This unretouched double-exposure photograph shows an individual shock wave from an exploding detonator. It was obtained by exposing a film to two successive images of the shock wave as revealed by discharging two condensers in succession through a spark gap.

The high intensity light flash for each image was of less than one microsecond duration, and the time interval between flashes was ten microseconds.

From such investigations, the efficiency of detonators is improved. The end result of research reaches the C-I-L customer in the form of improved products, and a higher standard of technical service which Canada needs for industrial progress.

C-I-L

## CANADIAN INDUSTRIES LIMITED

*Serving Canadians Through Chemistry*

Agricultural Chemicals • Ammunition • Coated Fabrics • Industrial Chemicals • Commercial Explosives • Paints • Plastics • Textile Fibres

# The Canadian Journal of Chemical Engineering

*formerly*

Canadian Journal of Technology

VOLUME 37 AUGUST, 1959 NUMBER 4

***Editor***
A. Cholette
Faculty of Science, Laval University
Quebec, Que.

***Managing Editor***
T. H. G. Michael

***Publishing Editor***
D. W. Emmerson

***Assistant Publishing Editors***
R. G. Watson
R. N. Callaghan

***Circulation Manager***
M. M. Lockey

**EDITORIAL BOARD**

*Chairman*
W. M. CAMPBELL, Atomic Energy of Canada Limited,
Chalk River, Ont.

L. D. DOUGAN, Polymer Corp. Limited,
Sarnia, Ont.

W. H. GAUVIN, McGill University,
Montreal, Que.

G. W. GOVIER, University of Alberta,
Edmonton, Alta.

J. W. HODGINS, McMaster University,
Hamilton, Ont.

A. I. JOHNSON, University of Toronto,
Toronto, Ont.

E. B. LUSBY, Imperial Oil Limited,
Toronto, Ont.

LEO MARION, National Research Council,
Ottawa, Ont.

R. R. McLAUGHLIN, University of Toronto,
Toronto, Ont.

G. L. OSBERG, National Research Council,
Ottawa, Ont.

J. H. SHIPLEY, Canadian Industries Limited,
Montreal, Que.

H. R. L. STREIGHT, Du Pont of Canada Limited,
Montreal, Que.

**EX-OFFICIO**

E. GORDON YOUNG, President, The Chemical Institute of Canada.

H. BORDEN MARSHALL, Chairman of the Board of Directors.

H. S. SUTHERLAND, Director of Publications.

Authorized as second class mail, Post Office Department, Ottawa. Printed in Canada

**Manuscripts** for publication should be submitted to the Editor: Dr. A. Cholette, Faculty of Science, Laval University, Boulevard de l'Entente, Quebec, Que. (Instructions to authors are on the next page).

**Editorial, Production and Circulation Offices:** 18 Rideau Street, Ottawa 2, Ont.

**Advertising Office:** C. N. McCuaig, manager of advertising sales, *The Canadian Journal of Chemical Engineering*, Room 601, 217 Bay Street, Toronto, Ont. Telephone—EMpire 3-3871.

**Plates and Advertising Copy:** Send to *The Canadian Journal of Chemical Engineering*, 18 Rideau Street, Ottawa 2, Ont.

**Subscription Rates:** In Canada—$3.00 per year and 75c per single copy; U.S. and U.K.—$4.00; Foreign—$4.50.

**Change of Address:** Advise Circulation Department in advance of change of address, providing old as well as new address. Enclose address label if possible.

**The Canadian Journal of Chemical Engineering** is published by The Chemical Institute of Canada every two months.

Unless it is specifically stated to the contrary, the Institute assumes no responsibility for the statements and opinions expressed in *The Canadian Journal of Chemical Engineering*. Views expressed in the editorials do not necessarily represent the official position of the Institute.

# The Canadian Journal of Chemical Engineering

*formerly*

## Canadian Journal of Technology

# INSTRUCTIONS TO AUTHORS

***Manuscript Requirements***

1. The manuscript should be in English or French.
2. The original and two copies of the manuscript should be supplied. These are to be on 8½ x 11 inch sheets, typewritten, and double spaced. Each page should be numbered.
3. Symbols should conform to American Standards Association. An abridged set of acceptable symbols is found in the third edition of Perry's Chemical Engineers' Handbook. Greek letters and subscripts and superscripts should be carefully made.
4. Abstracts of not more than 200 words in English indicating the scope of the work and the principal findings should accompany all technical papers.
5. References should be listed in the order in which they occur in the paper, after the text, using the form shown here: "Othmer, D. F., Jacobs, Jr., J. J., and Levy, J. F., Ind. Eng. Chem. 34, 286 (1942). Abbreviations of journal names should conform to the "List of Periodicals Abstracted by Chemical Abstracts". Abbreviations of the common journals are to be found in Perry's Handbook also. All references should be carefully checked with the original article.
6. Tables should be numbered in Arabic numerals. They should have brief descriptive titles and should be appended to the paper. Column headings should be brief. Tables should contain a minimum of descriptive material.
7. All figures should be numbered from 1 up, in Arabic numerals. Drawings should be carefully made with India ink on white drawing paper or tracing linen. All lines should be of sufficient thickness to reproduce well, especially if the figure is to be reduced. Letters and numerals should be carefully and neatly made, preferably with a stencil. Generally speaking, originals should not be more than twice the size of the desired reproduction; final engravings being 3¼ in. or 7 in. wide depending on whether one column or two is used.
8. Photographs should be made on glossy paper with strong contrasts. Photographs or groups of photographs should not be larger than three times the size of the desired reproduction.
9. All tables and figures should be referred to in the text.

***Submission of Manuscripts***

1. The three copies of the manuscript, including figures and tables, should be sent directly to:

   DR. A. CHOLETTE, editor,
   The Canadian Journal of Chemical Engineering,
   Faculty of Science, Laval University,
   Boulevard de l'Entente,
   Quebec, Que.
2. The authors addresses and titles should be submitted with the manuscript.
3. The author may suggest names of reviewers for his article, but the selection of the reviewers will be the responsibility of the editor. Each paper or article is to be reviewed by two chemical engineers familiar with the topic. Reviewers may request that they remain anonymous.
4. All correspondence regarding reviews should be directed to the editor.

***Reprints***

1. At least 50 free "tear sheets" of each paper will be supplied.
2. Additional reprints may be purchased at cost. An estimated cost of reprints, with an attached order form, will be sent to the author with the galley proofs.
3. Orders for reprints must be made before the paper has appeared in the Journal.

* * *

# Fundamental Aspects of Solids-Gas Flow

## Part I: Introductory Concepts and Idealized Sphere Motion in Viscous Regime[1]

*L. B. TOROBIN[2] and W. H. GAUVIN[2]*

**This article introduces a series of analytical and critical literature surveys which deal first with the individual fundamental momentum transfer phenomena associated with particulate motion as affected by particle shape, roughness, acceleration, concentration and rotation, as well as the turbulence characteristics and boundary conditions of the transporting fluid. This information will then be used as a basis of discussion and interpretation of the many investigations of multiparticle solids-gas conveying systems and contacting techniques reported in the literature.**

**This first paper reviews briefly some pertinent basic concepts of fluid mechanics, and then considers the development of the fluid velocity field and drag for single spherical particles moving rectilinearly at pre-wake-forming Reynolds Numbers through an infinite and undisturbed fluid.**

Of all the physical phenomena which, in various ways, affect man's daily life, his environment and his activities, few exert as profound an influence as those associated with the occurrence of solids-gas systems. Whether evidenced in the form of large-scale meteorological disturbances, such as sand and snow storms, or on a more modest scale, such as the dispersion of soot particles from a factory chimney, or finally in such short-range action as the entrainment of dust by vacuum-cleaning equipment, the behavior of solid particles in the presence of a gas stream significantly affects human welfare and economy. The range and variety of processes in which such systems play an important, if not a dominating part, is truly astounding: the spraying of insecticides, the dissemination of pollen, the motion of aircraft, rockets and missiles, the scattering of radioactive fallout, the inhalation of toxic dusts, the shifting of sand dunes, the erosion of soils, the color of the sky at twilight – these are but a few random examples of their occurrence.

The earliest harnessing of these systems for industrial uses was associated with materials handling and pneumatic conveying. Industrial equipment for this purpose was probably first reported in the literature in 1897 by Duckam (1), although it had been employed in small-scale operations as early as 1866 (2). Whereas the installations of the beginning of the century were used primarily for low-speed vacuum movement of grains, the newer high-speed conveying systems now handle chemicals, coal and a wide variety of industrial materials as well. Recent elaborations in these transport techniques have led to the development of dense-phase conveying (where, for example, 200 lb. of finely powdered coal can be transported in the presence of only one lb. of conveying air) and pneumatic stowing, used by modern mining technology to fill underground voids with crushed stones of relatively large size.

Chemical engineers were probably among the first to realize that the gas-phase component in this binary system could be made to play a more active role than that of a mere conveying medium. They were instrumental, during the past twenty years, in the development of new processes in which the unique contacting properties of solids-gas flow could be made to effect either simple physical operations, such as evaporation and drying (as in flash drying) or chemical reactions, as illustrated by moving-bed or fluidized-bed applications too numerous to mention.

It was inevitable that the spectacular achievements already obtained would cause a further intensification of research activities. As a result, two new contacting methods–the spouted-bed technique and the atomized suspension technique–have recently been reported, and new applications of solids-gas contacting are being developed at an ever-increasing rate.

The advantages resulting from the use of finely-divided solid reactants or catalysts in chemical processing are many. Chief among them are the ease of handling, the provision of large surface areas for mass and heat transfer, and the near-absence of internal diffusional resistance during reaction. The pulverization of the bulk raw material to yield particles small enough for efficient contacting presented until recently a number of technical or economic problems, but remarkable improvements in comminuting machinery which have occurred during the past few years now make it possible to subdivide effectively and economically not only very hard minerals such as taconites and jaspers, but even fibrous materials such as wet bark, sawdust, peat and lignite. These results have

[1]*Manuscript received February 23, 1959.*

[2]*McGill University and Pulp and Paper Research Institute of Canada, Montreal, Que.*

been achieved both by refinement of old designs (rod, ball or hammer mills) and by development of new principles of attrition (Aerofall mill, fluid erosion, explosive shattering).

As is commonly the case in many of the fast-developing areas of chemical engineering, practical know-how and purely technical considerations have far outdistanced basic studies of the principles underlying solids-gas contacting operations. Even in the field of solids-gas flow—which only involves considerations of momentum transfer—the approach is still largely empirical and rests heavily on arbitrary friction factors, specific to each application, from which generalization is utterly impossible. It is perhaps surprising to report that a large number of workers, currently active in the field, are still following this line of attack.

The discussion which follows was originally planned as a literature survey to record the results of experimental investigations of the conveying of solid particles by gas streams. Since in its broad aspects pneumatic conveying is a complex problem in fluid mechanics, the solution of which involves concepts of turbulence, flow fields, stochastic phenomena and boundary layer behavior, the search for experimental evidence had to be broadened beyond the usual limits of the chemical engineering literature, to include contributions from many diverse fields which include aerodynamics, fuel combustion, meteorology, acoustics, mining technology, industrial hygiene and toxicology, geophysics and applied mathematics. That this search was highly productive is attested by the large number of pertinent references—some obtained with difficulty—which have been consulted. The list is by no means complete.

As the review progressed, it was noted that a good many of the experimental investigations reported had been aware of only a few of the many possible system variables, so that they dealt with a comparatively narrow range of conditions. As a result, most of the published data on solids-gas systems were restricted in scope and frequently conflicting. Also, the scarcity of fundamental information and the lack of uniformity of presentation made a comparative study of the experimental evidence extremely arduous. It soon became evident that a mere recital of a large number of apparently unrelated facts would simply compound the confusion.

Although one of the purposes of the present work is still to record the published information as completely as possible, it was decided to place the main emphasis on critical analysis and interpretation of the experimental evidence, using the microscopic in an attempt to unravel the various macroscopic phenomena involved. In view of the complexity of the inter-relationships existing between the numerous variables, this was no easy task. The symbolism and nomenclature in themselves presented quite a problem; an attempt was made at unification, which may not have been successful.

To facilitate the presentation, the work has been divided into a number of self-contained articles, each with its own nomenclature and bibliography, starting with the behavior of a single spherical particle in infinite, turbulence-free surroundings, and then going on to consider all the various complicating factors, such as turbulent fields, effects of particle shape, roughness, acceleration and rotation, finally discussing the various aspects of multi-particle systems. Thus the pertinency of some of the definitions and topics discussed at the beginning to the problems of solids-gas flow may not become evident until much later.

In spite of its limitations, it is hoped that the present work will at least show the bolder outlines of this fascinating field and thus provide a better understanding of some of its fundamental aspects.

## I. FLUID PROPERTIES

The two broad classifications of fluid flow—laminar and turbulent—have been extensively discussed in the literature and excellent texts are available giving full treatment to the more recent work in the field [3, 4, 5, 6, 7]. A brief and at times oversimplified statement of some elementary concepts together with some less evident information which will be referred to in subsequent discussions will now be given.

### *Laminar Flow*

In this flow regime (also referred to as viscous or streamline flow) the fluid moves in layers or lamina. It possesses a definite "viscosity" which is made manifest by the internal frictional resistance which it offers to physical deformation. Fluid movement in the vicinity of a boundary will cause the layers to slip over one another, and they will produce a shearing stress given by the conventional Newtonian relationship. The generalized movement of an element of fluid resulting from its reaction to the viscous and pressure forces which it experiences is concisely stated by the vector form of the Navier-Stokes equation for incompressible flow:

$$\mathrm{D}\mathbf{u}/\mathrm{D}\theta = \mathbf{F} - (1/\rho)\,\mathrm{grad}\,\mathrm{p} + \nu \nabla^2\mathbf{u} \qquad \ldots\ldots(1)$$

where $\mathrm{D}\mathbf{u}/\mathrm{D}\theta$ is the total derivative of the velocity vector, $\mathbf{u}$, with respect to time, $\theta$, and represents the total acceleration of a fluid element due to changes of velocity in both space and time. $\mathbf{F}$ represents any body force (e.g. gravity); this term may be neglected in the case of submerged flow with no free surface, and, in this case, the x component of Equation (1) may be written out in full as follows:

$$\frac{\delta u}{\delta \theta} + u\frac{\delta u}{\delta x} + v\frac{\delta u}{\delta y} + w\frac{\delta u}{\delta z} = -\frac{1}{\rho}\frac{\delta p}{\delta x} + \nu\left(\frac{\delta^2 u}{\delta x^2} + \frac{\delta^2 u}{\delta y^2} + \frac{\delta^2 u}{\delta z^2}\right) \qquad \ldots\ldots(2)$$

From the law of conservation of mass, another important equation—the continuity equation—can be derived:

$$\mathrm{div}(\rho\mathbf{u}) = -\delta\rho/\delta\theta \qquad \ldots\ldots(3)$$

For an incompressible fluid, this expression may be written out in full:

$$\delta u/\delta x + \delta v/\delta y + \delta w/\delta z = 0 \qquad \ldots\ldots(4)$$

It should be noted that the assumption of incompressibility is valid for the gas phase in the immediate vicinity of a solid particle in most solids-gas systems.

The Navier-Stokes equations are at the core of any theoretical description of a real fluid system, so that their specific solution would predict all of the desired flow properties for that system. The equations, however, usually contain more unknowns than the number of known pertinent equations for the system and their solution presents almost insuperable mathematical complexity due to the non-linear terms.

Simplifying assumptions and secondary behavioral laws have been successfully employed to obtain solutions for a limited number of cases. Advances in the mathematical

sciences coupled with the evolution of physical laws resulting from experiment may be expected to increase the number of specific fluid systems for which a solution is available.

It is seldom justifiable in chemical engineering problems to assume that the fluid is inviscid, that is to say, that it possesses zero viscosity. In certain cases, however, where the movement of the main mass of fluid, away from solid boundaries, is of particular interest, such an assumption greatly simplifies the equations of motion. If the viscosity terms are neglected in (1) and (2), the resulting expressions are called the Euler equations of motion. A detailed discussion of the solution of these equations—the subject matter of classical hydrodynamics—does not properly belong in this report. Suffice it to say that to integrate these equations, it is convenient to introduce a new function $\phi$, which is called the *velocity potential*, the derivation of which in any direction gives the velocity in that direction, or:

$$\frac{\delta\phi}{\delta x} = u; \quad \frac{\delta\phi}{\delta y} = v; \quad \frac{\delta\phi}{\delta z} = w. \qquad \ldots\ldots\ldots\ldots(5)$$

If the flow is steady ($\delta u/\delta\theta = 0$), the equations of motion can be solved directly along a *streamline*, i.e., the line drawn tangent to the velocity vector at every point in the flow field.

If the flow is steady and also *irrotational*, that is:

$$\frac{\delta v}{\delta x} - \frac{\delta u}{\delta y} = 0; \quad \frac{\delta u}{\delta z} - \frac{\delta w}{\delta x} = 0; \quad \frac{\delta w}{\delta y} - \frac{\delta v}{\delta z} = 0. \qquad \ldots\ldots(6)$$

integration of the Euler equations for such a flow field (which is often called potential flow) yields the familiar Bernouilli equation (if gravity is the only external force acting on the fluid):

$$(1/2)(V^2/g_c) + gZ/g_c + p/\rho = \text{constant} \qquad \ldots\ldots\ldots(7)$$

The two-dimensional analysis of many problems involving inviscid fluids may be represented by a network of orthogonal lines consisting of streamlines and of equipotential lines. The latter are curves of equal velocity potential $\phi$, while the streamlines are curves of equal *stream function* $\psi$. The latter is mathematically defined, for two dimensional incompressible flow, by:

$$\delta\psi/\delta y = u \text{ and } \delta\psi/\delta x = -v \qquad \ldots\ldots\ldots\ldots(8)$$

It should be noted that although the velocity potential concept is valid only for potential (or irrotational) flow, that of the stream function is equally applicable to viscous systems and is frequently used to map out complex laminar flow systems, such as the viscous flow around an object submerged in a moving fluid.

If the flow is no longer irrotational, the three equations (6) will not be equal to zero, but will represent twice the value of the angular fluid velocity, or the components of *vorticity*. Thus:

$$\delta v/\delta x - \delta u/\delta y = 2\omega_z = \text{vorticity in a plane parallel to the z axis} \qquad \ldots\ldots(9)$$

and the terms on the left of the three equations (6) are the vorticity components. The concept of vorticity is very important in boundary layer theory or in the approach to turbulent motion. Mathematically, vorticity is a vector quantity obtained by taking the curl of the flow velocity, or:

$$\text{vorticity} = \text{curl } \mathbf{u} = \nabla \times \mathbf{u} \qquad \ldots\ldots\ldots\ldots(10)$$

Physically it is a measure of the rotating motion associated with an infinitesimally small volume sample taken from the fluid. The locus of the centres of the circulation are often referred to as the *vortex filaments* or *threads*.

***Transition to Turbulent Motion***

As the velocity of flow of a laminar network is increased, the stability of the laminar layers diminishes and at a sufficiently high velocity a confused eddying, indicating turbulent motion, begins to be observed.

There is as yet no clear understanding of the mechanism governing the transition from instability to full turbulence, although energetic inquiries towards this end have recently been reported [8, 9, 10, 11]. Hsu [12] has recently proposed a plausible conjectured model of transition to turbulence which is useful at this point in the discussion. The instability of a laminar layer is seen to produce a vortex filament, which moves relative to the ambient fluid. Since there is a drag force on the filament due to this relative motion, it is caused to accelerate. The acceleration causes increased vortex instability so that it breaks down resulting in the generation of smaller vortex filaments which are in turn accelerated and distorted by ambient vortex filaments or by a shear flow which may be present, and this cascade process will be continued so that after several cycles there is a random orientation and distribution and size spectrum of the vortex filaments resulting in a field of *random* vorticity referred to as turbulence. The flow may return to the laminar state if the necessary instability conditions or other factors specifically required at each stage of the cascade are not present to propagate the chain reaction.

In his classical treatise, Reynolds [13] found that the transition from laminar to turbulent motion of the flow in a pipe duct could be conveniently identified using the grouping of variables $\frac{DU\rho}{\mu}$ as a criterion. This dimensionless group is the ratio of a typical inertia reaction per unit volume $\frac{\rho U^2}{D}$, to a typical viscous force $\frac{U\mu}{D^2}$. It is a similarity parameter, and the greater its value, the smaller is the role played by viscous forces in determining the pattern of motion.

The Reynolds grouping designated by the symbol Re, has been employed to predict whether fluid motion in a pipe is laminar or turbulent. The lower critical value of Re for duct flow is defined as the one below which turbulence cannot exist, i.e. the viscous effects are sufficiently great to damp out and destroy fluctuations caused by momentary disturbances [14].

Typical of recent re-evaluations of Reynolds' data is a paper by Lindgren [15] who shows evidence that the classical experiments used to determine the lower critical value of Re in a conduit—usually given as 2100—have been misinterpreted and that there does not exist a critical value in this region. His experiments further indicate that (1) Re alone does not determine the state of motion of fluids in pipe; (2) the transition from laminar to turbulent motion continues at least to Re = 3300; (3) a sudden increase in resistance to flow at certain values of Re does not signify an instantaneous onset of turbulence; (4) the severity of the turbulence with high entrance disturbances decreases with the distance travelled; this has been observed with flows up to Re = 1,900,000; (5) in defining the state of motion in smooth cylindrical tubes, Re should be replaced by an expression which is a function of $\frac{(DU\rho)}{\mu}\frac{(D)}{L}$, where L is the downstream distance from the entrance. A comprehensive discussion of this subject is

available in the literature review presented by M. H. Smith [16].

The transition region at which the flow in a pipe becomes turbulent may be considerably altered by the presence of a solid phase, and this will be discussed more fully in a later section.

***Turbulent Flow***

It is convenient to regard the turbulent motion of a fluid as made up of two separate components: (1) a mean forward motion of the fluid which is steady with time; (2) a superimposed secondary randomly fluctuating motion of the fluid whose time-averaged value is everywhere null. Thus, if u, v, w and p are the instantaneous velocity components and pressure, the following typical relationship is obtained:

$$u = \bar{u} + u' \quad \ldots\ldots(11)$$

where u′ is the amount of fluctuation in the component velocity and $\bar{u}$ is its time average value, defined by:

$$\bar{u} = \frac{1}{\theta}\int_0^\theta u\,d\theta \quad \ldots\ldots(12)$$

The time interval $0 \rightarrow \theta$ is made sufficiently large to obtain a statistical sample so that a second sampling over this interval will not alter the average value $\bar{u}$.

It follows that:

$$u' = \frac{1}{\theta}\int_0^\theta u'\,d\theta = 0 \quad \ldots\ldots(13)$$

The mean square of the velocity fluctuation is defined by:

$$\overline{u'^2} = \frac{1}{\theta}\int_0^\theta u'^2\,d\theta \quad \ldots\ldots(14)$$

while the root mean square value of the fluctuation is given by:

$$\sqrt{\overline{u'^2}} = \frac{1}{\theta}\int_0^\theta \sqrt{u'^2}\,d\theta \quad \ldots\ldots(15)$$

Similar expressions can be written for the other velocity components and for the pressure.

Turbulent flow can be crudely visualized as being made up of eddies which vary continuously in size and translational speed. The nature of turbulent movement is very complex and statistical methods are therefore necessary for its analysis.

The root mean square values of the velocity fluctuations are referred to as the *intensities of the turbulence components*. They characterize the velocity within the eddies—packets of fluid which are constantly being formed and destroyed, their size varying from the order of the dimension of the pipe to vanishingly small "micro eddies".

Whereas in viscous flow the viscosity depends on the interaction of fluid molecules, fluid stresses being transmitted by inter-mixing and collision of neighbouring molecules, in turbulent motion there is still interchange of matter but now on a molar scale, and there is a diffusion in which fluid packets from low velocity regions are transferred to high velocity regions with an accompanying retardation to the latter.

The shearing stresses are therefore made up of two components: (1) the molecular action in the mean motion, and (2) the turbulent action in the secondary flow. The latter are made evident by the so-called Reynolds shear stresses, $-\rho\overline{u'v'}$, $-\rho\overline{v'w'}$ and $-\rho\overline{u'w'}$—three of six terms which occur in the turbulent flow form of the Navier-Stokes equations when the velocity is expressed as the sum of a mean and of a fluctuating component. The other three terms are the Reynolds normal stresses, $-\rho\overline{u'^2}$, $-\rho\overline{v'^2}$, and $-\rho\overline{w'^2}$.

There was an original tendency to draw an erroneous analogy between eddy motion and molecular motion which involves the movement of rigid particles, resulting in a number of crude concepts which did, nevertheless, prove useful in providing a framework for further theoretical and experimental work. Some of these expressions, which will arise in discussions in solids-gas flow, are listed below.

An *eddy viscosity* $\eta$ is defined by the expression:

$$\tau_{g_c} = (\mu + \eta)\,(du/dy) \quad \ldots\ldots(16)$$

In this expression $\tau$ is the total shear stress and is the sum of the laminar and of the turbulent shear stresses. The *kinematic eddy viscosity* is given by $\eta/\rho$.

Prandtl [17] defined a "mischungsweg" or *mixing length* l′ the eddy counterpart of the molecular free path, at the end of which the volume element would transfer all its momentum to the adjacent fluid, so that, instantaneously:

$$u' = l'(du/dy) \quad \ldots\ldots(17)$$

This implies that the eddy remains intact as a discrete entity over the length l′. Taylor [18] in an early work presented a vorticity transfer theory, which sought to remove some objections to the Prandtl concept, by considering a length l″ over which the volume element transferred all its excess vorticity rather than momentum so that, instantaneously:

$$u' = l''(du/dy) \quad \ldots\ldots(18)$$

The physical models upon which the above theories are based have since been shown to be entirely unrealistic. The eddies in a turbulent field are not discrete, and it is now considered naive to associate any of the length scales employed with a true physical picture of the turbulence.

Taylor [19, 20, 21] recognized that eddy diffusion involved a *continuous* change of the eddy mass and size, there being a constant decay and loss of eddies through viscous shear, in equilibrium with a constant generation by the instability of the flow. This seemingly chaotic system was therefore treated by statistical methods, and was characterized by the correlation of the components of the velocity fluctuations at different space and time intervals. The correlation between two infinitesimally displaced points is at a maximum (defined as unity) since the volume elements that would engulf one would be sure to include the other. The correlation would usually be expected to decrease as the intervals increased. Taylor defined a *correlating coefficient* $R_y$ by:

$$R_y = \frac{\overline{u'_1\,u'_2}}{\sqrt{u'^2_1}\sqrt{u'^2_2}} \quad \ldots\ldots(19)$$

where $u'_1$ and $u'_2$ are the velocity fluctuations at the points 1 and 2 separated in a direction transverse to the fluctuations by the distance y. Similar correlation coefficients can be defined for the directions x and z, and also for v′ and w′.

A *characteristic length scale* $L_E$ is associated with $R_y$ through the relationship:

$$L_E = \int_0^\infty R_y dy \quad \ldots\ldots\ldots\ldots\ldots\ldots (20)$$

This term is referred to as a *Eulerian scale.*

Obviously there are many Eulerian correlations possible corresponding to the different components of the velocity fluctuations and to the three directions, with no simple relationship existing between them, so that a given flow system is only partially characterized by a given Eulerian scale. Triple and quadruple correlations are also employed.

Consideration of the correlation between the velocity components of a fluid element separated by two intervals of *time* leads to the difficultly obtained *Lagrangian scale* $L_L$ defined by:

$$L_L = \sqrt{\overline{u'^2}} \int_0^\infty R_\theta d\theta \quad \ldots\ldots\ldots\ldots\ldots\ldots (21)$$

where

$$R_\theta = \frac{\overline{u'_\theta u'_{\theta+\Delta\theta}}}{\sqrt{\overline{u'^2_\theta}}\sqrt{\overline{u'^2_{\theta+\Delta\theta}}}}$$

There is no general relationship between the Eulerian and the Lagrangian scale [22] but limited proportionalities exist in certain cases. The *mean square eddy diffusion distance* $\overline{X^2}$ is given by Taylor's relationship:

$$\frac{1}{2}\frac{d\overline{X^2}}{d\theta} = \overline{u'^2} \int_0^\theta R_\theta \, d\theta \quad \ldots\ldots\ldots\ldots\ldots\ldots (22)$$

so that $\frac{1}{2}\frac{d\overline{X^2}}{d\theta}$ can be regarded as the eddy diffusion coefficient. Its measure is often employed to study the effect of entrained solids on the turbulence parameters of the gas phase of a solids-gas system [23, 24, 25, 26]. Other statistical precepts introduced by Taylor include that of the *turbulence spectrum,* by means of which is indicated the relative turbulent energies associated with the various frequencies of velocity fluctuations which go to make up the total field of random vorticity.

An idealisation removing almost insurmountable mathematical difficulties is the concept of homogeneous isotropic turbulence, the study of which was begun by Taylor in 1935. *Isotropic turbulence* infers that the mean values of functions of the flow variables are not affected by the translation, rotation and reflection of the axes of reference. As a consequence, the intensity components in such flow are equal, or:

$$\overline{u'^2} = \overline{v'^2} = \overline{w'^2} \quad \ldots\ldots\ldots\ldots\ldots\ldots (23)$$

The concept of *homogeneous turbulence* may be loosely defined by the condition that the intensity components should not be a function of position in space. In other words, although the three intensity components are not necessarily equal to each other, they remain unchanged at any point in the turbulent field.

It should be noted that, although homogeneous, the turbulence may be either isotropic or anisotropic. Isotropic turbulence appears to be statistically the more probable state, and it was thought at one time that any anisotropic turbulent motion rapidly approached the isotropic state, but recent experimental work has shown that the approach to isotropy is very slow [5].

Batchelor [4] points out that although the kinds of turbulent motion encountered in aeronautics, hydraulics and chemical engineering are usually more complicated than homogeneous turbulence, the study of the latter has practical utility in that an understanding of this simpler case will lead to comprehension of at least some of the aspects of non-homogeneous turbulence. On the other hand, there have been instances where investigators of solid-fluid flow have erroneously assumed isotropic turbulence to exist in a region of their experimental systems, and have then applied relationships derived from this assumption to obtain quantitative data.

Although the literature abounds with experimental probings of the intercorrelation of the turbulence properties, there has been little progress made towards the presentation of a universal theory of turbulence necessary if a solution to the Navier-Stokes equations for turbulent systems are ever to be solved. A typical illustration of the immaturity of our present state of knowledge is found in a recent paper by Betchov [27] who points out that attempts to enunciate the mysterious processes which determine and lead to the production of vorticity lead to systems of equations which are always less than the number of unknowns.

### *Fully Developed Turbulent Pipe Flow*

The turbulence structure of fully-developed particle-free pipe flow has been carefully studied by hot-wire methods [28, 29, 30, 31], the hot wire anemometer being a direction-sensitive instrument whose electrically-heated fine wire reacts to the instantaneous convective cooling caused by the fluctuating flow [32, 33, 28].

Laufer showed the pipe flow field to be divided into three concentric regions: (1) the wall vicinity in which the production and diffusion of turbulence, and viscous action play equally important roles; (2) the central portion of the pipe cross-section in which energy diffusion was found to be the important phenomenon; (3) the intermediate region in which the energy obtained by diffusion was dominated by the local rate of change of turbulent energy production. Typical turbulence profiles of the axial intensity as a function of ratio of the distance from the pipe center-line r to the pipe radius $r_o$ are given by Laufer in Figures 1 and 2, the latter amplifying the interesting intensity peaks occurring near the pipe wall. Figure 3 shows the somewhat similar behavior of the tangential and radial turbulence components but they clearly indicate that the flow is homogeneous and isotropic only over the centre fifth of the duct. The intensities in these plots were taken as the ratio of the occurring fluctuation to the friction velocity $U_\tau$ defined by:

$$U_\tau^2 = \nu \left(\frac{dU}{dr}\right)_{r=r_0} \quad \ldots\ldots\ldots\ldots\ldots\ldots (24)$$

Turbulence intensities for pipe flow are usually quoted as the ratio $\frac{\sqrt{\overline{u'^2}}}{U_c}$ where $U_c$ is the mean fluid velocity at the axis; stated in this manner, the intensities at the axis would be approximately 2.7%. If the local results are given as the *local* intensities, i.e. using the local mean velocities as the denominator, this would indicate local turbulence intensity values which are as high as 60% for the pipe wall region.

Similar, though less detailed results were obtained by Hall [34], Newman [35] and Sandborn [31], the latter showing that the longitudinal turbulence intensity at the pipe centre was given by the general expression:

$$\frac{\sqrt{\overline{u'^2}}}{U_c} = 0.144 \, Re^{-0.146} \quad \ldots\ldots\ldots\ldots\ldots\ldots (25)$$

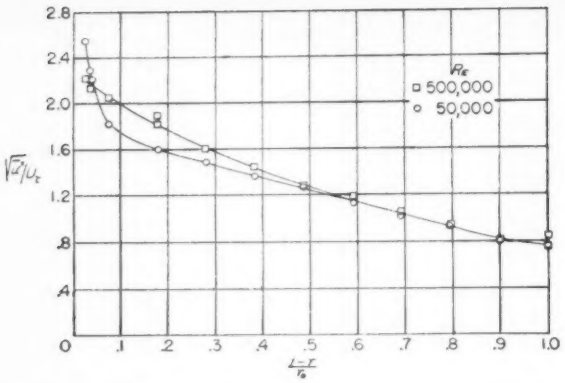


**Figure 1—Intensity of turbulence $\sqrt{u'^2}/U_\tau$ versus distance from pipe wall (Laufer).**

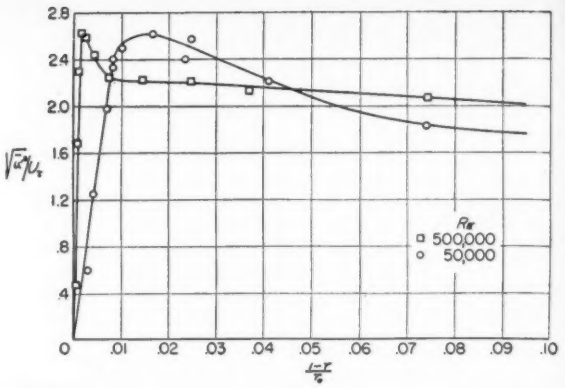


**Figure 2—Intensity of turbulence $\sqrt{u'^2}/U_\tau$ versus distance from pipe wall in wall vicinity (Laufer).**

Mickelsen [36] found that the Eulerian and Lagrangian scales at the pipe centre in fully-developed pipe flow were roughly related by the expression:

$$L_E = 0.6L_L \quad \ldots\ldots\ldots\ldots\ldots\ldots\ldots\ldots (26)$$

for turbulence intensities (reported as $\sqrt{u'^2}$) of 1.8 to 14 feet per second.

## II. FLUID RESISTANCE TO UNIFORM MOTION OF SINGLE SPHERICAL PARTICLES

### *Spherical Particle Behavior in a Laminar Fluid—The Drag Coefficient*

The laws of motion of a single spherical particle in an undisturbed fluid stream (i.e. one in which there is no secondary motion) have been the subject of a great many investigations performed during the past two centuries.

Newton [37] in 1719 presented experimental data for the retardatory air force on hollow spheres which he dropped from the dome of St. Paul's Cathedral, and he derived the following equation which seemed to predict his results theoretically:

$$R = (\pi/2)\,\rho r_p^2 V^2 \quad \ldots\ldots\ldots\ldots\ldots\ldots\ldots\ldots (27)$$

Equation (27) also roughly approximates some of the results of more recent experience, although the premises on which the derivation is based appear to have little or no validity. This must be stressed, since it is often assumed to be a successful solution to the problem. It will be subsequently shown that it is no paradox that subsequent writers have been unable to propose a complete theoretical solution for the flow regime for which Newton's law seems to be valid. Zahm [38] gives the following summary of Newton's assumptions: (1) the fluid is a discontinuous rare medium consisting of infinitely small equal particles, freely disposed at equal and great distances from each other; (2) these fluid particles, in uniform rectilinear motion, strike only the front part of the solid body immersed in it, leaving a vacuum behind extending to infinity and bounded by parallel streamlines grazing the body; (3) the particles striking the hard smooth front retain their tangential velocity component and lose their normal component if inelastic, or have it reversed if elastic. In all cases before and after rebound, they continue in straight lines without mutual interference, i.e. they have substantially infinite free paths.

The laws of resistance derived from these premises are absolutely valid for such a system, but this system differs vastly from a natural fluid. The Newtonian conception of fluid resistance has been replaced by the hydrodynamical conception, according to which the resistance consists of pressure differences and frictional stresses arising from the fluid around the body [39].

The phenomenon of fluid resistance is extremely complex and no simple formula can express the relationship between the fluid flow and the force on the spherical particle. Limited success has been attained for restricted conditions; however, results covering a wide range of conditions can only be given graphically.

A most important simplification was discovered by Lord Rayleigh [40] when he found that a single graph

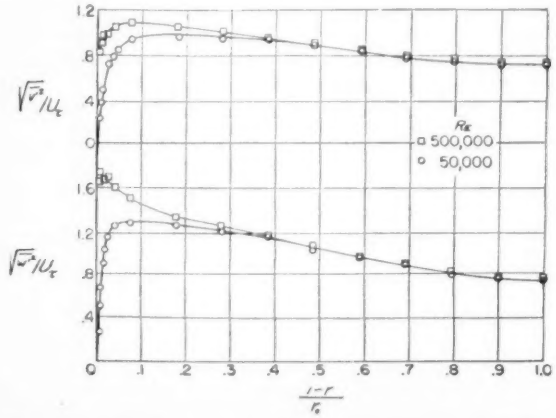


**Figure 3—Intensity of turbulence $\sqrt{v'^2}/U_\tau$ and $\sqrt{w'^2}/U_\tau$ versus distance from pipe wall (Laufer).**

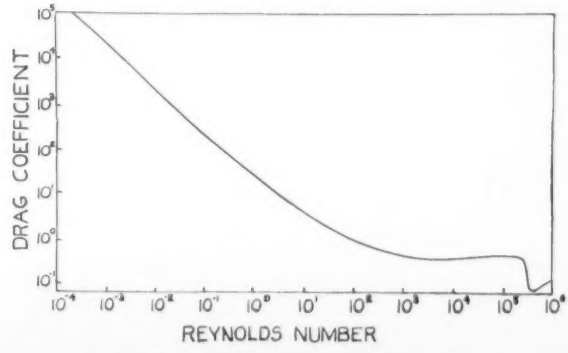


**Figure 4—Standard drag coefficient curve.**

could be used to present data for the motion in a laminar fluid of spheres of all sizes, and fluids of all densities and viscosities. One of the coordinates uses a ratio of inertia reaction to viscous reaction on the sphere, and it is expressed as a modified Reynolds Number $(d_p V\rho)/\mu$– where $d_p$ is now the diameter of the sphere. The other coordinate is a force coefficient $R/(1/2)\rho V^2 A_p$ in which R is the resistance of the fluid to the motion of the sphere and $A_p$ is the cross-sectional area of the particle. This dimensionless group is generally referred to as the coefficient of drag and is designated by the symbol "$C_D$".

The results of the many investigations were collected and graphically correlated using the drag coefficient and the particle Reynolds Numbers as coordinates. This has been presented by Castleman [41], Eisner [42], Muttray [43], Rouse [44], and most recently in a plot by Lapple and Shepherd [45].

Plotted on logarithmic coordinates, as shown in Figure 4, the drag coefficient falls linearly from a value of 100,000 at a Reynolds Number of 0.00025 to a value of 240 at $Re_p = 0.1$. This is the Stokes Law region, the significance of which will be discussed further on. It then decreases more moderately to a minimum of 0.38 at $Re_p = 5000$ and rises gently to a plateau of 0.47 at $Re_p = 100{,}000$. It falls off sharply to a value of approximately 0.1 at $Re_p = 300{,}000$ and again rises slowly with the Reynolds Number past that point.

At first glance it would appear that the determination of the drag coefficient would require only a minimal program of experimentation, involving the efforts of only a handful of workers. However, the wide discrepancy in the original results emphasizes the difficulties in obtaining the required idealized environmental conditions and in making accurate velocity measurements. The authors have therefore deemed it pertinent and informative to list, in a chronological sequence, the more significant contributions made towards the evolution of the standard resistance curve for spheres. This curve is meant to apply only to smooth non-rotating spheres, moving at a constant relative velocity in an infinite fluid free from any disturbances. Conditions of observation not complying with these restrictions usually result in values which deviate from the curve in some instances, as will be seen, by as much as several thousand percent.

In 1867, Rittinger [46] sought to verify Newton's "Law" by investigating particles whose Reynolds Numbers were in the vicinity of 10,000. He concluded that Newton's formula was not valid since constant $k_2$ in the relationship:

$$R = k_2(\pi/2)r_p^2 V^2 \qquad (28)$$

was not unity, but varied with the particle Reynolds Number.

A fuller Reynolds Number spectrum of from 0.009 to 8200 was investigated in 1900 by Allen [47], who developed a stereoscopic photography technique to measure the velocities of essentially spherical air bubbles and spheres of amber, paraffin and steel moving in water and aniline. His values of $C_D$ are at times low, possibly because the terminal velocities may not have been attained. They are also complicated by boundary or wall effects.

Arnold in 1911 [48] reported the fall velocities of rose metal spheres of diameter 0.013 to 0.14 cm. in colza oil, corresponding to a particle Reynolds Number of 0.002 to 2.4; however, his results are complicated by a wall effect.

Since it is easier to measure the velocity of a fluid than that of the particle, a solution to the drag coefficient problem was sought by somehow measuring the force on spheres suspended in a laminar fluid stream. The errors due to unsteady relative motion which plague the fall velocity studies are eliminated if the fluid velocity is held constant. Other difficulties develop, however, due to the inherent instability of a laminar fluid moving in a large size duct, since its Reynolds Number would be in excess of 2000.

Becker in 1907 [49] measured the resistance of spheres suspended in an air stream, but his results are not valid because they are overshadowed by the effect of the supporting wires. There are two principal sources of error here: the evaluation of the fluid force on the support mechanism is difficult–this is no simple matter, since the *presence* of the sphere may alter this force; secondly, the perforation by the supports of the complex flow field in the immediate vicinity of the sphere may in some cases engender unexpectedly large changes in the drag. This effect will be discussed more fully in a following section. Similar difficulties were encountered by Constanzi who, in 1912 [50], reported data obtained for spheres suspended in a moving column of water.

Meanwhile work with spheres moving in stagnant fluids was continuing with the help of improved velocity measuring techniques. Eiffel in 1912 [51] obtained resistance coefficients for spheres dropped from the Eiffel Tower, over a path long enough to allow the attainment of a constant velocity. These values were later confirmed by Prandtl in an artificial current of air at the Goettingen wind tunnel [52].

Shakespear in 1914 [53] obtained very consistent results when measuring the fall velocity of weighted celluloid spheres in an air tower, by making use of an electrical timing system. His system was, however, incapable of investigating small Reynolds Numbers since it would have required extremely small and at the same time accurate spheres of low density. This region was therefore almost exclusively studied with a liquid as the fluid.

Schmidt in 1920 [54] recorded the velocities of wax spheres in water, as well as the rising velocity of balloons in air. His results are complicated by acceleration effects which will be discussed more fully in another section. In 1921 Krey [55] conducted an extensive series of tests with lead, glass, brass, steel, clay, hard rubber and wooden spheres in water. These covered the Reynolds Number range from 100 to 30,000, which he extended to a value of $1 \times 10^6$ by measuring the force on a wooden sphere suspended in an air tunnel.

The great surge of activity in the field of aeronautics which developed at the close of the first World War produced a need for air tunnels in which test models of aircraft would behave as they would in the effectually laminar conditions of the free atmosphere. The obstacles to be overcome were indeed the very same as those which caused error in the suspended-sphere experiments. It became evident that the turbulence present in the flow of the early wind tunnels caused the behavior of the model aircraft to be radically different from that of the prototype in the atmosphere, so that the success of a modern wind tunnel design is in part measured by its ability to maintain streamline flow at high *tunnel* Reynolds Numbers. The fluid movement is so adjusted that the turbulence which originates at the walls of the duct is not allowed to permeate the flow in the core (which contains the test section)–as would be the case in fully developed pipe flow. A wind tunnel which fulfilled these requirements was constructed at Goettingen, and in 1922 Wieselsberger [56] began a series of drag coefficient trials in which he suspended (with a minimum of error) aluminium spheres of 1 to 28 cm. in diameter to get particle Reynolds Numbers of from 700 to 770,000. His results

generally coincide with the modern standard curve, and this is a tribute to the uniformity and lack of turbulence in the laminar air stream produced at the Goettingen tunnel.

Some rather novel methods were employed to extend the drag coefficient range. Richardson in 1923 [57] measured the resistance of air to the movement of spheres by firing them upwards from the unrifled barrel of a cannon. His results are higher than the now accepted values because of acceleration effects. Bacon and Reid in 1924 [58] obtained results for very high particle Reynolds Numbers ($2.5 \times 10^5$ to $1.5 \times 10^6$) by observing the motion of wood and brass spheres dropped from a plane.

Very accurate results for low Reynolds Numbers were obtained by Liebster and Schiller (1924) using photographic methods incorporating a timing disc [59]. These experiments were performed with lead and steel spheres in liquids of various viscosities, and they covered the Reynolds Number range of 0.12 to 2000.

Knodel in 1926 [60] used a pendulum method to measure the resistance of aluminum spheres of radius 0.146 to 0.401 cm. suspended in a laminar stream in a relatively narrow pipe. He developed an ingenious procedure to compensate for the complications introduced by the presence of the suspending mechanism. His results agree with the resistance values given by Liebster and Schiller.

One of the most important contributions towards the evolution of the standard curve was submitted by Lunnon in 1926 who performed a lengthy series of trials with spheres of various densities and diameters dropped in air [61] and in water [62], and he was able to reproduce the results of Wieselsberger's air tunnel tests. This proved effectively that the fluid resistance encountered by a spherical particle depended only on the relative movement of the solid with respect to the fluid, and not on the absolute values. Lunnon also investigated the effect of the acceleration of the particles on the drag coefficient, and this will be discussed at length in another section.

Air tunnel drag tests done in the Langley Memorial Aeronautical Laboratory in 1929 by Jacobs [63] confirmed that specific drag coefficient value is obtained at a given particle Reynolds Number, irrespective of what combination of variables, i.e. kinematic viscosity, velocity and sphere size, is used to obtain that value of the Reynolds Number.

There are more recent works such as that by Moller [64] in which measurements generally confirming the drag coefficient curve have been made as a secondary issue. Minor corrections may result from the work of Wiselius [65] who in 1947 found minimum drag values of 0.05 for the $Re_p = 3 \times 10^6$ region.

The validity of the standard curve for the sensitive region of $10 < Re_p < 100$ has been questioned recently by McKnown [66], who cites experimental evidence which indicates that the results in this region are still suffering from wall effects.

The studies just discussed were primarily directed towards the measurement of drag coefficients for idealized conditions. The large amount of experimentation studying the—at times—over-riding effects of fluid turbulence and boundary conditions, as well as particle acceleration, rotation, surface roughness and shape, will be presented after a more detailed discussion of the aerodynamics of the idealized case.

### *Approximate Equations for the Drag Coefficient*

Empirical expressions of limited accuracy giving either the drag coefficient or the drag force on a sphere for restricted Reynolds Number regions are available, the following of which are representative.

Schiller and Nauman [67] found the following relationship to hold for $Re_p \leq 700$:

$$C_D = \left(\frac{24}{Re_p}\right)(1 + 0.15\ Re_p^{\ 0.687}) \quad \ldots\ldots(29)$$

Kliachko [68] used the approximate relationship:

$$C_D = \frac{24}{Re_p} + 4/(Re_p)^{1/3} \quad \ldots\ldots(30)$$

Langmuir and Blodgett [69] employed:

$$C_D \cdot \frac{Re_p}{24} = 1 + 0.197\ Re_p^{0.63} + 0.0026\ Re_p^{1.38} \quad \ldots\ldots(31)$$

with good accuracy for the range $1 < Re_p < 100$.

Budryk [70] felt that in the "intermediate range" of particle movement, (i.e., in the Reynolds Number range from 0.5 to 2,000) the drag force should be made up of the sum of the resistances given by Stokes Law and Newton's "Law", giving the relationship as:

$$R = 6\pi\mu r_p V + k_3\left(\frac{\pi}{2}\right) r_p^2 \rho V^2 \quad \ldots\ldots(32)$$

where $k_3$ is a constant associated with Newton's Law. This pseudo-theoretical equation deviates considerably from observed values. On the other hand, Froessling [71] and later Gumz [72, 73] successfully applied the following empirical relationship for this region:

$$\frac{1}{R} = \frac{1}{R_{St}} + \frac{1}{R_N} \quad \ldots\ldots(33)$$

where $R_{St}$ is the resistance given by Stokes Law and $R_N$ is a residual drag force found by using the following pseudo-drag values:

$$\begin{array}{ll} C'_D = 0.08741 & \text{for } 0 < Re_p < 8 \\ C'_D = 0.3 & \text{for } 8 < Re_p < 300 \\ C'_D = 0.28 & \text{for } 300 < Re_p < 2000 \end{array}$$

### *Flow Regime Variation with Reynolds Number*

A brief description will now be given of the alterations which occur in the flow field about an immersed sphere as the particle Reynolds Number increases, in order to define the various flow regimes which will be subsequently discussed in detail.

The velocity of the fluid moving past the sphere must be zero along the surface of contact with the solid. At very low Reynolds Numbers, the velocity will increase gradually as the distance from the surface increases, to attain eventually a value which is equal to the stream velocity. This flow has up- and down-stream symmetry. The elements of the fluid meeting the front of the sphere are slowly accelerated sideways, and the inertia effects are too small to cause a time lag in the closing up of the flow behind the body. This visualization corresponds to the Stokes Law region which ends at a Reynolds Number of approximately 0.1, ushering in a "transition" region which has customarily been assumed to extend up to a Reynolds Number of 20,000.

A separation process in the boundray layer is first hinted at a Reynolds Number of approximately one, at which the streamline patterns associated with Stokes' regime become deformed and curl up to form a stationary vortex ring imbedded in the boundary layer at the rear of the sphere [74]. This ring resembles a smoke ring and it has strict axial symmetry. The velocity of circulation of the vortex fluid in contact with the rear portion of the sphere appears to be much slower than that of the

fluid in contact with its forward portion [75]. The ring grows in size as the Reynolds Number is increased, the vorticity generated in the ring all the while being balanced by that which diffuses downstream from it.

As the Reynolds Number increases in the transition range, the velocity gradient in the boundary layer becomes more severe. Since the fluid elements meeting the front of the sphere are accelerated sideways, this increase in the fluid velocity is accompanied by a decrease in static pressure, i.e. a negative pressure gradient, around the surface of the sphere towards the equator and in the direction of flow. The velocity of the fluid just outside the boundary layer begins to decrease beyond the equator, and the decrease in velocity now produces a *positive pressure gradient*. In that region, the motion of a thin stratum of fluid adjacent to the wall of the sphere and wholly inside the boundary layer will be influenced by three forces: it will be pulled downstream by the viscous action exerted by the stream above it; it will be retarded by friction at the sphere surface; and it is further retarded by the positive, or "adverse" pressure gradient. This pressure gradient increases with an increase in the sphere Reynolds Number and the energy and momentum of the fluid in the boundray layer become insufficient for it to force its way for very long against it. The fluid in the boundary layer is therefore eventually brought to rest, with respect to the sphere surface, and farther on next to the wall. a slow back-flow in the direction of the pressure gradient may set in. The forward boundary layer stream will then leave the sphere surface, and the latitude at which this occurs is referred to as the *point of separation*. Figure 5 shows a tracer photograph of the flow in this region.

At a Reynolds Number of about 500 [64], for a stream free from turbulence, a point of imbalance is reached and the vorticity diffusion rate downstream can no longer keep up with that generated in the vortex ring. At this point, referred to as the *lower critical Reynolds Number*, the vortex system breaks away from the body and feeds into a flow regime at the rear of the sphere which is bounded by a free shear layer, i.e. the separated boundary layer, and is referred to as *the wake*. The instability at the lower critical Reynolds Number does not correspond to that occurring at laminar-turbulent transition. As the Reynolds Number increases, there is a laminar-turbulent transition in the free shear layer which draws nearer to the separation point, the position depending on the free stream turbulence [76].

The transition region is traditionally assumed to extend to approximately 20,000, after which the wake is supposed to be made up of completely random flow systems [77]. Recent investigations point out, however, that there is always a periodicity associated with the turbulence in the wake, with the proportion of turbulent fluctuations gradually taking the upper hand as the Reynolds number increases [78].

In the vicinity of $Re_p = 200{,}000$ the forward part of the boundary layer attached to the body becomes unstable and enters into a transitional state tending towards turbulence, producing an unsymmetrical turbulent wake in an unstable and shifting position. At the *higher critical value of the Reynolds Number* ($Re_p = 300{,}000$), the separation circle moves suddenly to the rear, and there is a sharp drop of $C_D$ from 0.40 to 0.1. At still higher values of the Reynolds Number, the boundary layer flow becomes turbulent and the wake, now relatively narrow, is also turbulent and statistically stable.

The resistance of a sphere to motion in a fluid is spoken of as being the sum of a frictional effect, or *skin drag*, and a pressure gradient effect referred to as the *form drag* which is intimately associated with the mechanism of flow in the wake region. The relative contribution from each type of resistance varies with the flow regime, the former accounting for two-thirds of the total drag in the Stokes Law region and its contribution steadily diminishing to a negligible value as the particle Reynolds Number is increased beyond this range.

The ability to describe experimentally and theoretically the fluid behavior about a spherical particle seems to decrease with increasing Reynolds Numbers. Successful solutions to the Navier-Stokes equations have been given only for very low values and the degree of approximation increases as the lower critical Reynolds number is approached. The transition region has not been sufficiently probed by experiment, and has received only partial semi-theoretical treatment by boundary-layer theory methods. The developed wake regime has been even less fully described, and because of its complexity theoretical treatments deal only with the inter-relationships between arbitrary parameters.

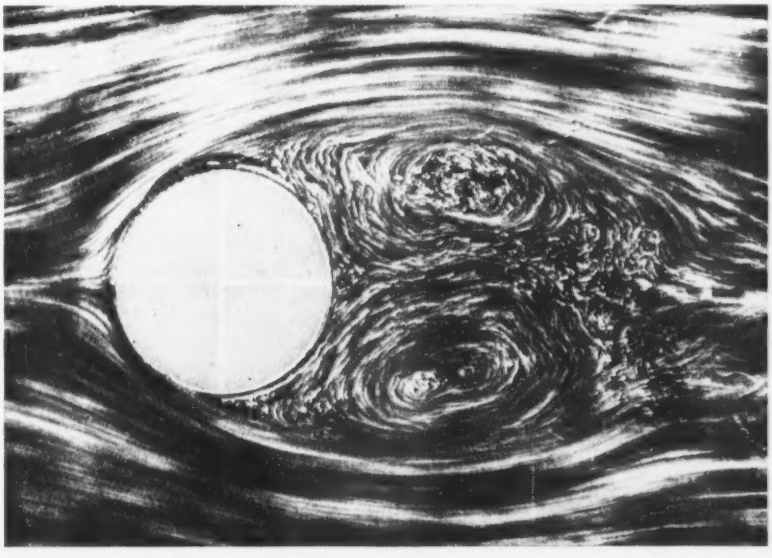

**Figure 5—Flow around submerged body in the vicinity of the lower critical Reynolds number.**

Our detailed discussion will follow this pattern, starting with the successful mathematical solutions available for the lower Reynolds Number region and ending with the most recently proposed concepts of wake flow behavior.

## III. THEORETICAL TREATMENT OF FLUID RESISTANCE TO SPHERE MOTION

### *Stokes' Solution*

A theoretical analysis of the problem of sphere motion should provide solutions for two major considerations: the first would permit calculation of the drag force for all Reynolds Number values. The second would provide a complete description of the flow field, so that the fine details of the changes occurring with increased velocities —which can often not be discerned by experiment—would be revealed. In turn, the validity of a presented solution could be evaluated by a comparison with the available experimental evidence—the drag criterion being the less sensitive one, and in some instances being unreliable as was illustrated by the Newton's "Law" case. Successful solutions would ultimately be extended to the less idealized systems having boundary conditions imposed by shape, surface roughness, rotation, free stream turbulence, etc. As will be seen from what is to follow, incorporation of these additional complexities in a theoretical treatment will not be possible in the immediate future.

In 1850 Stokes [79] succeeded in solving the equations for the resistance encountered by a sphere moving very slowly in a fluid, and this is the only case where a full theoretical solution has been obtained. The troublesome inertia terms of the Navier-Stokes equations may now be neglected so that it is reduced to the readily solvable form:

$$\text{grad } p = \mu \nabla^2 \mathbf{u} \quad \ldots\ldots\ldots\ldots\ldots\ldots (34)$$

The net force on the sphere is given by

$$R_{St} = 3\pi d p \mu U \quad \ldots\ldots\ldots\ldots\ldots\ldots (35)$$

two-thirds of which are shown to be due to the shearing stress exerted by the fluid on the sphere surface, while the remaining third is due to pressure distribution. The resulting drag coefficient 24/Re corresponds exactly to experience up to a Reynolds Number of 0.1.

This solution, considered a triumph of applied mathematics, is given in a simpler vector analysis form by Page [80] and represents the only successful fully theoretical derivation for the drag force on a particle imbedded in a fluid to date. Stokes' analysis provides a good description for the ambient flow except in the region away from the sphere where the fluid movement approaches that of the free stream.

### *Oseen's Approximation*

Neglect of the inertia terms becomes increasingly important at Reynolds Numbers above 0.1 and the Stokes resistance becomes correspondingly deficient. Whitehead [81] attempted unsuccessfully to calculate the flow pattern for finite Reynolds values by assuming an expansion of the flow in terms of Re. Oseen [82] pointed out that the result could not satisfy the boundary conditions, and he then proposed an approximation to the Navier-Stokes equations which considered the missing inertia terms to be important only in that region of the field approaching uniform flow. For this region the Navier-Stokes equations were reduced to the linear form:

$$\mathbf{U} \cdot \text{grad } \mathbf{u} = -\frac{1}{\rho} p + \nu \nabla^2 \mathbf{u} \quad \ldots\ldots\ldots\ldots\ldots\ldots (36)$$

where **U** is the free stream velocity vector. The Oseen equation has often been given in a different form resulting from representation of the velocity distribution as the sum of a constant velocity **U** and a disturbance velocity **u** [7], but Proudman and Pearson [87] point out that although it is formally the same as Equation (36) it is conceptually incorrect and has led to misleading and erroneous conclusions. They also feel that although Oseen's method of solution had seemed to give drag results which correspond to experiment, it could not be considered superior to that of Stokes for the derivation of the drag.

Goldstein [83] in 1929 succeeded in providing a complete solution for the Oseen approximation, and the following drag coefficient expression resulted:

$$C_D = (24/Re_p)(1 + 3Re_p/16 - 19Re_p^2/1280 + 71Re_p^3/20480 - \ldots\ldots) \quad (37)$$

This yields values which are within 5% of experience at $Re_p = 1$ and 20% in excess at $Re_p = 10$. Even more important are the flow patterns which are predicted by the solution, since the sphere now enters a Reynolds Number region which sees the emergence of wake phenomena together with the development of the complex wake structure. It was not until 1950 that the massive computations involved were performed by Tomotika and Aoi [74]. Their calculated pattern of streamlines clearly indicated the formation of a fixed vortex ring at the rear of the sphere at Reynolds Numbers as low as 0.1. In 1955, however, Pearcy and McHugh [84] armed with a digital computer repeated these calculations, and were surprised to find that the solution did not show the faintest suggestion of the formation of the vortex ring even at Reynolds Numbers as high as 10, where these rings had already been observed experimentally. Aside from pointing out serious errors in the work of Tomotika and Aoi, the calculations showed that the Oseen approximation indicates the formation of a strongly marked wake at Reynolds Numbers as low as one, and a boundary layer type of flow appeared on the sphere surface in the vicinity of $Re_p = 10$. Pearcy and McHugh's results began to raise serious doubts as to the validity of the Oseen approximation for the flow about a sphere since it seemed that it was not capable of indicating a vortex no matter how high the Reynolds parameter.

Stewartson [85] felt that since the Oseen equation would have to be used as a guide in the eventual solution of the exact Navier-Stokes equations, he would investigate its validity by inspecting the flow which it would indicate at high Reynolds Numbers. The solution maps out flow lines indicating a boundary layer on the forward portion, and a wake extending to infinity at the rear in the form of a cylinder with its axis parallel to the flow. The equations indicate that the wake is bounded by a shear layer, the flow inside and at infinity moving with the free stream velocity. At no time is a vortex indicated. This of course does not correspond to the actually observed system. The Oseen approximation of the Navier-Stokes equations is unacceptable as a description of the flow at high Reynolds Numbers since its solution indicates: (a) a boundary layer at the sphere front of order $\nu$, i.e. 0 ($\nu$) whereas it is observed to be 0 ($\nu^{1/2}$)—as indicated by the Navier-Stokes equation; (b) the Oseen-derived boundary layer does not break down when the skin friction vanishes on the body surface whereas in 1948 Goldstein [86] obtained a Navier-Stokes solution agreeing

with the observed fact that it does end and leave the surface of the body when this occurs; and (c) the solution for the pressure drag coefficient for $U\rho/2\mu \rightarrow \infty$ gave a value of 0.35. This, coupled with the Tomotika and Aoi solution for the Oseen approximation indicating that for all values of $U\rho/2\mu$ the skin friction is $\frac{3}{4}$ of the total drag, would indicate an obviously incorrect drag coefficient of 1.05 as $U\rho/2\mu$ (and therefore the Reynolds group) approach infinity.

In the light of the above, the Oseen approximation cannot, as it stands, be employed to further the theoretical advance towards a description of the flow for sphere Reynolds Numbers encompassing the formation and evolution of the wake regime. Proudman and Pearson [87] have very recently presented an interesting solution for the stream functions for small particle Reynolds Numbers by obtaining *separate* expansions of the stream functions for the region close to and far away from the body immersed in the flow, referred to as the Stokes and Oseen expansions respectively. For the first expansion, the boundary condition dictates that there must be no slip at the surface, while for the second the stream must be uniform at the boundary. Although unique solutions could not be obtained, the authors succeeded in using a "matching" procedure which produced the alternate terms of each expansion. The solution was applied to the flow around spheres and cylinders, and for the former the following expression for the drag coefficient was obtained:

$$C_D = (24/Re_p)[1 + (3/16)Re_p + (9/160)Re_p^2 \log Re_p + O(Re_p^2/4)] \quad \ldots\ldots (38)$$

The flow patterns about the sphere resulting from the solution have not as yet been calculated, so it is not known whether they would predict the vortex formation.

### *Kawaguti's Approach*

An interesting attempt to obtain an approximate solution of the Navier-Stokes equations for Reynolds Numbers in the vicinity of the lower critical value has recently been reported by Kawaguti [88, 89]. He employed a Galerkin method which involved the assumption of various functional forms with unknown parameters for the stream function $\psi$, the unknowns being solved for by the boundary conditions and some simplification of the Navier-Stokes equations. Many forms were attempted and the following form was successful for the range $10 < Re < 80$:

$$\psi = (1/2r^2 + A_1/r + A_2/r^2 + A_3/r^3 + A_4/r^4)\sin^2\theta + (B_1/r + B_2/r^2 + B_3/r^3 + B_4/r^4)\sin^2\theta\cos\theta \quad \ldots (39)$$

where r and $\theta$ are the polar coordinates and

$$A_2 = -\left(\frac{120}{29} + \frac{75}{29}A_1\right);$$

$$A_3 = \left(\frac{153}{29} + \frac{63}{29}A_1\right);$$

$$A_4 = -\left(\frac{95}{58} + \frac{17}{29}A_1\right);$$

$$B_2 = -\frac{23}{9}B_1;$$

$$B_3 = -\frac{19}{9}B_1;$$

$$B_4 = -\frac{5}{9}B_1$$

Values for $A_1$ and $B_1$ were obtained and the solution gave drag coefficients which are in excellent agreement with the experiment values in this range. Kawaguti reasoned that if Equation (39) is indeed correct, then the addition of a mathematically expressed small disturbance or perturbation of the proper form to the equations would yield the value of the lower critical Reynolds Number. The disturbance would die out for any Reynolds Number smaller than this value and would increase for larger ones. In this manner a lower critical Reynolds Number of 51 which Kawaguti compared with an experimental Reynolds Number of 100 was found. This comparison is approximate since the lower critical Reynolds Number occurs in the vicinity of 500 for a turbulence-free stream; all in all, however, this creditable approach shows promise.

Kawaguti's solution is not completely theoretical, since it relies on a comparison with experimental data for the selection of a proper mathematical form for the stream function. The work points out, however, that the exact solution of the Navier-Stokes equations together with the knowledge of the proper perturbation function could be expected to give the lower critical Reynolds Number as a function of the free stream conditions.

### *Numerical Solutions*

Approximate numerical methods using finite difference approximations have been employed in attempts to obtain solutions at specific Reynolds Numbers [90, 91]; however, in order to obtain workable boundary conditions the sphere is usually assumed to be in a flow which is bounded by a wall which invariably exerts a marked stabilizing influence on the sphere velocity field. The most recent example of this approach is found in a paper by Jenson [92] in which the ambient fluid is contained in a cylinder having six times the diameter as the contained sphere, and the solutions which were obtained for Reynolds Numbers of 5, 10, 20, and 40, show separation angles which are consistently lower than the experimental results reported by Garner [75], and wake dimensions which are smaller than those observed by Taneda [93].

In summary, although much effort has been expended in the study of the action on an immersed sphere by a turbulence-free flow, a theoretical description of the important region above a Reynolds Number of unity, where the inertia terms of the Navier-Stokes equation begin to exert an influence, has yet to be attained. The recent increased activity in the field has been coincident with the evolution of improved mathematical methods and the application of computing devices to cope with the ponderous numerical calculations which are required to plot the flow fields.

A subsequent paper will complete the discussion of the system of a smooth sphere moving in steady rectilinear motion through an essentially infinite and undisturbed fluid, by dealing at length with the many theoretical and experimental probings of the very important wake region.

The idealized boundary conditions thus far reviewed are seldom realized in industrial solids-gas systems, and the at times over-riding effects of non-steady motion, rotation, shape, roughness, wall proximity and high relative intensities of turbulence will be discussed.

## Nomenclature

Any consistent set of units may be employed. Those listed are merely illustrative.

| | |
|---|---|
| $A_p$ | = characteristic particle cross-sectional area, ft.$^2$ |
| $C_D$ | = particle drag coefficient, dimensionless. |
| $C'_D$ | = pseudo-drag coefficient used by Gumz, dimensionless Eqn. (33). |
| D | = duct diameter, ft. |
| $d_p$ | = characteristic particle diameter, ft. |
| **F** | = body force, lb. force. |
| g | = local acceleration of gravity, ft./sec.$^2$ |
| $g_c$ | = conversion factor 32.17 (lb. mass) (ft.)/(lb. force) (sec.$^2$). |
| $k_2$, $k_3$ | = Newton's "Law" correction coefficients, dimensionless. |
| L | = downstream length, ft. |
| $L_E$ | = Eulerian length scale, ft. |
| $L_L$ | = Lagrangian length scale, ft. |
| $l'$ | = Prandtl mixing length, ft. |
| $l''$ | = Taylor mixing length, ft. |
| R | = particle resistance, lb. force. |
| $R_N$ | = residual particle resistance given by Gumz, lb. force, Eqn. (33). |
| $R_{St}$ | = particle resistance given by Stokes law, lb. force, Eqn. (35). |
| Re | = system Reynolds Number, dimensionless. |
| $Re_p$ | = particle Reynolds Number, dimensionless. |
| $R_y$ | = Eulerian correlation coefficient, dimensionless. |
| $R_\theta$ | = Lagrangian correlation coefficient, dimensionless. |
| r | = distance from duct center, ft. |
| $r_o$ | = pipe radius, ft. |
| $r_p$ | = particle radius, ft. |
| U | = mean stream velocity, ft./sec. |
| **U** | = uniform stream velocity vector. |
| $U_c$ | = velocity at duct axis, ft./sec. |
| $U_f$ | = friction velocity, ft./sec., Eqn. (24) |
| **u** | = velocity vector, ft./sec. |
| u, v, w | = velocity components of **U** in Cartesian coordinates x, y and z, respectively, ft./sec. |
| u', v', w' | = instantaneous components of velocity fluctuation in x, y, z, ft./sec. |
| $\bar{u}$ | = time average value of u, ft./sec. |
| V | = bulk fluid velocity, ft./sec. |
| $\overline{X^2}$ | = mean square eddy diffusion distance, ft.$^2$ |
| Z | = height, ft. |
| $\delta$ | = partial differential operator. |
| $\eta$ | = eddy viscosity, lb. mass/ft. sec. |
| $\theta$ | = time, sec. |
| $\mu$ | = viscosity, lb. mass/ft. sec. |
| $\nu$ | = kinematic viscosity, ft.$^2$/sec. |
| $\rho$ | = fluid density, lb. mass/ft.$^3$ |
| $\tau$ | = shear stress, lb. force/ft.$^2$ |
| $\phi$ | = velocity potential, ft.$^2$/sec., Eqn. (5). |
| $\psi$ | = stream function, ft.$^2$/sec., Eqn. (8). |
| $\omega$ | = rotational velocity, radians/sec. |
| $\nabla$ | = vector operator del. |


## Acknowledgments

The authors wish to express their appreciation for the continued assistance given to them by Librarians A. Finnemore and L. Lefebvre of the Pulp and Paper Research Institute of Canada, and P. Keir of McGill University, in obtaining the many papers reviewed in this series. The permission of J. Laufer to reproduce Figures 1, 2 and 3, is gratefully acknowledged. L. B. Torobin is indebted to the Scientific Research Bureau, Trade and Commerce Department, Province of Quebec, for three consecutive Fellowships in support of his research program.


## References


(1) Duckham, F. E., Engineer, Jan. 29 (1897).
(2) Hudson, W. G., "Conveyors and Related Equipment". John Wiley and Sons, Inc., New York (1944).
(3) Pai, S. I., "Viscous Flow Theory". Van Nostrand Co., Princeton (1956).
(4) Batchelor, G. K., "The Theory of Homogeneous Turbulence". Cambridge University Press, Cambridge (1953).
(5) Townsend, A. A., "The Structure of Turbulent Shear Flow". Cambridge University Press, Cambridge (1956).
(6) Agostini, L. and Bass, J., N.A.C.A. T.M. 1377 (1955).
(7) Schlichting, H., "Boundary Layer Theory". Translated by J. Kestin. McGraw-Hill Book Co., Inc., New York (1955).
(8) Schubauer, G. B. and Klebanoff, P. S., N.A.C.A. T.R. 1289 (1956).
(9) Preston, J. H., J. Fluid Mech. 3: 373 (1958).
(10) Narasima, R., J. Aeronaut. Sci. 24: 711 (1957).
(11) Dhawan, S. and Narasima, R., J. Fluid Mech. 3: 418 (1957).
(12) Hsu, C. S., J. Aeronaut. Sci. 24: 313 (1957).
(13) Reynolds, O., Phil. Trans. Roy. Soc. (London) 124: 935 (1883).
(14) Rouse, H., and Howe, J. W., "Basic Mechanics of Fluids". John Wiley and Sons, Inc., New York (1953).
(15) Lindgren, E. R., Ark. Fysik 7: Paper 23, 293 (1953).
(16) Smith, M. H., "Bibliography on the Origin of Turbulence and Related Subjects". Princeton University, Princeton (1957).
(17) Prandtl, L., "Essentials of Fluid Dynamics". Blackie and Son Ltd., London and Glasgow (1952).
(18) Taylor, G. I., Proc. Roy. Soc. (London) 135A: 685 (1932).
(19) Taylor, G. I., Proc. Roy. Soc. (London) 120A: 13 (1928).
(20) Taylor, G. I., Proc. Roy. Soc. (London) 151A: 421 (1935).
(21) Taylor, G. I., Proc. Roy. Soc. (London) 164A: 476 (1938).
(22) Uberoi, M. S. and Corrsin, S., N.A.C.A. T.N. 2710 (1952).
(23) Latinen, G. A., Ph.D. Thesis, Princeton University, Princeton (1951).
(24) Hanratty, T. J., Ph.D. Thesis, Princeton University, Princeton (1953).
(25) Hanratty, T. J., Latinen, G. and Wilhelm,, R. H., A.I.Ch.E. Journal 2: 372 (1956).
(26) Soo, S. L., Chem. Eng. Science 57 (1956).
(27) Betchov, R., J. Fluid Mech. 1: 497 (1956).
(28) Newman, B. G. and Leary. B. G., A.R.L. Report No. A-72 (1950).
(29) Towle, W. L. and Sherwood, T. K., Ind. Eng. Chem. 31: 457 (1939).
(30) Laufer, J., N.A.C.A. T.R. 1174 (1954).
(31) Sandborn, U. A., N.A.CA. T.N. 3266 (1955).
(32) Cooper, R. D. and Tulin, M. P. AGARDograph No. 12 (1955).
(33) Van Der Leeden, P., Liem., D. N. and Suratman, P. C., Appl. Sci. Res. Sect. A, 5: 338 (1955).
(34) Hall, W., A.R.C. Tech, Rept. R. and M. 1842 (1938).
(35) Newman, B. G. and Leary, B. G., Dept. of Supply, Aero. Res. Lab. Rept. A 72, (Nov. 1950).
(36) Mickelsen, W., N.A.C.A. T.N. 3570 (1955).
(37) Newton, I., Philos. Nat. Primo. Math. 2, Sect. 2: 7 (1710).
(38) Zahm, A. F., J. Franklin Inst. 217: 153 (1934).
(39) Prandtl, L. and Tiejens, O. G., "Applied Hydro and Aero Mechanics". McGraw-Hill Book Co. Inc., New York (1934).
(40) Rayleigh, E., Phil. Mag. (5) B4: 59 (1892).
(41) Castleman, R. A., N.A.C.A. T.N. 231 (1926).
(42) Eisner, F., Proc. 3rd Intern. Congr. Appl. Mech., Stockholm (1931).
(43) Muttray, H., "Handbuch der Experimental Physik". Wien and Harms, Leipzic (1932).
(44) Rouse, H., "Nomogram for Settling Velocity of Spheres". Ann. Rept. Comm. Sed., Nat. Res. Council (1937).
(45) Lapple, C. E., "Fluid and Particle Mechanics". University of Delaware, Newark, Delaware (1954).
(46) Rittinger, P. and Ritter, V. "Lehrbuch der Aufbereitungskunde". Ernst und Korn, Berlin (1867).
(47) Allen, H. S., Phil. Mag. (5) 20: 323, 519 (1900).
(48) Arnold, H. D., Phil. Mag. (6) 22: 755 (1911).
(49) Becker, A., Ann. Physik. 24: 863 (1907).
(50) Constanzi, S., Alcune Esperienze di Idrodynamica 2, No. 4 (1912).
(51) Eiffel, G., Compt. rend. 155: 1597 (1912).
(52) Prandtl, L., Nachr. d.k. Ges. d. Wissensch. in Göttingen; Math.–Naturw. (1914).
(53) Shakespear, G. A., Phil. Mag. (6) 28: 728 (1914).
(54) Schmidt, F. S., Ann. Physik (4) 61: 633 (1920).
(55) Krey, H., "Mitteilungen versuch. Wasserbau u. Schiffbau". Mittler and Sohn, Berlin (1921).
(56) Wieselsberger, C., Physik. Z. 23: 219 (1922).
(57) Richardson, L. F., Phil. Trans. A 223: 351 (1923).
(58) Bacon, D. L. and Reid, E. G., N.A.C.A. Rept. 1185 (1924).
(59) Liebster, H. and Schiller, L., Physik Z. 25: 670 (1924).
(60) Knodel, A., Ann. Physik 80: 533 (1926).
(61) Lunnon, R. G., Proc. Roy. Soc. (London) 110A: 302 (1926).
(62) Lunnon, R. G., Proc. Roy. Soc. (London) 118A: 680 (1928).
(63) Jacobs, E. N., N.A.C.A. T.N. 312 (1929).
(64) Moller, von W., Physik Z. 39: 57-80 (1938).
(65) Wiselius, S. I., N.A.R.I. Rep. A 950, Amsterdam (1947).
(66) McKnown, J. S., Lee, H. M., McPherson, M. B. and Engez, S. M., Proc. 7th Intern. Congr. Appl. Mech. (London), (1948).
(67) Schiller, L. and Nauman, A., Z. Ver. deut. Ing. 77: 318 (1933).

(68) Kliachko, L. S., Heat and Ventilation (U.S.S.R.) No. 4 (1934).
(69) Langmuir, I. and Blodgett, K., A.A.F. T.R. 5418 (1946).
(70) Budryk, W., Rev. Ind. Miner. 16: 740 (1936).
(71) Froessling, N., Gerlands Beitr. Geophysik. 51: 167 (1937).
(72) Gumz, W., Feuerungstech. 26: 253 (1938).
(73) Gumz, W., Arch. ges. Warmetech. 1: 25 (1950).
(74) Tomotika, S., and Aoi, T. Quart. J. Mech. Appl. Math. 3: 140 (1950).
(75) Garner, F. H., Chemistry and Industry, Feb. 25, 141 (1956).
(76) Schiller, L. and Linke, W., N.A.C.A. T.M. 715 (1933).
(77) Nemenyi, P., Trans. Am. Geophys. Union 21: 633 (1940).
(78) Cometta, C., Brown U., Div. Eng., TR WT-21 (AFOSR TN 57-760).
(79) Stokes, G. G., Trans. Camb. Phil. Soc. 9, Part 2: 51 (1851).
(80) Page, L., "Introduction to Theoretical Physics". D. Van Nostrand Co., Inc., New York (1928).
(81) Whitehead, A. N., Quart. J. Math. 23: 143 (1889).
(82) Oseen, C. W., Ark. f. Mat. Astr. och Fys. 6, No. 29 (1910).
(83) Goldstein, S., Proc. Roy. Soc. (London) 123A: 225 (1929).
(84) Pearcy, T. and McHugh, B., Phil. Mag. 7th Ser. 46: 783 (1955).
(85) Stewartson, K., Phil. Mag. 8th Ser. 1: 345 (1956).
(86) Goldstein, S., Quart. J. of Mech. and Appl. Math. 1: 43 (1948).
(87) Proudman, I. and Pearson, J. R. A., J. Fluid Mech. 2: 237 (1957).
(88) Kawaguti, M., Rep. Inst. Sci. Technol. Tokyo 8: 1 (1954).
(89) Kawaguti, M., J. Phys. Soc. Japan 10: 694 (1955).
(90) Kawaguti, M., Rep. Inst. Sci. Technol., Tokyo, 4: 154 (1950).
(91) Lister, M., Ph.D. Thesis, London (1953).
(92) Jenson, V. G., Proc. Roy. Soc. (London) 249 A:347 (1959).
(93) Taneda, S., Rep. Inst. Appl. Mech. (Japan), 4: 99 (1956).

★ ★ ★

# Thermodynamic Properties of Some Organic Compounds[1]

## I. PVT Relationships and Calculated Thermodynamic Properties for Normal Butanol*

*L. W. SHEMILT*[2], *R. W. ESPLEN*[3] *and R. SINGH MANN*[4]

**Pressure-volume-temperature measurements on *n*-butanol have been carried out using the Kay type of pressure-block apparatus and glass capillary cell. Determinations were made isothermally in the saturated vapor and liquid and superheated vapor regions to above the critical point. Compressibility factors have been calculated. Constants in the Beattie-Bridgman equation of state have been determined from 250° to 300°C. at pressures up to 75 atmospheres.**

**The thermodynamic properties of normal butanol have been calculated over a temperature range of 0°C. to 300°C. and at pressures up to 1000 lb./sq. in. abs. from the PVT data. Values for the saturated liquid, saturated vapor, and superheated vapor are presented on a pressure-enthalpy diagram with specific volume and entropy as parameters. The entropy of the saturated vapor increases with temperature over a considerable region, indicating a positive specific heat of the saturated vapor in contrast to the lower alcohols of the same series.**

THE growing importance of processes involving high pressure and high temperature conversions has made the accurate determination of the pressure-volume-temperature (PVT) relationships of many compounds increasingly important. As part of an investigation into the thermodynamic properties of alcohols, the determination of PVT values on normal butanol has been carried out to provide data not available previously, and to allow compilation and calculation of the enthalpy values in the saturated, two-phase, and superheated regions.

Analytical representation of PVT data is achieved through equations of state, of which only a few such as those of Benedict, Webb and Rubin [1] and of Beattie and Bridgman [2] have attained practical importance. These are all empirical and while theoretical equations of state based on statistical thermodynamics have been attempted, there has been as yet no development possible of wide application. In this work the Beattie and Bridgman equation of state has been selected to represent the PVT data, and to be used in the calculation of other thermodynamic properties.

Graphical presentation of the PVT data and the calculated thermodynamic functions are also given.

### *Available data*

The amount of information on the PVT properties of *n*-butanol is relatively sparse. Vapor pressures up to the normal boiling point have been determined by Kahlbaum [3] and by Butler and co-workers [4]. Dreisbach [5] has reported boiling points at 4 different pressures below atmospheric. The definitive normal boiling point determination for *n*-butanol appears to be that of Wojciechowski [6] at 117.726°C., along with a coefficient of increase in boiling point with increase in pressure, $\frac{dp}{dt} = 0.0372$°C. per mm. Hg. Other values accepted by Timmermans [7] range from 117.77 to 118.0°C. Tukuzo and Koe [8] have reported the density of the saturated liquid from 0°C. to −80°C. while numerous determinations at single temperatures have been made [7]. Critical temperatures have been determined several times without reference to other critical properties [9, 10, 11], and the critical pressure has been reported by Herz and Neukirch [12]. New values have been given recently by Kay and Donham [13] who also reported orthobaric densities and vapor pressures up to the critical point. The most extensive determination of critical properties, including critical density and an equation for rectilinear diameters, formed the preliminary work in this investigation [14]. Densities for the saturated vapor and the corresponding equilibrium liquids were reported at the same time for a temperature range from 155° to 286°C. A tabulation of critical constants appearing earlier [14] has been revised and is shown in Table 1.

Early work on the heat capacity of *n*-butanol [15, 16] was limited to providing single values for the liquid, or a mean value over a limited temperature range. Parks [17] provided low temperature data including liquid butanol from its melting point to 20°C., while Williams and Daniels [18] gave a value for constant pressure heat capacity as a function of temperature for the range 30-80°C.

[1]*Manuscript received August 6, 1958.*
[2]*Professor, Department of Chemical Engineering, The University of British Columbia, Vancouver, B.C.*
[3]*Present address: Imperial Oil Limited, Sarnia, Ont.*
[4]*Present address: Bureau of Mines, Ottawa, Ont.*
*Contribution from the Department of Chemical Engineering, The University of British Columbia, Vancouver, B.C.*
**Grateful acknowledgement is made of financial assistance from the National Research Council.*

TABLE 1

CRITICAL PROPERTIES OF NORMAL BUTANOL

| Date | $t_c$°C | $P_c$ atm. | $\rho_c$ g./c.c. | Investigators |
|---|---|---|---|---|
| 1883 | 287.1 | | | Pawlewski [11] |
| 1884 | 270.5 | | | de Heen [10] |
| 1923 | | 48.4 | | Herz and Neukirch [12] |
| 1943 | 288.0 | | | Fischer and Reichel [9] |
| 1955 | 289.74 | 43.6 | 0.267 | Kay and Donham [13] |
| 1955 | 286.95 | 48.60 | 0.2700 | Singh and Shemilt [14] |

Francis [19] assembled previous data in the form of temperature dependent equations.

The only values for heat capacities in the vapor state were given by Sinke and de Vries [20] for the range 120-165°C. at 750 mm. pressure.

***Experimental***

1. *Materials*

The *n*-butanol (c.p. grade) was distilled at high reflux in a glass-helici packed column and middle cuts further refluxed and distilled successively from calcium oxide, fresh magnesium and activated alumina. In all distillations only the middle fraction (one-third) was collected. The final product gave a refractive index of 1.3973 at 25°C. measured on a carefully calibrated Abbe-type refractometer, a density of 0.80565 at 25°C. and a boiling point of 117.77°C. using a thermometer calibrated against a laboratory standard with an N.B.S. certificate. Two separate lots of *n*-butanol were prepared and gave identical results within the precision of the measurements (0.0001 refractive index units, 0.00003 in density, and 0.03°C. respectively).

The mercury used in contact with the *n*-butanol was triple distilled. Chlorobenzene, aniline, methyl salicylate, bromonaphthalene, n. butyl phthalate, and benzophenone used for the constant temperature column were reagent grade or better and were further purified by distillation at high reflux.

2. *Apparatus and procedures*

The apparatus, designed after that of Kay [21, 22] consisted of an adjustable steel block filled with mercury and connected to a calibrated glass capillary containing the sample and enclosed in a constant temperature apparatus. The pressure in the capillary of 2 mm. true bore tubing, was transmitted by mercury to an oil line leading to a dead weight gauge tester. A piston in the compressor block could be moved to adjust the pressure and keep the mercury-oil level constant, as shown by an electrical relay arrangement. For temperature measurement a copper-constantan thermocouple was used with a type K-2 potentiometer having a Weston Standard cell with an N.B.S. certificate. The temperature was kept constant around the capillary tube by boiling a purified organic compound under a controlled pressure. By selection of the proper compound a wide range of temperatures was obtainable. The pressure was measured by a manometer and controlled by a manostat operating through an electronic relay.

The constant temperature vapor bath was a silvered, vacuum-jacketed distillation column 4 feet long with sufficient expansion bellows to allow a temperature differential up to 340°C.

The compressor block contained the mercury-oil interface detector. The capillary was mounted by packing and a special-type gland. The piston was sealed with a special V-leather packing and could be moved in or out without loss of mercury up to operating pressures of 1200 lbs./sq. in.

The internal diameter of the "constant-bore" capillary tubing throughout its total length, and the volumes in the region of tubing joins and the volume of the sealed tip were obtained by weighing amounts of triple distilled mercury released from the tubing and measuring the height difference with a Gaertner cathetometer previously calibrated against a metre stick with an N.B.S. certificate.

The capillary tubing was filled by means of a carefully cleaned filling tube to a depth of about 6 inches with purified *n*-butanol which had just been boiled vigorously to remove dissolved gases. The tubing was inserted into a simple filling apparatus where a vacuum ($3 \times 10^{-5}$ cms. of mercury pressure, was applied until about 50% of the *n*-butanol was vaporized and removed. Purified mercury contained in the filling apparatus was then spilled into the capillary tubing sealing in the liquid butanol sample, and the tubing was inserted into position in the pressure block.

The copper-constantan thermocouple was constructed from Leeds and Northrup glass-insulated duplex thermocouple wire No. 30 B. & S. gauge, and was calibrated against a 2.5 ohm platinum-resistance thermometer with an N.B.S. certificate. The latter was also independently checked against the ice-point. The average deviation throughout the range to be used was $\pm$ 0.03°C. The dead weight test gauge, manufactured by Barrett, had a range up to 4000 p.s.i. Piston diameters and the weights used were checked for accuracy and found to agree with the manufacturer's listing (i.e. maximum total error less than 0.1%).

The general operating procedure involved manipulation of the compressor block piston and the weights on the test gauge pan to maintain correct mercury levels. Beginning with a liquid sample, vaporization was carried out to give as large a vapor-to-liquid ratio as possible for all two-phase readings. Condensation from a vapor state was also carried out to ensure the approach to equilibrium from "both sides". Thermal equilibrium was considered established when temperature readings changed less than 0.1°C. for a period of one hour, and the mercury level changed less than 0.5 cm. in the same period, indicating practically no vaporization or condensation and hence no large heat transfer demand. For this period also, room temperatures were maintained constant to 1°C. and atmospheric pressure continually noted. Following establishment of equilibrium, readings were made of the weights on the gauge tester, and of mercury levels throughout the system including meniscus height, and position of liquid meniscus when present. Temperatures ranged from 117.6°C. to 305.5°C. Below the critical point both liquid and superheated vapor systems as well as the two-phase equilibrium system were examined.

The actual weight of the samples used was obtained by measurements of liquid volume below 80°C. and utilization of known liquid density data [7]. Isothermal volume measurements for a completely and partially vaporized sample were used to give saturated liquid and vapor densities. Dew points were obtained by increasing pressure incrementally on the superheated vapor at constant temperature, and noting the point when the superheated vapor specific volume decreased significantly.

Two completely independent samples were used for purification and for measurement purposes. Comparison

of boiling-points, refractive indices, and vapor pressures at two different temperatures showed no difference beyond that inherent in the methods of measurement.

Corrections were applied for the mercury meniscus in accordance with values given in the International Critical Tables [23]. Volume corrections for the expansion of the glass capillary tubing due to temperature were made according to the equation [24].

$$V = V_o(1 + \alpha t)$$

where $\alpha$ = cubical expansion coefficient, $9.9 \times 10^{-6}$;
and $t$ = temperature change in °C.

The effect of pressure on the glass capillary volume was calculated by the equation [25]

$$\Delta V = V_o(30.27 \times 10^{-7}p + 9.9 \times 10^{-12}p^2)$$

where $p$ = pressure, Kg/cm²
and $V_o$ = original volume, cc's.

***Results and calculations***

1. *PVT Measurements.*

The results of the PVT measurements are presented in Table 2 and graphically in Figure 1, and cover a range of temperatures from 197°C. to 305°C. and pressures from 100 to 1000 psia.

The original results obtained as isothermal data were transformed to isometrics by a method similar to that used by Andrews [26], and modified by Beattie and Bridgman [2]. The transformation was effected by calculating the quantity (PV-RT) for each measurement on a given isothermal. A straight line was then passed through the point of zero density (where PV-RT = O), and the highest measured density on the isotherm. Deviation of the observed values from this line were plotted against density. From this plot values of PV-RT and hence of the pressure (considered as observed pressure) were interpolated for a set of evenly spaced densities, the same density being used at each isothermal. The data, smoothed with respect to volume are presented in Table 3.

Vapor pressure results ranging from the normal boiling point to the critical point are given in Table 4, along with saturated vapor and liquid densities previously reported [14].

2. *Equation of state.*

The PVT data were used for calculation of the constants in the Beattie-Bridgman equation of state [2]

where

$$P = \frac{RT(1 - E)}{V^2}(V + B) - \frac{A}{V^2}$$

$$\text{where } A = A_o\left(1 - \frac{a}{V}\right)$$

$$B = B_o\left(1 - \frac{b}{V}\right)$$

$$E = \frac{C}{VT^3}$$

The isometrics (Table 3) were each straightened by using a correction factor C, and that value of C was chosen which straightened out the most curved isometric. The Beattie-Bridgman procedure [2] was followed using a "corrected pressure" $p^1$ defined as

$$p^1 = p + F(V,T) = T\psi(V) - \phi(V)$$

For each isometric, plotted as $p^1$ vs. T, there were obtained values of $\Psi(V)$ and $\Phi(V)$ appearing as slope and intercept. Since

$$V + B = \frac{V^2 \cdot \psi(V)}{R}$$

$$\text{and } A = V^2 \cdot \phi(V)$$

TABLE 2

ISOTHERMAL PRESSURE-VOLUME DATA (OBSERVED) FOR *n*-BUTANOL

P = Pressure, p.s.i.a. V = Volume, ccs/gm.

| Temp = 197.28°C. | | Temp. = 209.11°C. | | Temp. = 221.80°C. | | Temp. = 232.45°C. | | Temp. = 244.63°C. | | Temp. = 260.55°C. | |
|---|---|---|---|---|---|---|---|---|---|---|---|
| P | V | P | V | P | V | P | V | P | V | P | V |
| 113.72 | 59.63 | 118.73 | 59.83 | 123.71 | 59.55 | 124.06 | 61.99 | 129.01 | 61.35 | 134.05 | 61.44 |
| 122.87 | 54.28 | 137.26 | 50.36 | 142.52 | 50.68 | 142.62 | 52.43 | 147.64 | 52.64 | 152.74 | 53.09 |
| 127.49 | 51.84 | 156.07 | 42.80 | 161.18 | 43.44 | 161.50 | 45.34 | 166.58 | 45.76 | 171.52 | 46.45 |
| 128.94 | 49.72 | 170.19 | 37.87 | 180.27 | 37.69 | 180.63 | 39.54 | 204.98 | 35.61 | 210.16 | 36.59 |
| | | | | 199.51 | 32.95 | 199.83 | 34.75 | 243.83 | 28.38 | 258.83 | 28.20 |
| | | | | 214.02 | 29.84 | 219.19 | 30.80 | 282.98 | 23.02 | 307.88 | 22.19 |
| | | | | | | 238.65 | 27.37 | 302.61 | 20.69 | 357.17 | 17.73 |
| | | | | | | 258.11 | 24.31 | 322.29 | 18.63 | 406.57 | 13.94 |
| | | | | | | 263.91 | 23.34 | 327.21 | 18.13 | 421.41 | 12.93 |
| | | | | | | 264.7 | 23.32 | | | | |

| Temp. = 268.90°C. | | Temp. = 272.25°C. | | Temp. = 276.48°C. | | Temp. = 283.94°C. | |
|---|---|---|---|---|---|---|---|
| P | V | P | V | P | V | P | V |
| 138.90 | 60.43 | 278.13 | 28.25 | 278.04 | 28.37 | 288.16 | 28.37 |
| 157.65 | 52.51 | 336.38 | 21.30 | 355.79 | 19.59 | 356.25 | 20.52 |
| 195.84 | 40.92 | 355.87 | 19.40 | 404.87 | 16.14 | 405.23 | 17.30 |
| 244.33 | 31.34 | 404.87 | 15.70 | 453.96 | 13.37 | 454.40 | 14.30 |
| 293.29 | 24.86 | 483.58 | 11.80 | 552.57 | 8.646 | 503.98 | 12.10 |
| 342.53 | 20.00 | 541.71 | 9.77 | 601.21 | 7.160 | 553.01 | 9.92 |
| 391.93 | 16.10 | 620.86 | 8.74 | 700.55 | 2.180 | 602.49 | 7.83 |
| 441.42 | 13.00 | 650.85 | 2.218 | 800.52 | 2.117 | 651.48 | 5.80 |
| 481.03 | 10.70 | 700.84 | 2.170 | 900.50 | 2.083 | 730.86 | 2.439 |
| | | 800.82 | 2.110 | 1000.48 | 2.040 | 800.82 | 2.297 |
| | | 900.80 | 2.051 | | | 900.79 | 2.220 |
| | | 1000.79 | 2.014 | | | 1000.77 | 2.156 |

| Temp. = 286.99°C. | | Temp. = 294.68°C. | | Temp. = 300.56°C. | | Temp. = 305.52°C. | |
|---|---|---|---|---|---|---|---|
| P | V | P | V | P | V | P | V |
| 405.31 | 17.40 | 366.47 | 20.80 | 308.09 | 27.29 | 279.26 | 31.07 |
| 454.63 | 14.60 | 405.68 | 17.56 | 366.56 | 22.36 | 308.23 | 27.68 |
| 503.92 | 12.00 | 454.94 | 15.53 | 405.77 | 18.31 | 376.32 | 21.04 |
| 602.74 | 10.20 | 504.19 | 13.44 | 454.97 | 15.67 | 405.92 | 19.68 |
| 632.41 | 7.10 | 553.36 | 11.52 | 504.30 | 13.64 | 455.10 | 16.89 |
| 661.86 | 5.85 | 603.09 | 9.76 | 553.72 | 11.82 | 504.43 | 14.61 |
| 671.60 | 5.50 | 652.56 | 8.13 | 603.25 | 10.13 | 603.86 | 12.68 |
| 711.28 | 3.170 | 702.28 | 6.73 | 652.79 | 8.64 | 653.34 | 9.68 |
| 731.06 | 2.590 | 751.17 | 5.674 | 702.41 | 7.29 | 703.34 | 8.34 |
| 751.03 | 2.403 | 801.22 | 4.863 | 752.01 | 6.28 | | |
| 800.97 | 2.300 | 851.06 | 4.296 | 801.66 | 5.472 | | |
| 850.96 | 2.223 | 900.99 | 3.850 | 851.31 | 4.782 | | |
| 900.96 | 2.203 | 950.96 | 3.459 | 901.09 | 4.255 | | |
| 1000.94 | 2.195 | 1000.45 | 3.053 | 950.90 | 3.850 | | |
| | | | | 1000.02 | 3.513 | | |

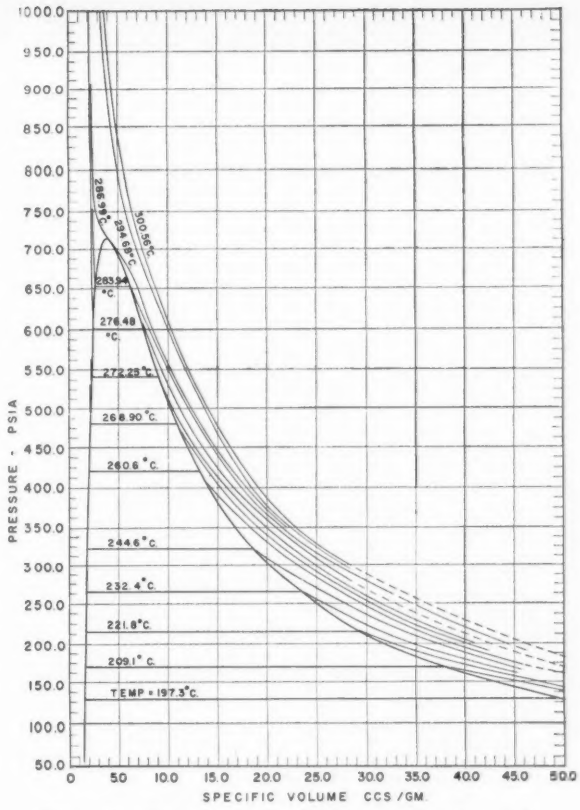


**Figure 1—Pressure-volume isotherms for *n*-butanol.**

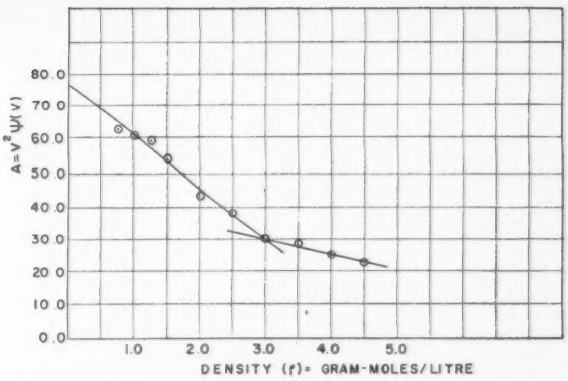


**Figure 2—The Beattie-Bridgman function, $A = V^2 \Psi (V)$. Related to density for *n*-butanol.**

the values of B and A for each isometric were found, and plotted as functions of density. These plots enabled the four remaining constants in the equation of state to be determined and are shown in Figures 2 and 3. A definite break occurred in the two plots at the region of $\rho = 3.00$; and hence two different sets of constants were obtained. Table 5 presents these compared with those of methanol, the only other normal alcohol for which results are available [27].

By using the virial form of the equation of state

$$P = RT\rho + \beta \cdot \rho^2 + \gamma \cdot \rho^3 + \delta \cdot \rho^4,$$

the virial coefficients may be evaluated from the Beattie-Bridgman constants as, for example, with the important second virial coefficient,

$$\beta = B_o - \frac{A_o}{RT} - \frac{C}{T^3}$$

3. *Compressibility*

The compressibility factor, $Z = \dfrac{PV}{RT}$, was evaluated from the experimental PVT data for isotherms from 197°C. to 305°C. and the values presented in Table 6. These results, expressed as a function of reduced pressure, are also given in a "compressibility chart", Figure 4, with

TABLE 3

ISOMETRIC PRESSURE-TEMPERATURE DATA (OBSERVED) FOR *n*-BUTANOL
Absolute pressure — atmos.

| Density gm. mole/(ρ) litre | Temp. °C. | | | | | | | | |
|---|---|---|---|---|---|---|---|---|---|
| | 260 | 265 | 270 | 275 | 280 | 285 | 290 | 295 | 300 |
| 0.50 | 18.00 | 18.42 | 18.85 | 19.22 | 19.60 | 20.00 | 20.40 | 20.80 | 21.20 |
| 0.75 | 23.60 | 24.11 | 24.70 | 25.25 | 25.00 | 26.37 | 26.95 | 27.50 | 28.05 |
| 1.00 | 27.90 | 28.70 | 29.60 | 30.40 | 31.23 | 32.10 | 32.95 | 33.80 | 34.65 |
| 1.25 | 30.40 | 31.50 | 32.65 | 33.85 | 35.00 | 36.15 | 37.30 | 38.50 | 39.68 |
| 1.50 | 32.50 | 33.90 | 35.30 | 36.80 | 38.25 | 39.70 | 41.20 | 42.65 | 44.10 |
| 1.75 | 33.35 | 35.00 | 36.70 | 38.40 | 40.13 | 41.82 | 43.58 | 45.30 | 47.00 |
| 2.00 | | | | | 41.50 | 43.40 | 45.45 | 47.50 | 49.50 |
| 2.50 | | | | | 44.30 | 46.90 | 49.55 | 52.20 | 54.80 |
| 3.00 | | | | | 47.60 | 50.50 | 53.40 | 56.40 | 59.20 |
| 3.50 | | | | | 49.80 | 53.50 | 57.20 | 60.95 | 64.60 |
| 4.00 | | | | | 52.50 | 56.70 | 60.85 | 65.00 | 69.20 |
| 4.50 | | | | | 54.70 | 59.58 | 64.40 | 69.20 | 74.00 |

TABLE 4

VAPOR PRESSURES AND ORTHOBARIC DENSITIES FOR *n*-BUTANOL

| Temp. °C. | Pressure p.s.i.a. | Density G/CC | |
|---|---|---|---|
| | | Liquid | Vapor |
| 117.58 | 14.65 | | |
| 126.85 | 20.36 | | |
| 131.83 | 23.79 | | |
| 155.77 | 48.61 | 0.70520 | 0.0079 |
| 155.99 | 48.74 | | |
| 167.74 | 66.97 | | |
| 173.30 | 77.17 | 0.67059 | 0.01249 |
| 175.78 | 81.64 | | |
| 183.61 | 97.85 | 0.62478 | 0.01587 |
| 198.89 | 137.17 | 0.61920 | 0.02106 |
| 209.11 | 170.19 | | |
| 212.02 | 179.16 | 0.59305 | 0.02775 |
| 221.59 | 215.81 | | |
| 221.80 | 216.53 | | |
| 232.45 | 264.41 | | 0.04280 |
| 237.31 | 287.06 | 0.53590 | |
| 244.63 | 326.99 | 0.51993 | 0.05516 |
| 260.55 | 421.22 | 0.48589 | 0.07733 |
| 268.90 | 481.03 | 0.45740 | 0.09480 |
| 272.2 | 541.0* | 0.43200 | 0.1023 |
| 276.5 | 601.0* | 0.42370 | 0.1300 |
| 283.9 | 653.0* | 0.3620 | 0.1681 |
| 285.7 | — | 0.3220* | 0.2402 |

*extrapolated values.

temperature as a parameter, and the calculated values in the form of smoothed curves.

4. *Volume, vapor pressure, and heat of vaporization.*

Saturated liquid volumes up to 100°C. were calculated from the Bridgman equation [28]

$$d = 0.82390 - 0.699 \times 10^{-3}t + 0.32 \times 10^{-6}t^2, \quad \ldots\ldots(1)$$

where t = temperature in °C.

These values on a large-scale plot, with the experimental ones from 155°C. to 287°C., allowed a smooth interpolation for the range 100° to 155°C. Saturated vapor volumes up to 155°C. were calculated using the compressibility factor from the generalized charts of Hougen and Watson [29].

The vapor pressure values available were plotted on a large scale Cox-type graph, a smooth curve drawn through the data, and vapor pressures read for the desired increments of temperature.

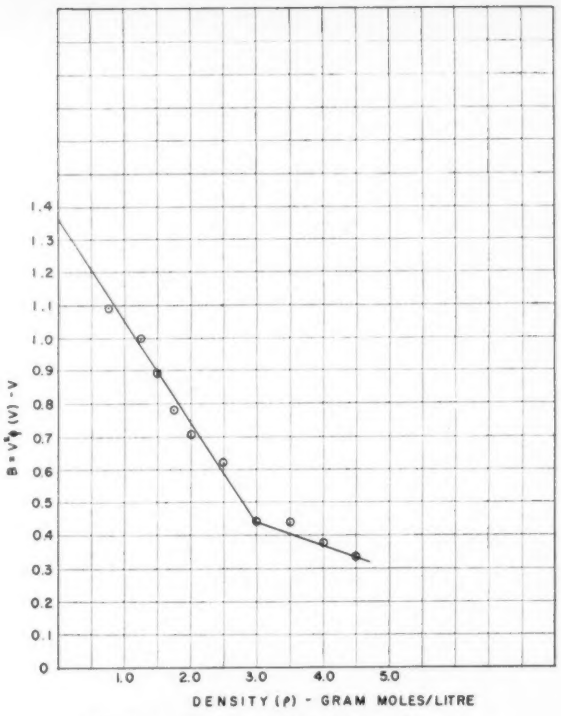


**Figure 3—The Beattie-Bridgman function, $B = V^2 \phi (V) - V$. Related to density for *n*-butanol.**

Latent heats of vaporization were calculated by the well-known Clapeyron equation [30], by the Othmer method [31], and by Othmer's method as modified by Thomas [32]. The values obtained by the three methods varied by less than 3% in all cases. A smooth curve averaging the results and extrapolating to a value of zero at the critical temperature was used to portray the best value.

5. *Enthalpy*

Liquid and vapor enthalpies were obtained from the enthalpies of the ideal gas, the equation of state, and the heats of vaporization in the following manner. First, the enthalpy of the ideal gas at zero pressure was obtained from a heat capacity equation. For this the heat capacity

TABLE 5

CONSTANTS FOR BEATTIE-BRIDGMAN EQUATION OF STATE

| | | n. butanol | | methanol |
|---|---|---|---|---|
| Range of temp. °C. | | 250–300 | 250–300 | — |
| Range of density gm. moles/litre | | 0.75–3.00 | 3.00–4.50 | — |
| Constant | Units | | | |
| a | litres/gm. mole | 0.20411 | 0.10730 | 0.09246 |
| $A_o$ | (atm.) (litres/gm. mole)² | 76.226 | 44.235 | 33.309 |
| b | litres/gm. mole | 0.2265 | 0.1047 | 0.09929 |
| $B_o$ | litres/gm. mole | 1.3513 | 0.6571 | 0.60362 |
| c | (litres/gm. mole)/°K³ | $4.00 \times 10^5$ | $4.00 \times 10^5$ | $3.2031 \times 10^5$ |

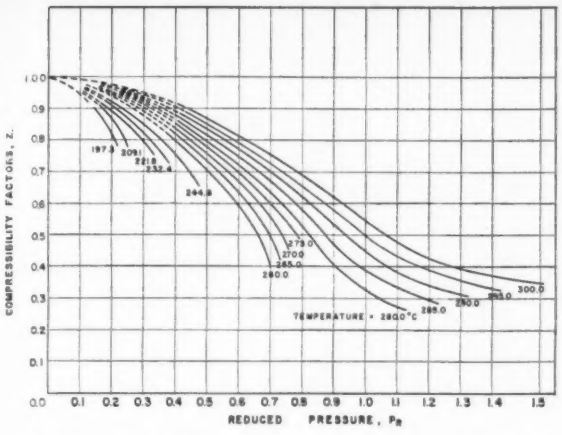


**Figure 4—Compressibility factors for *n*-butanol.**

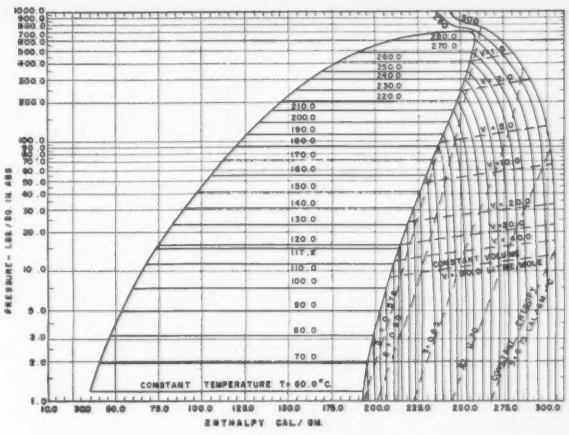


**Figure 5—Pressure-enthalpy diagram for *n*-butanol.**

TABLE 6 (a)

COMPRESSIBILITY FACTORS FOR *n*-BUTANOL

Volume — litres/gm. mole  Press. — atm.  Temp. — °C.

| Temp. | Volume | 1.50 | 1.75 | 2.00 | 2.25 | 2.50 | 2.75 | 3.00 | 3.25 | 3.50 | 4.00 | 4.50 |
|---|---|---|---|---|---|---|---|---|---|---|---|---|
| 197.3 | Press. | | | | | | | 10.23 | 9.79 | 9.27 | 8.39 | 7.65 |
| | Z | | | | | | | 0.7944 | 0.8240 | 0.8403 | 0.8692 | 0.8915 |
| 209.1 | Press. | | | | | 12.28 | 11.63 | 11.00 | 10.38 | 9.78 | 8.77 | 7.95 |
| | Z | | | | | 0.7758 | 0.8082 | 0.8339 | 0.8525 | 0.8650 | 0.8865 | 0.9090 |
| 221.8 | Press. | | | 15.58 | 14.38 | 13.33 | 12.42 | 11.62 | 10.88 | 10.23 | 9.16 | 8.23 |
| | Z | | | 0.7684 | 0.7979 | 0.8220 | 0.8423 | 0.8596 | 0.8720 | 0.8838 | 0.9041 | 0.9132 |
| 232.4 | Press. | | 17.78 | 16.27 | 15.00 | 13.87 | 12.90 | 12.04 | 11.27 | 10.60 | 9.950 | 8.580 |
| | Z | | 0.7499 | 0.7845 | 0.8133 | 0.8357 | 0.8549 | 0.8726 | 0.8835 | 0.8941 | 0.9156 | 0.9305 |
| 244.6 | Press. | 20.75 | 18.92 | 17.20 | 15.71 | 14.50 | 13.45 | 12.56 | 11.74 | 11.03 | 9.85 | 8.86 |
| | Z | 0.7261 | 0.7726 | 0.8025 | 0.8249 | 0.8457 | 0.8632 | 0.8794 | 0.8901 | 0.9006 | 0.9192 | 0.9291 |

TABLE 6 (b)

COMPRESSIBILITY FACTORS FOR *n*-BUTANOL

Volume — litres/gm. mole  Press. — atm.  Temp. — °C.

| Temp. | Volume | 0.222 | 0.25 | 0.2857 | 0.333 | 0.40 | 0.50 | 0.5714 | 0.666 | 0.80 | 1.00 | 1.33 | 2.00 |
|---|---|---|---|---|---|---|---|---|---|---|---|---|---|
| 260 | Press. | | | | | | | 33.35 | 32.50 | 30.40 | 27.90 | 23.60 | 18.00 |
| | Z | | | | | | | 0.4356 | 0.4952 | 0.5559 | 0.6377 | 0.7190 | 0.8228 |
| 265 | Press. | | | | | | | 35.00 | 33.90 | 31.50 | 28.70 | 24.11 | 18.42 |
| | Z | | | | | | | 0.4526 | 0.5109 | 0.5703 | 0.6495 | 0.7273 | 0.8339 |
| 270 | Press. | | | | | | | 36.70 | 35.30 | 32.65 | 29.60 | 24.70 | 18.85 |
| | Z | | | | | | | 0.4705 | 0.5275 | 0.5860 | 0.6641 | 0.7387 | 0.8459 |
| 275 | Press. | | | | | | | 38.40 | 36.80 | 33.85 | 30.40 | 25.25 | 19.22 |
| | Z | | | | | | | 0.4878 | 0.5449 | 0.6020 | 0.6758 | 0.7483 | 0.8548 |
| 280 | Press. | 54.70 | 52.50 | 49.80 | 47.60 | 44.30 | 41.50 | 40.13 | 38.25 | 35.00 | 31.23 | 25.80 | 19.60 |
| | Z | 0.2675 | 0.2891 | 0.3134 | 0.3492 | 0.3904 | 0.4571 | 0.5015 | 0.5617 | 0.6168 | 0.6880 | 0.7516 | 0.8636 |
| 285 | Press. | 59.58 | 56.70 | 53.50 | 50.50 | 46.90 | 43.40 | 41.82 | 39.70 | 36.15 | 32.10 | 26.37 | 20.00 |
| | Z | 0.2890 | 0.3095 | 0.3377 | 0.3675 | 0.4096 | 0.4738 | 0.5218 | 0.5778 | 0.6314 | 0.7008 | 0.7675 | 0.8736 |
| 290 | Press. | 64.40 | 60.85 | 57.20 | 53.40 | 49.55 | 45.45 | 43.58 | 41.20 | 37.30 | 32.95 | 26.95 | 20.40 |
| | Z | 0.3096 | 0.3291 | 0.3536 | 0.3851 | 0.4289 | 0.4918 | 0.5388 | 0.5943 | 0.6457 | 0.7130 | 0.7774 | 0.8829 |
| 295 | Press. | 69.20 | 65.00 | 60.95 | 56.40 | 52.20 | 47.50 | 45.30 | 42.65 | 38.50 | 33.80 | 27.50 | 20.80 |
| | Z | 0.3298 | 0.3485 | 0.3735 | 0.4032 | 0.4478 | 0.5094 | 0.5552 | 0.6093 | 0.6600 | 0.7250 | 0.8020 | 0.8923 |
| 300 | Press. | 74.00 | 69.20 | 64.60 | 59.20 | 54.80 | 49.50 | 47.00 | 44.10 | 39.68 | 34.65 | 28.05 | 21.20 |
| | Z | 0.3493 | 0.3678 | 0.3924 | 0.4192 | 0.4660 | 0.5262 | 0.5710 | 0.6245 | 0.6749 | 0.7367 | 0.7950 | 0.9015 |

of the vapor at zero pressure was determined by using the characteristic frequencies of all the intramolecular bonds as measured spectroscopically, and calculating by means of the appropriate Einstein functions. The frequency values of Bennewitz and Rossner [33], as subsequently modified by Dobratz [34], were used. The heat capacity equation thus obtained was

$$(C_P)_O = -8.324 \times 10^{-3} + 1.2778 \times 10^{-3}T - 0.48048 \times 10^{-6}T^2, \quad \ldots\ldots(2)$$

where T = temperature in °K.

Changes in enthalpy with pressure and temperature may be expressed by the equation

$$dH = C_p dT + \left[V - T\left(\frac{\partial V}{\partial T}\right)_p\right] dP \quad \ldots\ldots(3)$$

By integration of this equation and selection of an appropriate standard state, enthalpy values for the non-ideal saturated vapor state were obtained. The standard state selected was a value of zero enthalpy for the liquid at 0°C. The temperature term was integrated using Equation (2) above. The pressure term was integrated by the method of Hougen and Watson [35] up to 250°C. For the range 250° to 300°C., values of the pressure integral were determined from the constants of the Beattie-Bridgman equation of state, as suggested by Dodge [36] using a differentiation of the expanded form of the equation of state. The enthalpy value for the ideal gas at 0°C. and zero pressure was calculated by adding the heat of vaporization value at 0°C. to the standard state value for the liquid.

Liquid enthalpy values were then calculated by addition of latent heats of vaporization to the enthalpy values for the saturated vapor. Up to 90°C., they were also determined by Williams and Daniels' equation [18]

$$C_p = 0.49992 + 0.00263t + 0.0000018t^2, \quad \ldots\ldots(4)$$

where t = temperature in °C.

Up to 70°C. the values checked within 0.5%.

6. *Entropy.*

Entropies were calculated in a manner similar to that for enthalpies. Values for the vapor were obtained from the equation [37]

$$S = S_o + \int_{To}^{T} \frac{C_p}{T} dT - \int_{Po}^{P} \left(\frac{\partial V}{\partial T}\right)_p dP \quad \ldots\ldots(5)$$

where $P_o = 0$, $T_o = 0$°C.,
and $S_o$ = an arbitrary standard state value of entropy at 0°C. and zero pressure, and taken to be zero for liquid.

The temperature integral was evaluated using Equation (2). The pressure integral was determined for the range of 250°C.-300°C. from the Beattie-Bridgman constants as before, and up to 250° by the method of Hougen and Watson [38]. The values at 250°C. by the two methods checked within 1.5%.

Entropies for the liquid were obtained from the equation

$$S_L = S_V - \frac{\Delta H_v}{T} \quad \ldots\ldots(6)$$

where $S_L$ = entropy of liquid, cal. per mole per °K.
$S_V$ = entropy of vapor, cal per mole per °K.
$\Delta H_v$ = latent heat vaporization, cal. per mole.
and T = temperature in °K.

Liquid entropies were also determined for the temperature range 0°C.-80°C. from Daniel's equation of heat capacity and were found to agree within 0.8%.

Enthalpies and entropies for the superheated region were determined in a similar fashion to the saturated

TABLE 7

THERMODYNAMIC PROPERTIES OF *n*-BUTANOL — SATURATED ZONE

| Temp. °C. | Pressure p.s.i.a. | Volume liquid ccs./gm. | Volume vapor ccs./gm. | Enthalpy liquid cal./gm. | Heat of vaporiz'n cal./gm. tion | Enthalpy vapor cal./gm. | Entropy liquid cal./(gm.) (°C.) | Entropy of vaporiz'n cal./(g.m.) (°C.) | Entropy vapor cal./(gm.) (°C.) |
|---|---|---|---|---|---|---|---|---|---|
| 0 | 0.01938 | 1.2137 | 230315 | 0.0 | 172.34 | 172.34 | 0.0 | 0.6309 | 0.6309 |
| 10 | 0.03866 | 1.2242 | 136410 | 5.124 | 170.22 | 175.34 | 0.00704 | 0.6012 | 0.6082 |
| 20 | 0.08118 | 1.2348 | 58805 | 10.515 | 167.67 | 178.18 | 0.02394 | 0.5720 | 0.5959 |
| 30 | 0.17976 | 1.2459 | 27445 | 16.175 | 165.27 | 181.44 | 0.04143 | 0.5452 | 0.5866 |
| 40 | 0.35080 | 1.2564 | 16504 | 22.110 | 162.56 | 184.67 | 0.0593 | 0.5191 | 0.5784 |
| 50 | 0.66456 | 1.2688 | 7903.7 | 28.322 | 160.47 | 188.79 | 0.0756 | 0.4966 | 0.5722 |
| 60 | 1.17159 | 1.2807 | 4620.0 | 34.816 | 158.93 | 192.75 | 0.0942 | 0.4740 | 0.5682 |
| 70 | 1.97600 | 1.2929 | 2815.0 | 40.592 | 155.24 | 195.83 | 0.1118 | 0.4524 | 0.5642 |
| 80 | 3.2088 | 1.3055 | 1784.8 | 46.575 | 152.42 | 198.99 | 0.1303 | 0.4316 | 0.5619 |
| 90 | 4.987 | 1.3186 | 1018.05 | 52.610 | 149.59 | 202.20 | 0.1451 | 0.4119 | 0.5570 |
| 100 | 7.519 | 1.3319 | 803.28 | 59.887 | 146.63 | 206.52 | 0.1628 | 0.3920 | 0.5548 |
| 110 | 11.147 | 1.3456 | 557.74 | 67.495 | 143.59 | 211.08 | 0.1808 | 0.3747 | 0.5555 |
| 117.7 | 14.696 | 1.3580 | 428.37 | 72.63 | 141.26 | 213.89 | 0.1980 | 0.3616 | 0.5596 |
| 120 | 16.165 | 1.3630 | 404.05 | 75.00 | 139.80 | 214.80 | 0.2040 | 0.3556 | 0.5596 |
| 130 | 23.219 | 1.3810 | 275.67 | 82.10 | 136.50 | 218.60 | 0.2217 | 0.3386 | 0.5603 |
| 140 | 30.567 | 1.3990 | 212.83 | 89.65 | 132.80 | 222.45 | 0.2403 | 0.3214 | 0.5617 |
| 150 | 41.148 | 1.4170 | 160.54 | 97.22 | 129.00 | 226.22 | 0.2582 | 0.3048 | 0.5630 |
| 160 | 55.257 | 1.4350 | 115.50 | 104.85 | 125.10 | 229.95 | 0.2779 | 0.2881 | 0.5660 |
| 170 | 71.275 | 1.4750 | 88.00 | 111.39 | 121.00 | 232.39 | 0.2950 | 0.2730 | 0.5680 |
| 180 | 90.38 | 1.520 | 70.30 | 118.92 | 117.00 | 235.92 | 0.3128 | 0.2582 | 0.5710 |
| 190 | 113.16 | 1.570 | 57.00 | 126.37 | 113.00 | 239.37 | 0.3280 | 0.2439 | 0.5719 |
| 200 | 140.35 | 1.620 | 46.75 | 133.95 | 108.80 | 242.75 | 0.3462 | 0.2300 | 0.5762 |
| 210 | 173.12 | 1.680 | 37.00 | 140.75 | 104.40 | 245.15 | 0.3650 | 0.2161 | 0.5811 |
| 220 | 209.42 | 1.742 | 30.00 | 147.28 | 100.05 | 247.33 | 0.3795 | 0.2029 | 0.5824 |
| 230 | 252.42 | 1.813 | 24.65 | 154.46 | 95.20 | 249.66 | 0.3963 | 0.1892 | 0.5855 |
| 240 | 302.74 | 1.890 | 20.30 | 161.73 | 90.12 | 251.85 | 0.4151 | 0.1756 | 0.5907 |
| 250 | 355.64 | 1.972 | 16.50 | 169.01 | 84.00 | 253.01 | 0.4307 | 0.1605 | 0.5912 |
| 260 | 417.37 | 2.060 | 13.30 | 178.21 | 77.12 | 255.33 | 0.4507 | 0.1446 | 0.5953 |
| 270 | 498.19 | 2.220 | 10.64 | 191.06 | 64.95 | 256.01 | 0.4705 | 0.1196 | 0.5901 |
| 280 | 604.01 | 2.469 | 7.117 | 211.55 | 44.95 | 256.50 | 0.4986 | 0.0812 | 0.5798 |
| 287 | 714.00 | 3.707 | 3.707 | 250.0 | 0.0 | 250.0 | 0.5504 | 0.0 | 0.5504 |

vapor by using the Beattie-Bridgman constants from 250°C.-300°C., and the Hougen and Watson method [39] from 117.7°C.-250°C. Values below 117.7°C. were obtained by extrapolation.

7. *Thermodynamic network.*

The thermodynamic properties measured and calculated as above are presented for the saturated zone in Table 7, for the superheated region in Table 8, and graphically in Figure 5.

***Discussion of results***

A high degree of purity for the *n*-butanol was obtained. The density measurement of 0.80565 compares to the values of 0.80567, 0.80572, 0.8057, 0.8057 selected by Timmermans [7]. The refractive index value of 1.3973 compares to the critically selected values of 1.3974 and 1.3970. The normal boiling point obtained during purification was 117.77 ± 0.03°C. After the purified material was enclosed in the PVT apparatus, a series of readings at different times gave an average value of 117.69 ± 0.03°C. This agreement between a static and dynamic method appears quite acceptable. It also compares favorably to Timmermans [7] selection of 10 values ranging from 117.7 to 118.0°C., and Kay and Donham [13] who reported 117.73°C.

In addition a further criterion of purity was used. The average pressure rise on condensation was determined from the dew-point pressure and the pressure value at complete condensation. Over a series of temperatures from 220°C. to 270°C. this value averaged 0.15 p.s.i., somewhat more favorable than the single value of 0.32 p.s.i. reported by Kay and Donham [13] at 230°C. A similar gauge of the purity showed in determinations of vapor pressures with widely varying percentages of vaporized material. At 185°C., for example, the deviation was less than 0.04% for a change from 20% to 80% vaporized.

All the usual corrections to pressure and volume were applied, with the exception of any correction for the presence of mercury vapor. The usual correction consists of subtracting the vapor pressure of mercury from the measured pressure, allowing for the effect of the total pressure on this vapor pressure value (the so-called Poynting effect). Jepson and Rowlinson [40] have recently discussed this correction and applied additional corrections for deviations from ideality in the gaseous solution of mercury and the contained vapor. However, in the measurements reported here an extremely small mercury surface was available to the system. In addition precise duplication of results on the two-phase system when approaching it both from a superheated vapor and a total liquid state, confirmed that no mercury vapor correction was required.

The vapor pressure data reported here show complete consistency with Butler's data below the normal boiling point when plotted on a large scale Cox-type chart. Moreover both an Antoine equation and another type of a 3-constant vapor pressure equation show no discontinuities at the boiling point when applied to all available data [41]. The isothermal plot (Figure 1) and the calculations used in determining the critical points [14] both indicate a high degree of self-consistency of the results given here. It is thus considered that precision of the measurements (0.01 atmospheres for pressure; 0.03°C. for temperature; and 0.5% for volumes) is satisfactorily reflected in the PVT values reported.

While data in the superheated region are available only from 197°C. to 305°C., measurements on properties of the saturated vapor and liquid are given from the normal boiling point to 287°C. The size of the sample that could be put in the apparatus limited the range of vapor volumes that could be measured at the lower temperatures. The fact that measurements could be made above the critical point meant however that the significant range of values was adequately covered.

The vapor pressure data used for the presentation of the thermodynamic network are based on actual measurements throughout the temperature range from 0°C. to the

TABLE 8

THERMODYNAMIC PROPERTIES OF *n*-BUTANOL
SUPERHEATED REGION

Temp. — °C. Press. — p.s.i.a.
volume, V — cc's/gm. = 62.43 (cu.ft./lb.)
enthalpy, H — cal./gm. = (B.t.u./lb.) $\left(\frac{1}{1.8}\right)$. Entropy, S — cal./(gm.) (°C.) = B.t.u./(lb.) (°F.).

| Press. | | Temp. 117.6 | 120 | 130 | 140 | 150 | 160 | 170 | 180 | 190 | 200 |
|---|---|---|---|---|---|---|---|---|---|---|---|
| 14.7 | V | 428.37 | 425.26 | 440.00 | 451.94 | 463.11 | 474.54 | 485.49 | 496.70 | 507.92 | 519.15 |
| | H | 213.89 | 214.88 | 219.20 | 223.48 | 227.97 | 232.58 | 237.16 | 241.87 | 246.64 | 251.50 |
| | S | 0.5596 | 0.5629 | 0.5780 | 0.5847 | 0.5955 | 0.6061 | 0.6167 | 0.6274 | 0.6378 | 0.6481 |
| 25.0 | V | | | | 264.07 | 270.73 | 277.01 | 283.79 | 289.69 | 297.02 | 304.79 |
| | H | | | | 222.85 | 227.48 | 232.19 | 236.57 | 241.25 | 246.07 | 250.98 |
| | S | | | | 0.5691 | 0.5799 | 0.5907 | 0.6012 | 0.6122 | 0.6241 | 0.6331 |
| 50.0 | V | | | | | | 134.33 | 137.27 | 140.68 | 143.78 | 148.13 |
| | H | | | | | | 230.23 | 234.84 | 239.60 | 244.40 | 249.51 |
| | S | | | | | | 0.5691 | 0.5802 | 0.5911 | 0.6020 | 0.6128 |
| 75.0 | V | | | | | | | | 91.82 | 95.14 | 97.21 |
| | H | | | | | | | | 238.01 | 243.04 | 247.95 |
| | S | | | | | | | | 0.5776 | 0.4889 | 0.5999 |
| 100 | V | | | | | | | | | 69.63 | 71.13 |
| | H | | | | | | | | | 241.39 | 246.32 |
| | S | | | | | | | | | 0.5785 | 0.5898 |

TABLE 8 (Continued)

| Press. | | 210 | 220 | 230 | 240 | 250 | 260 | 270 | 280 | 290 | 300 |
|---|---|---|---|---|---|---|---|---|---|---|---|
| 14.7 | V | 531.20 | 542.74 | 554.29 | 565.0 | 576.0 | 586.49 | 597.68 | 607.16 | 620.4 | 631.3 |
| | H | 256.48 | 261.51 | 266.71 | 271.80 | 277.08 | 282.37 | 287.01 | 293.34 | 298.87 | 304.4 |
| | S | 0.6586 | 0.6691 | 0.6794 | 0.6897 | 0.6999 | 0.7101 | 0.7204 | 0.7306 | 0.7403 | 0.7502 |
| 25.0 | V | 310.88 | 316.62 | 323.05 | 329.80 | 336.77 | 344.12 | 351.51 | 358.25 | 364.36 | 371.20 |
| | H | 255.95 | 260.94 | 266.14 | 271.24 | 276.56 | 281.91 | 286.51 | 292.90 | 298.43 | 303.97 |
| | S | 0.6437 | 0.6542 | 0.6645 | 0.6747 | 0.6849 | 0.6952 | 0.7056 | 0.7156 | 0.7256 | 0.7357 |
| 50.0 | V | 151.73 | 155.19 | 155.67 | 162.32 | 166.00 | 168.79 | 171.44 | 175.36 | 179.80 | 182.50 |
| | H | 254.44 | 259.51 | 264.74 | 269.93 | 275.28 | 280.57 | 285.00 | 291.58 | 297.25 | 302.76 |
| | S | 0.6233 | 0.6341 | 0.6445 | 0.6550 | 0.6654 | 0.6756 | 0.6861 | 0.6963 | 0.7060 | 0.7189 |
| 75.0 | V | 99.60 | 102.18 | 103.92 | 105.98 | 108.04 | 111.49 | 113.35 | 116.11 | 118.7 | 121.12 |
| | H | 253.02 | 258.17 | 263.45 | 268.51 | 273.82 | 279.38 | 284.00 | 290.47 | 296.10 | 301.71 |
| | S | 0.6107 | 0.6217 | 0.6321 | 0.6428 | 0.6597 | 0.6638 | 0.6742 | 0.6845 | 0.6944 | 0.7043 |
| 100 | V | 72.73 | 74.90 | 76.46 | 77.98 | 80.10 | 82.14 | 83.70 | 85.61 | 87.48 | 90.56 |
| | H | 251.37 | 256.63 | 261.95 | 267.11 | 272.58 | 278.09 | 282.76 | 289.15 | 296.78 | 300.69 |
| | S | 0.6023 | 0.6124 | 0.6230 | 0.6337 | 0.6450 | 0.6550 | 0.6555 | 0.6759 | 0.6859 | 0.6957 |
| 150 | V | 46.20 | 47.87 | 48.95 | 49.92 | 51.70 | 52.70 | 53.80 | 54.92 | 56.72 | 57.74 |
| | H | 248.01 | 253.44 | 258.83 | 264.13 | 269.81 | 275.21 | 279.99 | 286.33 | 292.23 | 297.83 |
| | S | 0.5870 | 0.5977 | 0.6088 | 0.6201 | 0.6312 | 0.6418 | 0.6530 | 0.6635 | 0.6735 | 0.6834 |
| 200 | V | | 33.37 | 35.07 | 35.76 | 36.70 | 37.50 | 38.26 | 39.73 | 41.32 | 42.89 |
| | H | | 249.39 | 255.63 | 260.89 | 266.66 | 271.95 | 276.76 | 283.40 | 289.84 | 295.80 |
| | S | | 0.5850 | 0.5970 | 0.6089 | 0.6208 | 0.6315 | 0.6420 | 0.6558 | 0.6642 | 0.6742 |
| 250 | V | | | 26.25 | 27.10 | 28.20 | 29.30 | 30.25 | 31.32 | 32.32 | 33.02 |
| | H | | | 251.58 | 257.16 | 263.11 | 269.03 | 274.20 | 280.71 | 287.17 | 292.92 |
| | S | | | 0.5872 | 0.5994 | 0.6114 | 0.6228 | 0.6344 | 0.6458 | 0.6562 | 0.6662 |
| 300 | V | | | | 20.92 | 21.60 | 22.47 | 23.30 | 24.33 | 25.48 | 26.60 |
| | H | | | | 252.96 | 258.82 | 264.21 | 270.16 | 273.42 | 280.30 | 286.90 |
| | S | | | | 0.5897 | 0.6014 | 0.6151 | 0.6282 | 0.6374 | 0.6490 | 0.6588 |
| 350 | V | | | | | 17.06 | 17.85 | 18.39 | 19.51 | 20.78 | 22.82 |
| | H | | | | | 254.00 | 260.27 | 265.57 | 273.41 | 280.30 | 286.90 |
| | S | | | | | 0.5951 | 0.6079 | 0.6196 | 0.6320 | 0.6428 | 0.6529 |
| 400 | V | | | | | | 14.23 | 14.52 | 15.93 | 17.51 | 17.62 |
| | H | | | | | | 255.77 | 259.94 | 268.90 | 277.60 | 284.49 |
| | S | | | | | | 0.6002 | 0.6126 | 0.6256 | 0.6369 | 0.6475 |
| 450 | V | | | | | | | 12.43 | 14.00 | 15.41 | 15.67 |
| | H | | | | | | | 256.29 | 266.61 | 274.50 | 281.33 |
| | S | | | | | | | 0.6053 | 0.6188 | 0.6311 | 0.6416 |
| 500 | V | | | | | | | | 11.36 | 13.34 | 13.65 |
| | H | | | | | | | | 263.03 | 271.55 | 279.05 |
| | S | | | | | | | | 0.6126 | 0.6250 | 0.6350 |
| 550 | V | | | | | | | | 9.35 | 11.45 | 11.83 |
| | H | | | | | | | | 260.07 | 268.75 | 276.33 |
| | S | | | | | | | | 0.6046 | 0.6180 | 0.6291 |
| 600 | V | | | | | | | | 7.966 | 9.690 | 10.13 |
| | H | | | | | | | | 256.99 | 265.20 | 273.43 |
| | S | | | | | | | | 0.5989 | 0.6119 | 0.6224 |
| 650 | V | | | | | | | | | 8.06 | 8.65 |
| | H | | | | | | | | | 262.64 | 270.07 |
| | S | | | | | | | | | 0.6037 | 0.6148 |
| 700 | V | | | | | | | | | 6.67 | 7.29 |
| | H | | | | | | | | | 258.69 | 261.43 |
| | S | | | | | | | | | 0.5908 | 0.6012 |
| 800 | V | | | | | | | | | 4.82 | 5.38 |
| | H | | | | | | | | | 241.30 | 250.51 |
| | S | | | | | | | | | 0.5420 | 0.5525 |
| 900 | V | | | | | | | | | 3.85 | 4.25 |
| | H | | | | | | | | | 238.20 | 244.50 |
| | S | | | | | | | | | 0.5358 | 0.5460 |
| 1000 | V | | | | | | | | | 3.05 | 3.51 |
| | H | | | | | | | | | 236.69 | 242.97 |
| | S | | | | | | | | | 0.5326 | 0.5427 |

critical point. The results of Kahlbaum [8] and of Butler [4] up to the normal boiling point agree very well. From there to the critical point the results reported here are considerably higher than those reported by Kay and Donham [18]. The difference is approximately 2% until close to the upper limit when it increases to 10%. There appears to be no obvious reason for the disagreement. It is felt, however, since a significantly lower pressure rise on condensation was obtained, and extreme caution used in establishing of equilibrium, that the values reported here are more reliable. One other interesting fact is that the application to the normal alcohols of the Riedel [42] and Lydersen [43] group contribution method for estimating critical properties, with due allowance for increasing chain length and molecular weight, indicates that the results reported here are more consistent with those of the other normal alcohols [41]. Better agreement with an Othmer-type of reference substance relationship is also obtained, and in addition a large scale plot of log p against 1/T shows the slight tendency to an S-shaped curve that has been noted for the corresponding paraffins [44]. These results were therefore used for all the thermodynamic calculations given here. Stull [45] has previously calculated vapor pressures from the normal boiling point to the critical point by an unstated extrapolation method. These deviate from the measured values used here by an average of 2%.

Evaluation of the constants for the Beattie-Bridgman equation of state was limited to the temperature range of 250-300°C. because insufficient volumetric data were available at lower temperatures. While such an equation, with 5 empirical constants, has been shown to fit PVT relations with a high degree of accuracy, its adequacy is illustrated by the necessity of using two sets of constants to cover the range of densities in this case. The values of the constants obtained for *n*-butanol are similar in magnitude to those for methanol and indicate their possible usefulness in homologous series calculations. They have also been applied to calculate other thermodynamic properties, and are of interest in calculating virial coefficients and hence for comparison with theoretical calculations of intermolecular forces and force constants.

The specific volumes of the superheated vapor at temperatures below 200°C. were not of as high order of accuracy due to the size of sample that had to be used, and the difficulty of actual measurements of large volumes at low temperatures and pressures. As a result the use of a generalized method appears satisfactory at temperatures under 200°C. At higher temperatures and particularly at higher pressures significant deviations occur from the usual generalized compressibility chart. From the PVT measurements reported here, the calculation of compressibilty factors has resulted in a chart (Figure 4) of limited but useful range. Some of the compressibility factors vary as much as 40% from those predicted by the generalized compressibility chart. Below the critical point the corrections are almost all negative, and above the critical point are all positive. The increasing use of a third parameter, such as Pitzer's acentric factor [46], or the critical compressibility [47], enables much more accurate generalized predictions. For intensive application such as in an homologous series, this still does not attain the accuracy possible through use of experimental data.

The close agreement shown between liquid enthalpy values based on Daniel's equation (measured heat capacity values) and those obtained by calculation from spectroscopic data and addition of heats of vaporization, indicates a high degree of consistency. It also lends validity to the use of spectroscopic calculations at higher temperatures where liquid heat capacity values were not available. While the vapor heat capacity values of Sinke and de Vries [20] are approximately 10% higher than those calculated with the data of Bennewitz and Rossner [38], the former were actually limited to a determination of 5 values over a narrow range. The overall effect on enthalpy values would be less than 0.3% in any case, and hence the use of the full range of calculated values was considered to be justified. Since the entropy values as calculated were based on the same data, the good accuracy of these is also indicated.

The thermodynamic properties reported are in reality overall or apparent values and do not take into account the effect of association between *n*-butanol molecules. From the practical standpoint such apparent values represent the actual behavior of *n*-butanol independent of whether or not the state of equilibrium between associated and unassociated molecules is known.

The entropy values for the saturated vapor are interesting from the design standpoint since there is a considerable region through which positive specific heats are indicated. This means that adiabatic compression from certain superheated vapor regions leads to the compressed vapor becoming "wet". In contrast to this both methanol [48] and ethanol [49] have saturated vapor entropies that decrease continuously with increasing temperature. The normal paraffins exhibit similar behavior [50].

From overall considerations of accuracy, it is estimated that the error in the thermodynamic properties now presented for *n*-butanol is within 1% for most of the range covered and not much in excess of that even at highest temperatures and pressures.

### *Nomenclature*

a, A, $A_o$, b, B, $B_o$, C, E = constants in Beattie-Bridgman equation of state.
$C_p$ = heat capacity, constant pressure
d = density (Bridgman equation)
d = differential operator
H = enthalpy
$\Delta H_v$ = latent heat of vaporization
$p^1$ = corrected pressure in Beattie-Bridgman equations
p = pressure, kg./cm.$^2$
P = pressure, psia.
R = universal gas constant
S = entropy
t = temperature, °C.
T = absolute temperature
V = specific volume
$\Delta V$ = volume change
Z = compressibility factor

### *Greek letters*

$\alpha$ = cubical expansion coefficient
$\beta, \gamma, \delta$ = virial coefficients
$\rho$ = density
$\Delta$ = finite difference
$\phi$ = function
$\psi$ = function.

### *Subscripts*

L = liquid
O = zero (pressure, temperature); original value (volume).
V = vapor.

## *References*


(1) Benedict, M., Webb, G. B., and Rubin, L. C., J. Chem. Phys. 8, 334 (1940).
(2) Beattie, J. A., and Bridgman, O. C., Proc. Am. Acad. Arts. Sci. 63, 229 (1928).
(3) Kahlbaum, G. W., Z. physik. Chem. 13, 14 (1894); 26, 577 (1898).
(4) Butler, J. A. V., Thompson, D. W., and Ramchandam, C. N., J. Chem. Soc. 280 (1935).
(5) Dreisbach, R. R., and Shrader, S. A., Ind. Eng. Chem. 41, 2879 (1949).
(6) Wojciechowski, M., J. Res. Nat. Bur Std. 17, 721 (1936).
(7) Timmermans, J., "Physico-Chemical Constants of Pure Organic Compounds" (Elsevier, New York, 1950) p. 319.
(8) Tokuzo, T., and Koe, U., Bull. Chem. Soc. Japan, 6, 118 (1931).
(9) Fischer, R., and Reichel, T., Mikrochemie, 31, 192 (1943).
(10) de Heen, Landolt and Bornstein (Verlag Julius Springer, Berlin, 1923) Vol. 1, p. 256.
(11) Pawlewski, B., Ber. deut. chem. Ges. 15, 2143, 2460 (1882).
(12) Herz, W., and Neukirch, E., Z. Physik, 104, 433 (1923).
(13) Kay, W. B., and Donham, W. E., Chem. Eng. Soc. 4, 1 (1955).
(14) Singh, R., and Shemilt. L. W., J. Chem. Phys. 23, 1370 (1955).
(15) Von Reis, M. A., Annalen der Physik, 13, 447 (1881).
(16) Longinine, W., Anales de chemie et de Phys., 13, 289 (1898).
(17) Parks, G. S., J. Am. Chem. Soc., 47, 415 (1951).
(18) Williams, J. W., and Daniels, F., J. Am. Chem. Soc. 46, 903 (1924).
(19) Francis, A. W., Ind. Eng. Chem. 20, 283 (1928).
(20) Sinke, G. C., and de Vries, T., J. Am. Chem. Soc. 75, 1815 (1953).
(21) Bahlke, W. H., and Kay, W. B., Ind. Eng. Chem. 24, 291 (1932).
(22) Kay, W. B., and Rambosek, G. M., Ind. Eng. Chem. 45, 221 (1953).
(23) International Critical Tables (McGraw-Hill, New York, 1926) Vol. I. p. 68-70.
(24) Corning Glass Works, Corning, New York, Cat. No. L.P. 34 (1954).
(25) Bridgman, P. W., Am. Sci. J. 7, 81 (1929).
(26) Andrews, Phil. Transactions, 166, 421 (1876).
(27) Beattie, J. A., and Stockmayer, W. H., Reports on Progress in Physics, 7, 195 (1940).
(28) Bridgman, P. W., Proc. Am. Acad. Arts & Scie., 66, 185 (1930).
(29) Hougen, O. A., and Watson, K. M., Chemical Process Principles (John Wiley & Sons) p. 489.
(30) Clausius, R. J. E., Ann. Phy. 79, 368 (1850).
(31) Othmer, D. F., Ind. Eng. Chem. 32, 841 (1940); 34, 1072 (1942).
(32) Thomas, L. H., J. Chem. Soc. 3415 (1949).
(33) Bennewitz, K., and Rossner, W., Z. Physik Chem. 39B, 126 (1938).
(34) Dobratz, C. J., Ind. Eng. Chem. 33, 759 (1941).
(35) Hougen, O. A., and Watson, K. M., Chemical Process Principles (John Wiley & Sons) p. 493.
(36) Dodge, B. F., Chemical Engineering Thermodynamics (1944). McGraw-Hill Book Co., New York, p. 219.
(37) Ibid. P. 231.
(38) Hougen, O. A., and Watson, K. M., Chemical Process Principles (John Wiley & Sons) p. 497.
(39) Ibid. P. 518.
(40) Jepson, W. B., and Rowlinson, J. S., J. Chem. Phys. 23, 1599 (1955).
(41) Shemilt, L. W., Unpublished work.
(42) Reidel, L., Chem. Ing. Tech. 24, 353 (1952).
(43) Lydersen, A. L., Univ. of Wisconsin, Eng. Expt. Station, Report No. 3 (1955).
(44) Thompson, A. W., Chem. Rev. 48, 1 (1946).
(45) Stull, D. R., Ind. Eng. Chem., 39, 517 (1947).
(46) Pitzer, K. S., J. Am. Chem. Soc. 77, 3427 (1955).
(47) (Lydersen, A. L., Greenkorn, R. A., and Hougen, O. A., Univ. of Wisconsin Eng. Expt. Station, Report No. 4 (1955).
(48) Smith, J. M., Chem. Eng. Prog. 44, 521 (1948).
(49) Reid, R. C., and Smith, J. M., Chem. Eng. Prog. 47, 415 (1951).
(50) Maxwell, J. B., "Data Book on Hydrocarbons", Van Nostrand. 1950. P. 128-135.


★ ★ ★

# Rate Control in the Hydrometallurgical Preparation of Uranium Dioxide[1]

*D. R. WILES*[2]

**Recent studies of the hydrogen-precipitation of uranium dioxide from alkaline carbonate solutions have been extended. It was revealed that the reduction takes place in two phases. The first of these is the one described by Forward and Halpern. The second stage, much slower than the first, appears to be associated with the complete covering of the catalyst by the solid product. It is shown that while quantitative information is unreliable, a good qualitative description of the second-stage reaction can be based on the diffusion of reactants through this product layer to the catalyst surface.**

One of the more active areas of research in hydrometallurgy in recent years has been that of the precipitation of metals from solution of hydrogen reduction [1, 2, 3]. By extension of this method, Forward and Halpern [4] found it possible to strip uranium from carbonate leach solutions by hydrogen precipitation of uranium dioxide. Analogous reactions have been investigated in vanadium [5]. A solid catalyst, such as nickel powder, is used.

The reduction of uranium was found [4] to occur as described in Equation (1):

$$UO_2(CO_3)_3^{-4} + H_2 \xrightarrow{(Ni)} UO_2 + 2HCO_3^- + CO_3^= \quad \ldots\ldots(1)$$

Forward and Halpern also studied the kinetics of the reaction. They found that the rate of the reaction is proportional to the catalyst surface area and to the first power of the hydrogen pressure, but that, except at the very end of the reaction, the rate is independent of the uranium concentration. They thus found that the rate of the reduction could be described by the equation,

$$-\frac{d[U]}{dt} = k[Ni]_s\,[H_2]\,e^{-\Delta H/RT} \quad \ldots\ldots(2)$$

During the course of a further investigation of this process, it has been discovered that the precipitation proceeds in two phases, giving the same product, but with quite different rates. It was found that, following the stage which was investigated by Forward and Halpern, there occurs a slower stage, characterized, it appears, by the fact that the catalyst is completely covered with a layer of the reaction product. It is likely that this condition will obtain in any industrial application of the process.

Bunji and Zogović have recently shown [6] that the product $UO_2$ can itself function as a catalyst for the reduction. However, catalysis by uranium oxide results in reduction at a rate very much slower than even the slow second stage in the presence of nickel.

### *Experimental*

The experiments to be described were performed using solutions of uranium trioxide in ethylenediaminium carbonate. This cation offers two advantages in the present case: its solutions are more stable than those containing ammonia, and the reduction rates obtainable in the amine solutions are much higher and more convenient for study than those obtained in sodium carbonate solutions. Since the cation does not appear explicitly in Equations (1) and (2), one would expect the choice of cation not to have a qualitative effect on the reaction. However, it will be pointed out later that there is a substantial difference in the rates in solutions using different cations.

Solutions were prepared by passing gaseous carbon dioxide into suspensions of uranium trioxide in aqueous ethylenediamine. After dissolution of the uranium, the pH was adjusted to 9.5 by addition of further $CO_2$. The uranium trioxide was prepared by heating uranium peroxide which was, in turn, precipitated with hydrogen peroxide from a sulphuric acid solution of sodium diuranate.

The ethylenediamine was technical grade, made by Carbide and Carbon Chemicals Corporation. Carbon dioxide and hydrogen were obtained in cylinders from liquid Carbonic Canadian Limited, and Canadian Liquid Air Company, respectively. The catalyst used was Sherritt Gordon nickel powder C50-275, with 80% of the particles having diameters between 100$\mu$ and 150$\mu$. The superficial area of this powder is computed to be about 55 cm$^2$ per gram. It had earlier been found [7] that the catalytic activity of this powder was very low for some minutes at the first of each experiment. This effect, perhaps due to the presence of an oxide film, was found to be eliminated by pre-treatment in the ethylenediaminium carbonate solutions, under several atmospheres of hydrogen pressure, and at the temperature of the subsequent experiment.

Experiments were carried out in a one-gallon autoclave, made by Autoclave Engineers Inc. Heating was done by a gas flame, controlled by a Wheelco controller, actuated by an iron-constantan thermocouple. The temperature was held constant to $\pm 1°C$. during each experiment. Values were reproducible to $\pm 1°C$. Stirring was done by means of a stainless steel impeller operated continuously at 700 r.p.m. Uranium was added at the beginning of each experiment, under operating pressure, in the

[1]*Manuscript received March 15, 1959.*
[2]*Present Address: Department of Chemistry, Carleton University, Ottawa, Ont.*
*Contribution from the Department of Mining and Metallurgy, The University of British Columbia, Vancouver, B.C.*

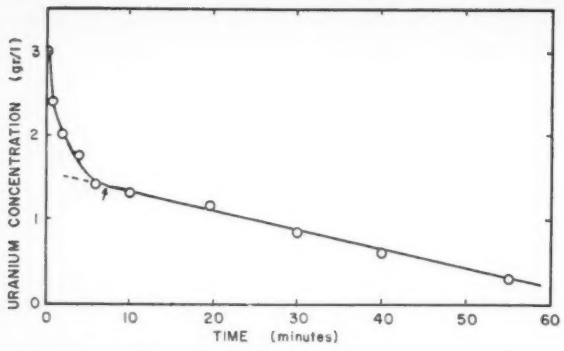


**Figure 1—Typical reduction, showing two phases.**

form of a strong (30 gr. U/L) solution of uranium in ethylenediamine carbonate. Samples were withdrawn periodically, and analysed for dissolved uranium by means of x-ray fluorescence. These measurements were made on acidified solutions containing a thorium internal standard, using a Norelco x-ray fluorescence apparatus. The intensity of the uranium Kα line was compared with that of the Kα line from a known amount of added thorium. Calibration and reproducibility tests indicate that the analytical errors are 1% or less.

***Results and Discussion***

The course of a typical reduction is shown in Figure 1, where two stages are clearly evident. The transition between the two stages occurred at various times and uranium concentrations, depending on the amount of catalyst present. The product was shown by x-ray diffraction to be the same in both cases–a form of uranium dioqide whose O:U ratio is somewhat greater than 2.0.

Also evident from the data shown in Figure 1 is the independence of the second-stage reduction rate of uranium concentration. The linearity of the first stage is not evident in Figure 1 because of its being of such short duration. Rate measurements on the second phase reaction were made using the best straight line drawn visually through the experimental points. Although it is very difficult to assess the accuracy of such measurements, the error in such a measurement is not likely to exceed 5%. Reproducibility of experiments was not so good, however, and deviations of 10-15% were common. This can possibly

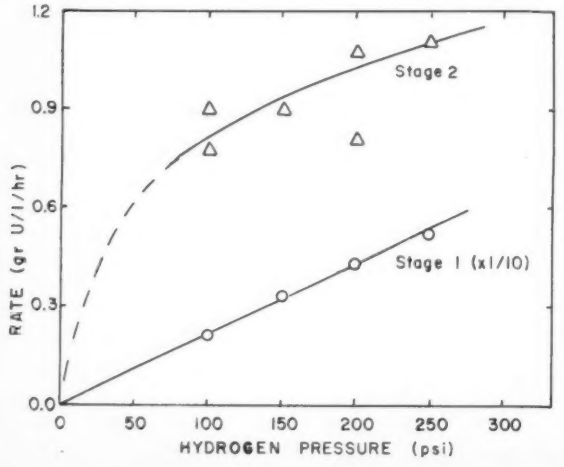


**Figure 3 — Dependence of reaction rate on hydrogen pressure.**

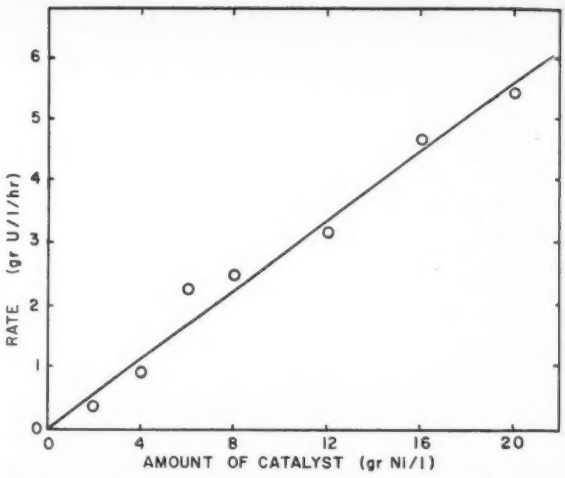


**Figure 2—Dependence of the second-stage rate on amount of catalyst.**

be attributed to variations in the activity of the catalyst surface, which is likely to be quite sensitive to the exact conditions of the experiment.

The dependence of the reaction rate on catalyst area is shown in Figure 2. The evident first-order dependence is to be expected for a reaction which takes place entirely at the catalyst surface.

The effect of hydrogen pressure on both the first and the second stages of the reaction is shown in Figure 3. The first-order dependence found for the first stage is in agreement with the results of Forward and Halpern. Two things are apparent regarding the second phase of the reaction: a marked increase in the scatter of the data, and a transition to a fractional order in hydrogen. Both these effects suggest that the reaction rate is controlled by some physical or mechanical process rather than by a chemical reaction.

The rate of the reaction was studied as a function of temperature and an apparent activation of 8,700 calories per mole was indicated. Comparison of this value with that of 9,800 calories per mole found [4] for the first stage reaction suggests that the rate controlling processes may be similar.

It was found that, in spite of the implication of Equation (1), the nature of the cation has a considerable effect on the rate of the reduction. As shown in Figure 4, the rates in ammonium carbonate and ethylenediaminium carbonate solutions are nearly the same, but about ten times faster than the rate in sodium carbonate solutions. The reason for this is not clear, but may lie in the fact that the faster rates are found in solutions which are strongly corrosive to nickel and maintain clean catalyst surfaces.

In spite of the thick coating of uranium oxide, it was found possible to conduct several successive precipitations using the same batch of catalyst. In such cases, each new charge of uranium was added to the solution without interrupting the pressure, temperature, or agitation.

Figure 5 shows a cross section of a catalyst particle coated with uranium oxide from five successive precipitations. Five layers are clearly visible, separated by darker regions. This darker material is associated with the continued action of the hydrogen on the precipitate after the solution has been completely stripped of uranium. It is likely that this dark material is a more highly reduced form of the uranium dioxide.

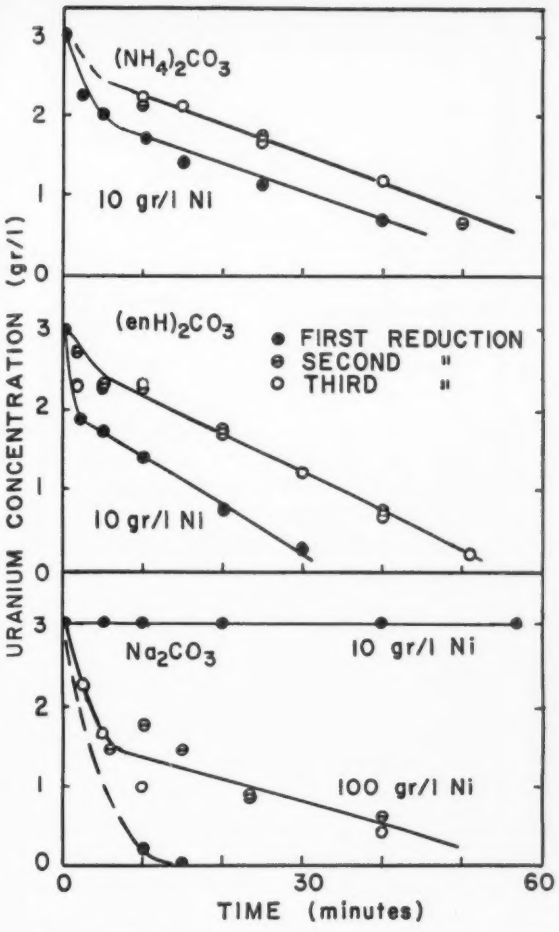


**Figure 4—Reduction rate curves for different cations.**

In Figure 6 is seen a cross section of a $UO_2$ layer deposited by two successive precipitations: the first of 3.0 grams per liter, and the second of 6.0 grams per liter. From the observation that the thinner layer is on the outside, it may be concluded that the reduction proceeds at the original nickel surface, after transport of the reactants through the deposited layer. It will be observed in Figure 6 that the outside layer is very thin compared to the inner one—much more than the expected factor of 2. This is not understood, although it may result partly from the fact that, being older, the outer layer has been subjected for a longer time to the compressive effect of collisions between particles.

Diffusion of reactants through this layer would suggest that the reaction rate should be dependent on the reciprocal of the total amount of uranium precipitated, in keeping with the well-known relation

$$\frac{dn}{dt} = D \cdot \frac{\Delta C}{\delta} \quad \ldots\ldots\ldots\ldots\ldots\ldots (3)$$

where the thickness, $\delta$, of the diffusion layer depends on the mass of product precipitated. The reactant whose diffusion limits the rate is evidently molecular hydrogen, although the fractional order suggests that the control may be shared with some other reactant.

If the density of the deposited material is constant, one would expect that the rate of the reaction could be

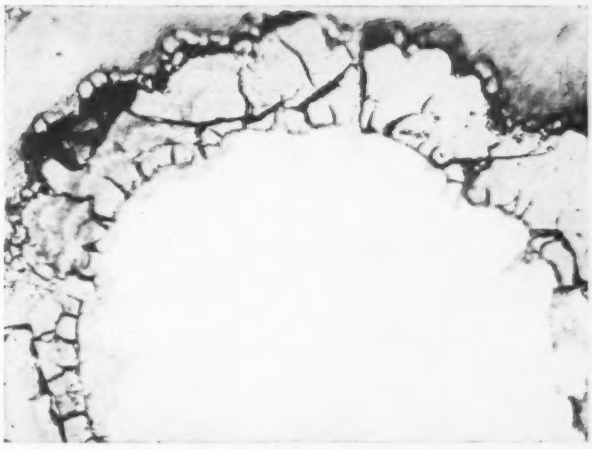

**Figure 5 — Photomicrograph of a polished section of a $UO_2$-covered catalyst particle. (Cracking likely took place on drying). (X 720).**

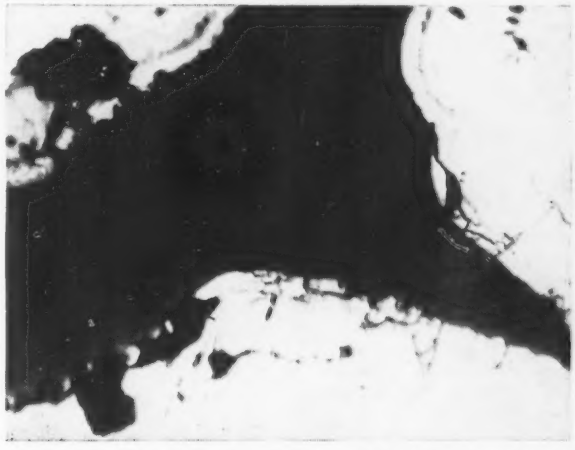

**Figure 6—Photomicrograph of a polished section of $UO_2$-covered catalyst particles, showing the first-formed layer on the outside. (X 720).**

related to the amount, M, of uranium precipitated, by the equation

$$\frac{d[U]}{dt} = \frac{A}{M} \quad \ldots\ldots\ldots\ldots\ldots\ldots (4)$$

where A is a constant. Figure 7 is a plot showing the rates of several successive reductions, plotted according to Equation (4). It is evident from Figure 7 that the data can best be fitted by an expression of the form

$$\frac{d[U]}{dt} = \frac{A}{M} + B \quad \ldots\ldots\ldots\ldots\ldots\ldots (5)$$

The additional term, B, in Equation (5) is interpreted as representing the effect of abrasion or flaking of the $UO_2$ layer, so as to reduce the thickness of the diffusion barrier. Once a complete layer has been formed, this abrasion may be more or less constant. This postulated abrasive effect is supported experimentally by the observation that an appreciable fraction of the uranium oxide is always found to be free of the nickel catalyst.

The initial deposition of $UO_2$ appears to occur on active areas, such as grain boundaries and certain grain faces. This is shown in Figures 8 and 9, which are photomicrographs of the surface of a nickel sheet used as catalyst for a very short time.

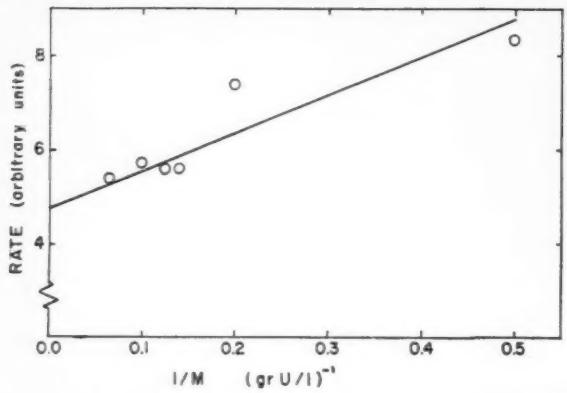


**Figure 7 — Dependence of the rate on the amount of uranium precipitated.**

From this it can be deduced that for a heterogeneous surface the transition from the first to the second stage of the reduction should be of the form

$$\log \left\{ \frac{[U]_t - [U]_2}{[U]_o - [U]_2} \right\} = - Ct \quad \ldots\ldots\ldots\ldots\ldots\ldots (6)$$

where $[U]_2$ is the uranium concentration in solution at the point when the catalyst surface is completely covered with $UO_2$. This point can be identified experimentally as the first point where the data begin to fall on the straight line for the second stage, as indicated by an arrow in Figure 1. Experimental results support this deduction, as can be seen from Figure 10, which shows the data from two separate experiments plotted according to Equation (6).

The gross features of the process seem now to be clear: The first deposition is at active sites, dependent on the surface structure of the nickel, giving a rate which is constant in time. The deposition spreads laterally until the surface is covered, giving rise to a logarithmic transition stage. Reaction proceeds by virtue of diffusion of the reactants through the deposited layer. This last step is altered in nature by a gradual flaking off or abrasion of the deposited layer, which causes serious deviation of the rate from the expected parabolic behavior.

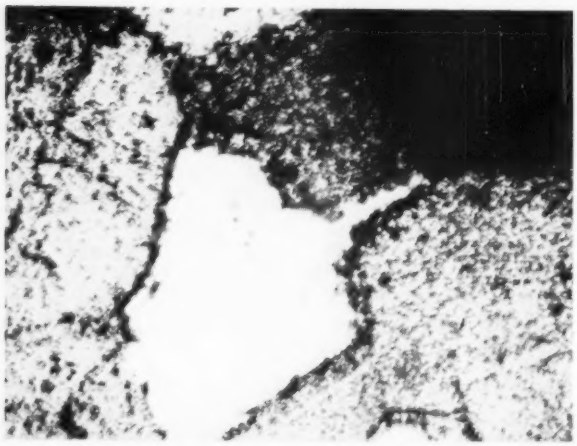

**Figure 9—Photomicrograph showing the effect of grain boundaries on the catalytic activity of the surface. (X 16).**

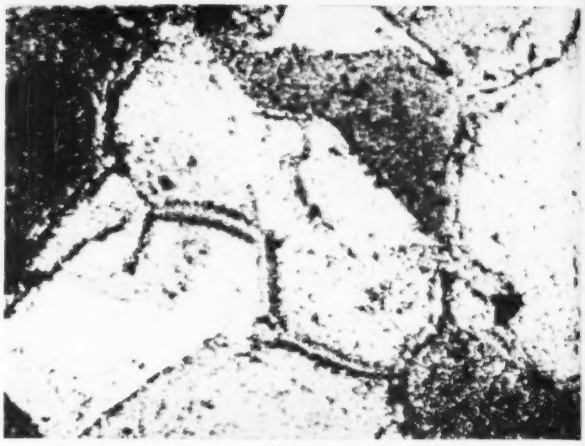

**Figure 8—Photomicrograph showing the effect of crystal orientation on the catalytic activity of the surface. (X 16).**


### *Acknowledgements*

The author is very grateful to E. A. Hahn, G. Nakazawa, J. P. Viszolyi, and B. Zogovic, who performed the experiments and to R. G. Butters for valuable advice regarding the x-ray fluorescence analysis. The financial assistance of Eldorado Mining and Refining (1944) Limited and the National Research Council of Canada is greatly appreciated.


### *Nomenclature*

| | | |
|---|---|---|
| A, B, C | = | undefined constants. |
| $\Delta C$ | = | concentration difference across the diffusion barrier |
| D | = | diffusion constant. |
| $\Delta H$ | = | experimental activation energy. |
| k | = | rate constant. |
| M | = | mass of $UO_2$ precipitated. |
| $(dn/dt)$ | = | amount of material across the diffusion barrier per $cm.^2$ per sec. |
| $R_2$ | = | rate of the second-stage reduction. |
| $\delta$ | = | thickness of the diffusion layer. |
| $[H_2]$ | = | hydrogen pressure. |
| $[Ni]_o$ | = | initial catalyst surface area. |
| $[U]_t$ | = | uranium concentration in solution at time t. |
| $[U]_o$ | = | initial uranium concentration in solution. |
| $[U]_2$ | = | uranium concentration in solution at the point when the catalyst first becomes completely coated with uranium oxide. |

### *References*


(1) Forward, F. A., J. Inst. Metals, 82, 113 (1954).
(2) Schaufelberger, F. A., J. Metals, 8, 695 (1956).
(3) Knacke, O., Pawlek, F., and Süssmuth, E., Z.f. Erzbergbau u. Metallhuttenws, IX, (12) 1 (1956).
(4) Forward, F. A. and Halpern, J., Trans. C.I.M., LVI, 355 (1953).
(5) O'Brien, R. N., Forward, F. A., and Halpern, J., Trans. C.I.M., LVI, 359 (1953).
(6) Bunji, B., and Zogovic, B., II Int. Conf. on the Peaceful Uses of Atomic Energy, Geneva, Sept. 1958, A Conf/15/P/485.
(7) Halpern J., personal communication.


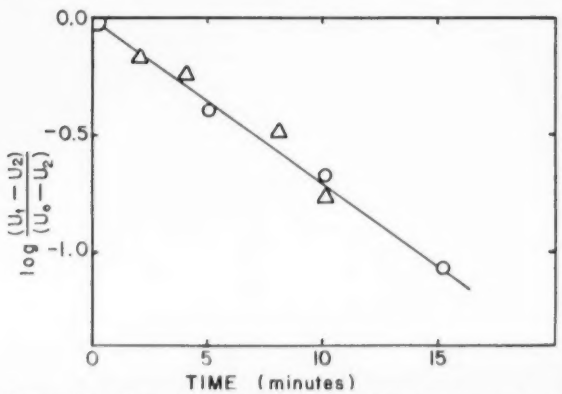


**Figure 10—Plot of data showing logarithmic nature of the transition stage.**

★ ★ ★

# Aeration in Tower-Type Fermenters[1]

*D. MURPHY*[2], *D. S. CLARK*[3] *and C. P. LENTZ*[4]

**The effects of air flow rate, oxygen partial pressure, aeration disk size and porosity, liquid height, and surface-active agents on aeration were studied in two unstirred towers or column-type vessels of different diameters using the sodium sulphite oxidation method. The coefficient of oxygen transfer increased with air flow rate up to the "flooding" point. The air flow rate required to cause "flooding" was increased by increasing the area of the aeration disk relative to the cross-sectional area of the tower. Within limits, aeration was improved by using disks of finer porosity. Under most conditions the coefficient of oxygen transfer was much higher in the small tower. The coefficient of transfer was not affected by liquid height in the tower, but efficiency of absorption increased with height. Aeration was adversely affected by all surface active agents tested.**

AERATION was found to be the most important factor in scaling up a submerged fermentation of the beet sugar molasses for the production of citric acid in unstirred tower-type fermenters (1). The results of that study, in which the fermentation was transferred from a small glass tower (2.5 liters operating volume) to a larger one (36-40 liters operating volume), both aerated through sintered glass disks, indicated that more information on the physical factors governing aeration in this type of vessel should be obtained.

Although a considerable amount of work has been published on mass transfer from bubbles leaving an orifice (2, 3, 4, 5) on mass transfer in column-type gas-liquid contactors (6, 7), on aeration in fermenters (8, 9, 10, 11, 12), and in scaling up fermentation equipment (12, 13, 14, 15, 16), it is of indirect value in scaling up the citric acid fermentation mentioned above. Information directly applicable to the equipment and conditions in use should be obtained before a further increase in scale is attempted. The work on mass transfer from bubbles, for example, shows that orifice size and shape affect bubble size and in turn mass transfer, but this information can not be used to predict the performance of a series of sintered glass disks. The work on tower-type gas-liquid contactors does not cover disk area in relation to column area, oxygen absorption, or a suitable range of disk porosities, and in addition most of the work is devoted to higher rates of gas flow than are of interest in the fermentation under study. Most of the work on fermentation equipment deals with relatively short, mechanically agitated vessels rather than unstirred columns or towers (8, 9, 10, 11, 12, 13, 14, 15, 16).

In the present work aeration studies were made with two sizes of glass towers similar to those used by Martin and Waters (17) and Steel *et al* (1). The work included determination of the effect of factors such as gas flow rate, disk area and porosity, column diameter and height, oxygen partial pressure, and antifoam agents on the absorption of oxygen by copper catalyzed aqueous sodium sulphite solutions in the towers (12). The sulphite oxidation method has been shown to provide a satisfactory indication of the relative effects of physical factors such as fermenter size, agitation, and air flow rate on the rate of oxygen absorption (12, 13, 18).

### *Experimental*

The small tower consisted of a section of 2.5 in. (6.3 cm.) diameter pyrex pipe 120 cm. in length with an additional 6 cm. section containing the aeration disk at the bottom. The aeration section was made from a male 60/50 pyrex joint fused to a Buchner funnel containing a sintered glass disk. A wet test gas meter was used to set the gas flow at the desired rate and a rotameter was used in maintaining a constant flow. The tower was filled to a depth of 96 cm. in most experiments; where greater depth was required, an addition section was added to the top of the tower. The temperature of the solution in the tower was thermostatically controlled at 25°C. during experiments by cool water flowing down the outside of the tower. Samples were drawn from the center of the tower through a glass tube set into the wall of the tower through a glass tube set into the wall of the tower about 30 cm. above the aeration disk.

The large tower was made from flange-connected sections of six inch (15.2 cm.) diameter pyrex pipe; the total height was 270 cm. The bottom section contained a rubber covered steel plate in which cut-down Buchner funnels with sintered glass disks were set (1). This tower was filled to a depth of 192 cm. in most experiments. Temperature was controlled at 25°C. by means of a U-shaped copper cooling coil in the tower. Sampling and gas flow regulating equipment was similar to that used with the small tower.

Medium porosity disks of sintered pyrex were used in most experiments, with fine and coarse disks being used to determine the effect of porosity. Maximum pore sizes in the three grades of disk were 77.4, 12.2 and 5.4 microns (19). Except where the effect of disk area was being measured, one disk, 3.8 cm. in diameter and 4 mm. thick,

[1]*Manuscript received February 20, 1959.*
[2]*Present address: Chemistry Department, University College, Science Buildings, Dublin, Ireland.*
[3]*Assistant Research Officer, National Research Council, Ottawa, Ont.*
[4]*Associate Research Officer, National Research Council, Ottawa, Ont.*
*Contribution from the Division of Applied Biology, National Research Council, Ottawa, Canada. Issued as N.R.C. No. 5276.*

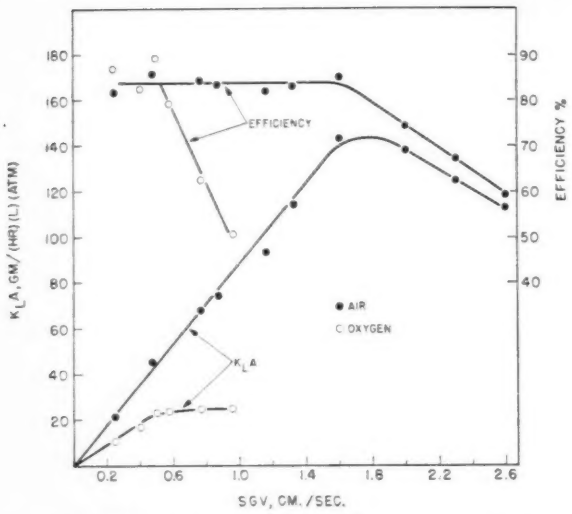


**Figure 1—Effect of gas flow rate on coefficient of oxygen transfer and efficiency of oxygen absorption. (Small tower with medium porosity disk covering 42% of tower cross-sectional area).**

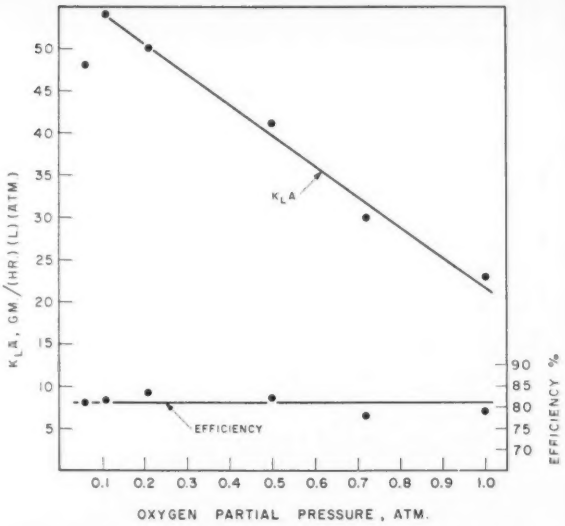


**Figure 2—Effect of oxygen partial pressure on coefficient of oxygen transfer and efficiency of oxygen absorption. (Small tower with medium porosity disk covering 42% of tower cross-sectional area; superficial gas velocity 0.57 cm./sec.).**

was used in the small tower, and seven similar disks in the larger tower. This represented about 45% of the cross-sectional area of each tower. A medium porosity disk the full diameter of the large tower was also tested.

The rate of oxygen transfer was determined by iodometric titration of the sulphite remaining in the reaction solution at various times during the test. Tap water was used to make up the reaction solution, and all chemicals were reagent grade. The initial concentration of sodium sulphite was 0.2 N in most tests, and the concentration of $CU\ SO_4 5H_2O$ was $8 \times 10^{-5}$ M, well above the minimum level established by Fuller and Crist [20]. To prevent loss of sulphite, flasks and pipettes used in sampling were flushed with nitrogen before use. Other measurements made included gas flow rate, pressure loss through the aeration disk, and hold-up or volume of bubbles in the liquid column.

The superficial gas velocity (S.G.V., cm./sec.), the coefficient of oxygen transfer ($K_LA$, gm./(l.) (hr.) (atm.), and the "retention" ($cm.^3/l.$) were calculated from the measurements made (see appendix). The superficial gas velocity was determined by dividing the volume rate of gas flow by the cross-sectional area of the tower. It was used instead of the volume rate of gas flow in order that results obtained with towers of different diameters could be compared directly. The coefficient of oxygen transfer was calculated by dividing the grams of oxygen absorbed per hour per liter of sulphite solution by the log mean of the inlet and outlet partial pressures. This is a modified coefficient which includes the surface area of the bubbles as well as the actual coefficient of transfer [8]. The known partial pressure of the oxygen in the gas entering the tower and the partial pressure in the gas leaving the tower, calculated from the sulphite oxidation rate, were used in obtaining the log mean pressure. Graphical integration based on partial pressure determinations at various liquid levels in the towers confirmed the validity of using log mean pressure values at all except the highest and lowest superficial gas velocities. At these velocities the error was appreciable but not large enough to affect conclusions drawn from the results. The retention was determined by dividing the volume of gas held in the aerated column of solution by the number of liters of solution in the tower. The efficiency, or proportion of oxygen absorbed to that entering the tower, was also calculated for some tests.

### *Results and discussion*

*Superficial gas velocity and oxygen pressure*

In the small tower the coefficient of transfer ($K_LA$) of oxygen from air increased linearly with the volume rate of gas flow until "flooding" occurred (Figure 1). In the flooding range there was a gradual change in bubble size and in the character of their movement; bubbles coalesced and became large and turbulence at the top of the liquid increased markedly. The predominance of large bubbles in the flooding range suggested that the decrease in $K_LA$ and hence efficiency was caused mainly by decreased bubble area.

The coefficient of transfer decreased linearly with increasing partial pressure of oxygen in the gas (Figure 2). Since approximately 80% of the oxygen entering the tower was absorbed for all partial pressure values tested, the decrease in $K_LA$ can be ascribed mainly to a reduction in bubble area. However, the greater reduction in transfer area for bubbles of pure oxygen compared to bubbles with a lower oxygen partial pressure, for the same efficiency of oxygen absorption, explained these decreases in $K_LA$ for low superficial gas velocities only (Figure 1). The rapid falling-off of $K_LA$ and efficiency at higher gas velocities with pure oxygen as compared to air suggested some other factor (Figure 1).

*Disk porosity and area*

The medium porosity disk produced much higher values of $K_LA$ (Figure 3) and retention (Figure 4) than the coarse disk. There was no appreciable difference, however, in $K_LA$ and retention values between the medium and fine disks.

Pressure loss through the aeration disks increased sharply with decreasing pore size, but only slightly with rate of gas flow. At a superficial gas velocity of 1 cm./sec.,

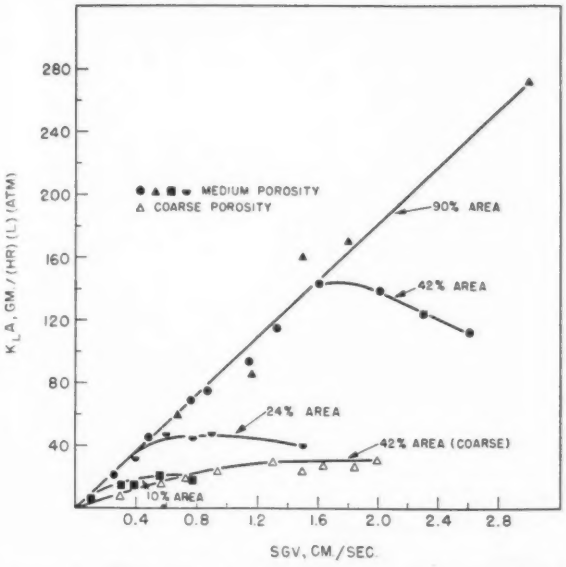


**Figure 3—Effect of disk area and porosity on coefficient of oxygen transfer. (Small tower).**

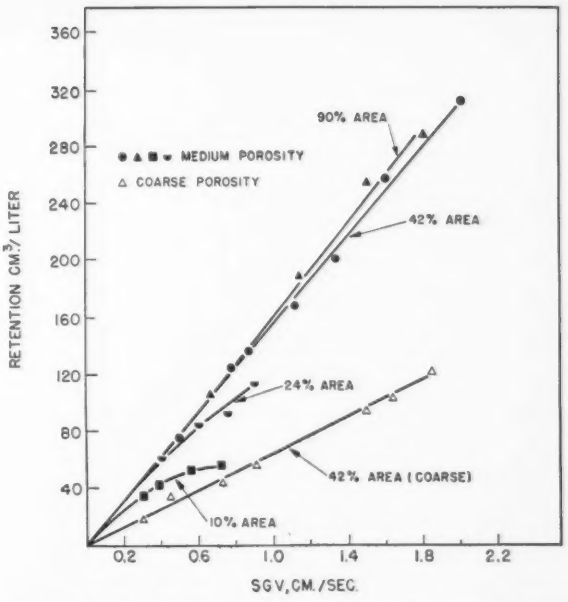


**Figure 4—Effect of disk area and porosity on gas retention. (Small tower).**

for example, the pressure losses for the coarse, medium and fine disks were 8.5, 40 and 72 cm. of mercury, respectively, while the corresponding pressure losses at a velocity of 2 cm./sec. were 9, 44, and 76 cm. of mercury. The relatively small change in pressure loss with increasing rate of gas flow was caused by the increasing number of pores through which gas flowed as the flow rate was increased.

The main effect of increasing disk area relative to the cross-sectional area of the tower was to raise the flow rate at which flooding occurred (Figure 3). The relation between disk size and the flow rate at which flooding started suggested that flooding was mainly a function of the gas flow per unit area of disk, although the rate at which $K_L A$ decreased in the flooding ranges for the different sizes of disks indicated that the relative size of the tower was also involved. Retention increased approximately linearly with superficial gas velocity for all disks over the entire range of velocities tested (Figure 4).

*Diameter and height of tower*

In the large tower (approximately twice the diameter of the small tower) the effects of superficial gas velocity and of disk porosity and area on $K_L A$, retention, and efficiency were similar to those in the small tower, but values of $K_L A$ under comparable conditions (except for tower diameter) below the flooding point were approximately half those observed for the small tower, or inversely proportional to the increase in diameter ratio

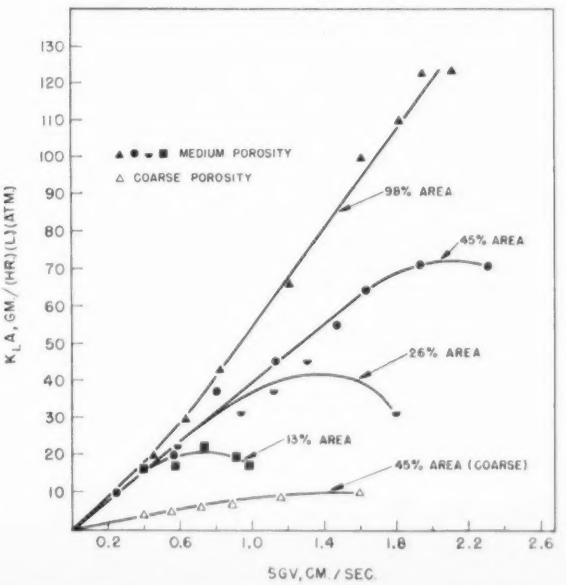


**Figure 5—Effect of disk area and porosity on coefficient of oxygen transfer and efficiency. (Large tower).**

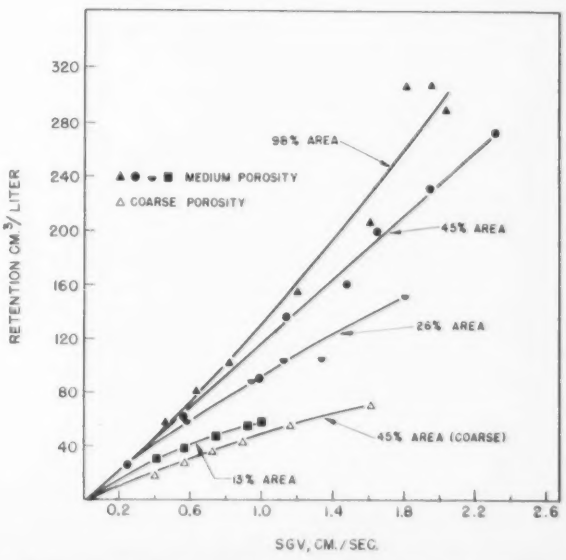


**Figure 6—Effect of disk area and porosity on gas rentention. (Large tower).**

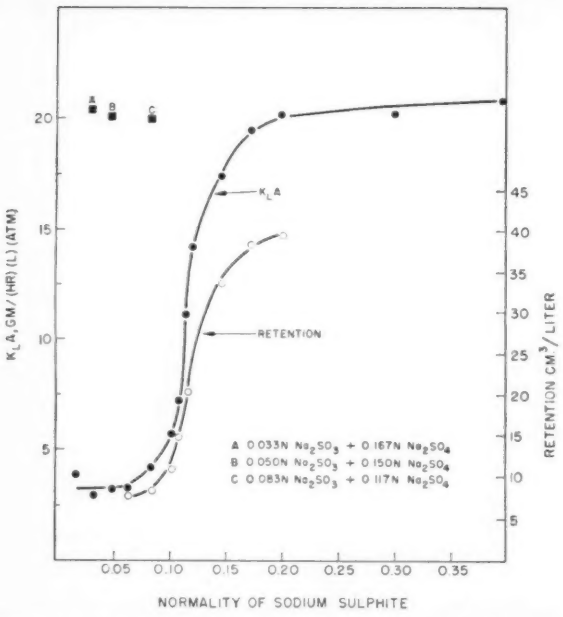


**Figure 7 — Effect of sodium sulphite concentration on coefficient of oxygen transfer and gas rentention. (Small tower with medium porosity disk covering 42% of tower cross-sectional area; superficial gas velocity 0.24 cm./sec.).**

(compare Figures 3, 4, 5 and 6). In most instances, depending upon the superficial gas velocity and cross-sectional area of the disk used, the retention in the large tower was about $\frac{2}{3}$ that in the small tower for comparable conditions. The superficial gas velocity at which flooding occurred was higher in the larger tower. With disks of small cross-sectional area (less than 40% of the tower cross-sectional area) the maximum values of $K_LA$ reached were about equal, but with disks the next size larger (Figure 3, 42%; Figure 5, 45%) the maximum for the small tower was double the maximum for the large tower.

Tests made with air over a range of liquid levels between 24 and 192 cm. in both large and small towers, showed that the values of $K_LA$ did not change appreciably with height if a correction were made for the effect of oxygen absorption on bubble area. Efficiency, of course, varied sharply with liquid height in these experiments because of the high rate of oxygen absorption by the sulphite solution. This effect is, therefore, a characteristic of the sulphite method.

*Sulphite concentration, antifoam agents, pulp suspensions*

Tests with initial concentration of sodium sulphite between 0.02N and 0.40N showed that the rate of oxidation was highly dependent on initial concentration in the range 0.10N and 0.20N (Figure 7). In any given test the rate of oxidation remained constant until most of the sulphite was used, but this rate depended on the initial sulphite concentration. Tests in which sodium sulphate was added to the solution showed that the rate depended on the total amount of sulphite and sulphate rather than on sulphite alone (Figure 7, A, B, C), and the reaction rate was approximately the same for total concentrations over 0.20N.

Photographs taken during tests using sodium sulphite solutions of different normality showed that bubble size, and hence total bubble area available for mass transfer, varied markedly with sulphite concentration (Figure 8). This probably accounted for most of the effect of sulphite

TABLE 1
EFFECT OF SURFACE-ACTIVE AGENTS ON OXYGEN ABSORPTION
(Tests made in small tower, medium porosity disk 42% of tower cross-sectional area in size, superficial air velocity 0.3 cm./sec.)

| Agent | Type | Concentration (ppm) | $K_LA$ | Efficiency (%) |
|---|---|---|---|---|
| None | – | – | 25 | 84 |
| Lard oil | Antifoam | 50 | 18 | 73 |
| | | 400 | 18 | 73 |
| 3% Octadecanol in mineral oil | Antifoam | 400 | 18 | 72 |
| Antifoam 60[1] | Antifoam | 10 | 6.0 | 34 |
| | | 50 | 2.0 | 13 |
| | | 100 | 2.5 | 16 |
| | | 400 | 2.4 | 15 |
| Aerosol OT[2] | Wetting agent | 4 | 15 | 66 |
| | | 10 | 16 | 67 |
| Dreft[3] | Detergent | 10 | 14 | 64 |
| | | 20 | 12 | 58 |

[1]General Electric Company, silicone products Department, Waterford, N.Y., U.S.A.
[2]American Cyanamid Company, Industrial Chemicals Division, New York, N.Y., U.S.A.
[3]Procter and Gamble Limited, Toronto, Ont.

concentration on $K_LA$. Bubbles did not appear to decrease further in size as the normality was increased above 0.175.

All of the antifoam and surface-active agents tested affected aeration adversely (Table 1). The magnitude of the effect varied widely, depending on the agent used, but with the exception of antifoam 60, did not vary appreciably with the amount of the agent added. Under the conditions used these agents did not affect bubble size noticeably.

The addition of small amounts of finely ground filter paper affected $K_LA$ markedly (Figure 9). The variation of $K_LA$ with gas flow rate with any given amount of pulp was similar to the relation under comparable conditions without pulp.

***Conclusions***

The results obtained in this study may be summarized as follows:

(1) The coefficient of oxygen transfer ($K_LA$) increased with gas flow rate up to the limit imposed by "flooding".

(2) $K_LA$ decreased with increasing oxygen pressure.

(3) $K_LA$ increased with decreasing aeration disk pore size, within limits.

(4) Aeration disk area relative to the cross-sectional area of the tower affected $K_LA$ markedly by raising the gas flow rate at which "flooding" occurred.

(5) Values of $K_LA$ were generally much lower in the larger diameter tower than in the smaller one.

(6) $K_LA$ was not affected appreciably by the height of the liquid column, but efficiency increased with height.

(7) $K_LA$ was adversely affected by all of the surface-active agents tested.

Comparison of the results obtained in the towers (maximum values of $K_LA$ = 140-150) with those obtained in mechanically agitated vessels by Cooper, Fernstrom and Miller [12], maximum values of Kv equivalent to $K_LA$ = 50-60) shows that the towers provide a relatively high degree of aeration. Nonetheless, the limits imposed by conclusions (1) to (6) above indicate that baffles, mechanical agitation, and elimination of antifoam agents may be necessary to obtain the required level of aeration for the submerged fermentation mentioned earlier [1], if it is to be successful in larger vessels.

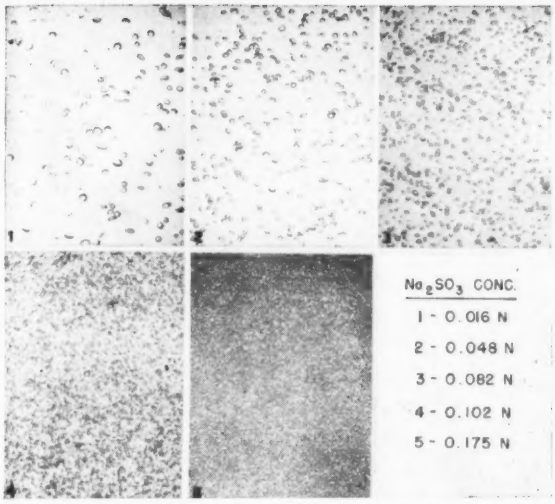


**Figure 8—Effect of sodium sulphite concentration on bubble size. (Small tower with medium porosity disk covering 42% of tower cross-sectional area; superficial gas velocity 0.24 cm./sec.).**

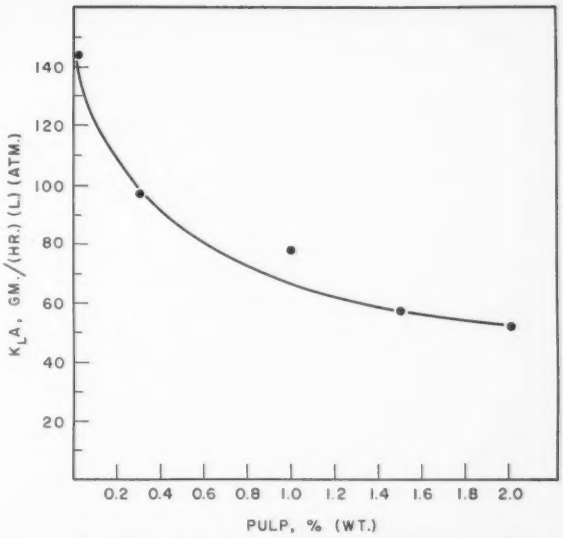


**Figure 9—Effect of finely ground paper pulp on coefficient of oxygen transfer. (Small tower with medium disk covering 42% of tower cross-sectional area; superficial gas velocity 1.7 cm./sec. Wt. of pulp expressed as per cent of wt. of liquid in tower).**


### *Acknowledgement*

The authors wish to thank N. U. Cholette for technical assistance during this investigation.


### *References*


(1) Steel, R., Lentz, C. P., and Martin, S. M., Can. J. Microbiol. 1, 299 (1955).
(2) Datta, R. L., Napier, D. H., and Newitt, D. M., Trans. Inst. Chem. Engrs. (London) 28, 14 (1950).
(3) Pattle, R. E., Trans. Inst. Chem. Engrs. (London) 28, 27 (1950).
(4) Pattle, R. E., Trans. Inst. Chem. Engrs. (London) 28, 32 (1950).
(5) Coppock, P. D., and Meiklejohn, G. T., Trans. Inst. Chem. Engrs. (London) 29, 75 (1951).
(6) Verschoor, H., Trans. Inst. Chem. Engrs. (London) 28, 52 (1950).
(7) Shulman, H. L., and Molstad, M. C., Ind. Eng. Chem. 42, 1058 (1950).
(8) Hixon, A. W., and Gaden, E. L. Jr., Ind. Eng. Chem. 42, 1792 (1950).
(9) Bartholomew, W. H., Karow, E. O., Sfat, M. R., and Wilhelm, R. H., Ind. Eng. Chem. 42, 1801 (1950).
(10) Bartholomew, W. H., Karow, E. O., Sfat, M. R., and Wilhelm, R. H., Ind. Eng. Chem. 42, 1810 (1950).
(11) Maxon, W. D., and Johnson, M. J., Ind. Eng. Chem. 45, 2554 (1953).
(12) Cooper, C. M., Fernstrom, G. A., and Miller, S. A., Ind. Eng. Chem. 36, 504 (1944).
(13) Karow, E. O., Bartholomew, W. H., and Sfat, M. R., J. Agric. and Food Chem. 1, 302 (1953).
(14) Bartholomew, W. H., Karow, E. O., and Sfat, M. R., Ind. Eng. Chem. 42, 1827 (1950).
(15) Buelow, G. H., and Johnson, M. J., Ind. Eng. Chem. 44, 2945 (1952).
(16) Shu, P., Can. J. Tech. 33, 279 (1955).
(17) Martin, S. M., and Waters, W. R., Ind. Eng. Chem. 44, 2229 (1952).
(18) Schultz, J. S., and Gaden, E. L. Jr., Ind. Eng. Chem. 48, 2209 (1956).
(19) British Standards, No. 1969, British Standards Institution, London (1953).
(20) Fuller, E. C., and Crist, R. H., J. Am. Chem. Soc. 63, 1644 (1941).


## APPENDIX

### *Sample calculations*

The following calculations illustrate the methods used in determining SGV, $K_LA$, efficiency and retention. The particular example selected corresponds to points (0.87, 74.8) and (0.87, 83.5) on Figure 1 and point (0.87, 135) on Figure 4.

1. *Known experimental conditions*

| | |
|---|---|
| Temperature of reaction medium (T) | = 25°C. |
| Partial pressure of oxygen in air entering tower ($P_1$) | = 0.21 atmos. |
| Volume of liquid in tower (V) | = 2.5 l. |
| Cross-sectional area of tower (A) | = 27 sq. cm. |
| Airflow rate (R) | = 85.0 l./hr. (23.6 cm.³/sec.) |

(Procedure as outlined in "Procedure")

2. *Results measured*

| | |
|---|---|
| Increase in liquid head caused by air bubbles (H) | = 12.5 cm. |
| Amount of oxygen absorbed based on average value obtained from idometric titration of 10 successive samples of sulphite solution ($Q_1$) | = 7.85 g $O_2$/(l.) (hr.) |

3. *Results calculated*

Amount of oxygen supplied by air entering tower

$$(Q_2) = \frac{(32)\ (R)\ (P_1)}{(24.4)\ (V)} = \frac{(32)\ (85)\ (0.21)}{(24.4)\ (2.5)} = 9.4\ \text{g}\ O_2/(\text{l.})\ (\text{hr.})$$

(Molecular wt. of oxygen = 32. Volume occupied by one gram mole of oxygen at 25°C and 760 mm Hg = 24.4 l.). Partial pressure of oxygen in gas escaping from top of tower

$$P_2 = \frac{1 - \frac{Q_1}{Q_2}}{\frac{1}{P_1} - \frac{Q_1}{Q_2}} = \frac{1 - \frac{7.85}{9.4}}{\frac{1}{0.21} - \frac{7.85}{9.4}} = 0.042\ \text{atmos.}$$

Log mean partial pressure in liquid column

$$(P_3) = \frac{P_1 - P_2}{\log_e \frac{P_1}{P_2}} = \frac{0.21 - 0.042}{1.59} = 0.105\ \text{atmos.}$$

$$\text{SGV} = \frac{R}{A} = \frac{23.6}{27} = 0.87\ \text{cm./sec.}$$

$$K_LA = \frac{Q_1}{P_3} = \frac{7.85}{0.105} = 74.8\ \text{g}\ O_2/(\text{l.})\ (\text{hr.})\ (\text{atmos.})$$

$$\text{Efficiency} = \frac{Q_1}{Q_2} \times 100 = \frac{7.85}{9.4} \times 100 = 83.5\%$$

$$\text{Retention} = \frac{(H)\ (A)}{V} = \frac{(12.5)\ (27)}{2.5} = 135.0\ \text{cm.}^3/\text{l.}$$

★ ★ ★

# The Effect of Pressure on the Enthalpy of Gases[1]

*REZA KORDBACHEN*[2] *and CHI TIEN*[3]

**A generalized enthalpy-correction chart based on the law of corresponding states was constructed using the compressibility factor information reported by Nelson and Obert [6, 7]. The range of pressures covered the region from $P_r = 0.02$ to $P_r = 40$, and the temperature extended from $T_r = 0.265$ to $T_r = 12.5$. The results produced from the correlation of this work have been found to agree with those obtained from some of the more sophisticated methods already presented in the literature.**

THE pressure effect on enthalpy for any real gases has long been recognized. Watson and Nelson [1] constructed the enthalpy correction chart for hydrocarbon mixtures and subsequent work by Hougen and Watson [2] gave the first generalized chart for enthalpy correction. Their work is based on the principle of corresponding states and the numerical values of $\frac{H^* - H}{T_c}$ resulted from compressibility factor information reported by Dodge [3]. The inadequacy of this chart has been repeatedly indicated by the large deviation when compared with actual experimental data.

The recent contribution of Lydersen et al [4] and also that of Curl and Pitzer [5] point to the inability of the law of corresponding states to treat all substances alike. To overcome this limitation they have suggested the introduction of a third parameter in addition to the conventional parameters of $P_r$ and $T_r$. This is accomplished by using critical compressibility factor, $Z_c$, in Lydersen's work, and the so-called accentric factor in Curl and Pitzer's work. In theory, this approach is undoubtedly superior to the conventional procedures already in existence. However, the introduction of an additional parameter increases the complexity of computations and requires additional information besides the critical temperature and pressure. In many cases, the third parameter is rather difficult to obtain.

For certain preliminary engineering calculations, there still is a need for a simpler generalized chart based on two parameters. The purpose of this paper is to present such a chart capable of producing reliable enthalpy corrections without recourse to the use of the more refined approaches suggested recently. The greater accuracy is made possible by using the compressibility factor information reported recently by Nelson and Obert [6, 7]. The superiority of Nelson and Obert's work is indicated by the fine agreement between the predicted values based on their work and the actual values. Also the work of fugacity coefficient [8] has proved to be worthwhile.

[1]*Manuscript received December 20, 1958.*
[2]*Graduate student, Department of Chemical Engineering, Oklahoma State University, Stillwater, Oklahoma, U.S.A.*
[3]*Assistant professor, Department of Chemical Engineering, The University of Tulsa, Tulsa, Oklahoma, U.S.A.*
*Contribution from the Department of Chemical Engineering, The University of Tulsa, Tulsa, Oklahoma, U.S.A.*

### *Development of Correlation*

The enthalpy, as a thermodynamic propery, can be considered as a function of temperature and pressure. The partial derivative of H (enthalpy) with respect to P (pressure) is given by

$$\left(\frac{\partial H}{\partial P}\right)_T = V - T\left(\frac{\partial V}{\partial T}\right)_P \quad \ldots\ldots\ldots\ldots\ldots\ldots (1)$$

Since at zero pressure all gases behave ideally, by integrating Equation (1), we have

$$(H^* - H)_T = \int_0^P \left[T\left(\frac{\partial V}{\partial T}\right)_P - V\right]_T dp \quad \ldots\ldots\ldots (2)$$

where $H^*$ and H are the enthalpy at temperature T for P =O and P respectively.

From the equation of state, we have

$$PV = ZRT \quad \text{or} \quad Z = \frac{PV}{RT} \quad \ldots\ldots\ldots\ldots\ldots (3)$$

Differentiating equation (3) with respect to P and substituting into Equation (2), it gives

$$\left[\frac{H^* - H}{T_c}\right]_{T_r} = RT_r^2 \int_0^{P_r} \left(\frac{\partial Z}{\partial T_r}\right)_{P_r} \frac{dP_r}{P_r} \quad \ldots\ldots\ldots (4)$$

Equation (4) served as the basis for the construction of the present chart. Numerical values of the compressibility factor z as reported by Nelson and Obert [6, 7] were replotted as z vs $T_r$ with $P_r$ as parameter. The partial derivative, $\left(\frac{\partial Z}{\partial T_r}\right)_{P_r}$ is then evaluated by graphical differentiation using the technique described by Worthing and Geffner [9].

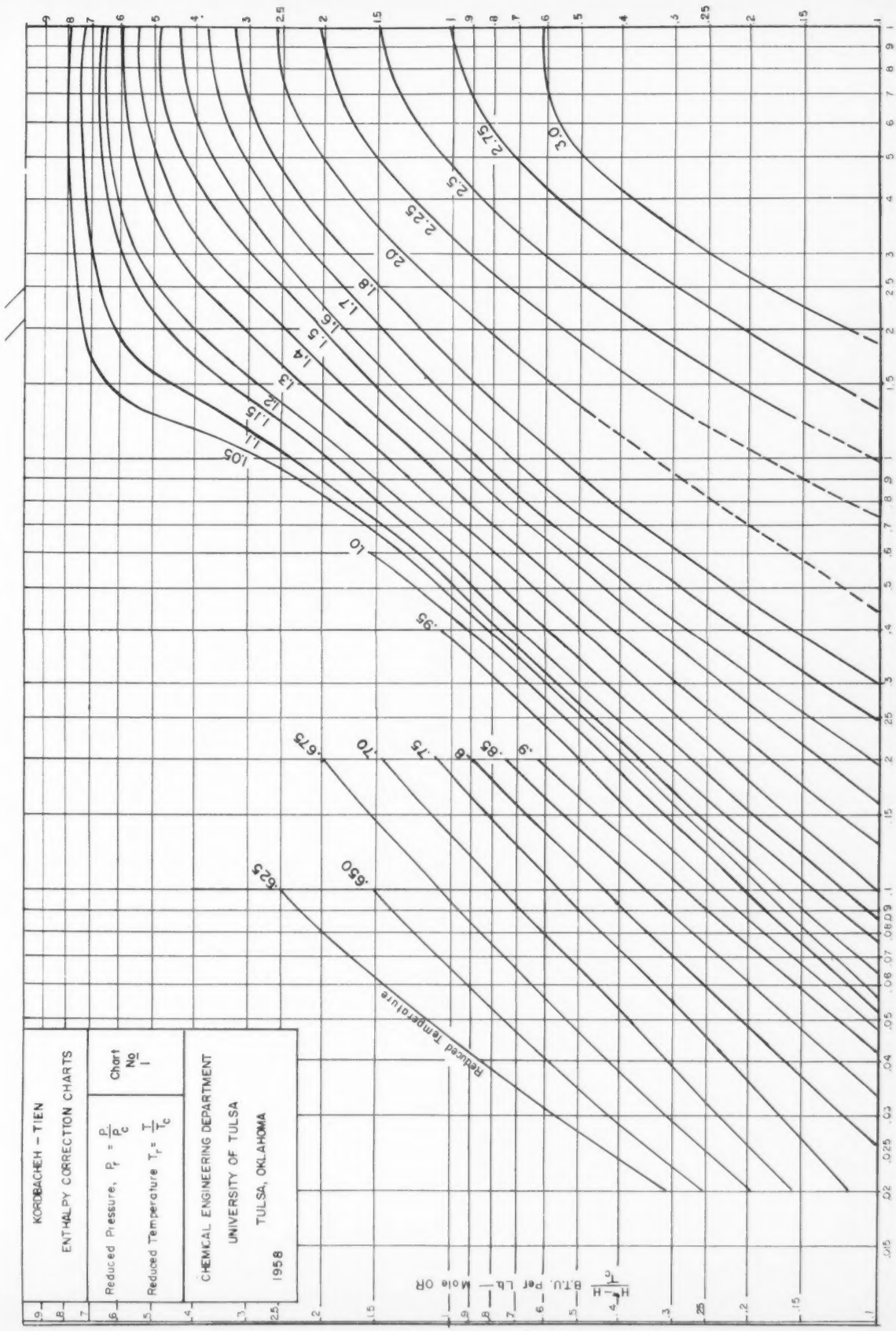
KORDBACHEH – TIEN
ENTHALPY CORRECTION CHARTS
Reduced Pressure, $P_r = \frac{P}{P_c}$
Reduced Temperature $T_r = \frac{T}{T_c}$
Chart No. I
CHEMICAL ENGINEERING DEPARTMENT
UNIVERSITY OF TULSA
TULSA, OKLAHOMA
1958
Reduced Temperature
Reduced Pressure, $P_R$
$\frac{H^\circ - H}{T_c}$ B.T.U. Per Lb. — Mole OR
3.0
2.75
2.5
2.25
2.0
1.8
1.7
1.6
1.5
1.4
1.3
1.2
1.15
1.1
1.05
1.0
.95
.9
.85
.8
.75
.70
.675
.650
.625

Figure 1.

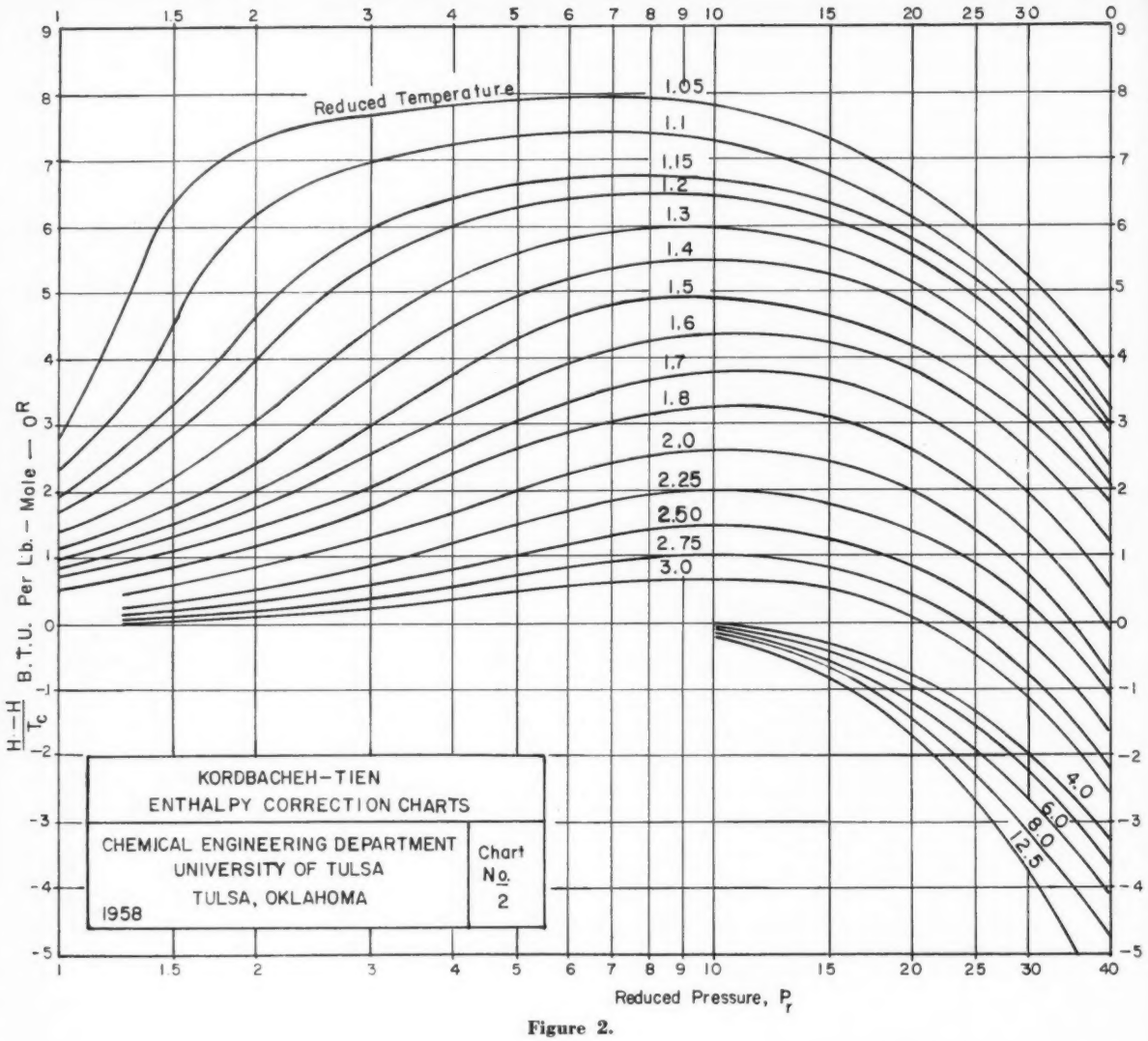


**Figure 2.**

With $\left(\frac{\partial Z}{\partial T_r}\right)_{P_r}$ known, the quantity, $\frac{H^* - H}{T_c}$, can easily be computed from Equation (4) by means of graphical integration.

***Results and Comparison***

Figures 1 and 2 are plots of the calculated results obtained in this work. These figures give the plots of the enthalpy correction term, $\frac{H^* - H}{T_c}$, versus reduced pressure, $P_r$, with $T_r$ as parameters. The use of this generalized chart is simple and straightforward. For any given compounds at specified temperature and pressure, it is only necessary to compute the reduced temperature and pressure and the subsequent value of $\frac{H^* - H}{T_c}$ can then be obtained from the chart.

Comparisons were made between this work and some other existing methods which include those by Hougen and Watson [2], Lydersen et al [4] and by Curl and Pitzer [5]. Results of the preceding methods of computation were also compared with experimental data for carbon dioxide, methane, ethane, isobutane, n-pentane, and ammonia [4, 10, 11]. These comparisons are presented in Table 1.

The comparisons indicate that in several cases the predicted value from this work is the lowest among all the existing methods. In the case of carbon dioxide, the agreement with experimental values is very good with an average deviation of less than 2%. This represents a better agreement than is possible from the work of Curl and Pitzer, Lydersen, Greenkorn and Hougen. The previous two-parameter charts give an average deviation of approximately 7%. Similarly this work gives fair agreement in the case of ethane. The deviations for the cases of isobutane and n-pentane are somewhat greater, but it should be noted that the other methods also have correspondingly greater deviation for these two compounds.

It would be of interest to compare results for two extreme cases of this method of computation with other methods: methane with $Z_c = 0.289$, and ammonia with $Z_c = 0.234$. For methane, this work gives better agreement at low temperature while that by Hougen and Watson fits the experimental values better at higher temperatures. The values based on Lydersen, Greenkorn and Hougen give better agreement for $T_r = 2.068$, but for lower temperatures this work gives better results. In all cases, the predicted values from this work as well as that by

TABLE 1

COMPARISON OF PREDICTED AND EXPERIMENTAL VALUE OF $(H^* - H)/T_c$

Compound: Carbon Dioxide $P_c = 73.0$ atm. $T_c = 304.1°K$ $Z_c = 0.275$

| | $T_r = 1.1$ | | | | | | | | | $T_r = 1.2$ | | | | | | | | |
|---|---|---|---|---|---|---|---|---|---|---|---|---|---|---|---|---|---|---|
| $P_r$ | Expt. | C.P. | % Dev. | H.W. | % Dev. | L.G.H. | % Dev. | K.T. | % Dev. | Expt. | C.P. | % Dev. | H.W. | % Dev. | L.G.H. | % Dev. | K.T. | % Dev. |
| 0.5 | 0.953 | 1.05 | 10.0 | 1.05 | 10.0 | 6.93 | −2.0 | 0.98 | 3.0 | 0.775 | 0.795 | 2.5 | 0.88 | 13.5 | 0.715 | −7.6 | 0.772 | −0.2 |
| 1.0 | 2.325 | 2.36 | 1.5 | 2.50 | 7.5 | 2.325 | 0.0 | 2.36 | 1.5 | 1.77 | 1.77 | 0.0 | 1.90 | 7.5 | 1.73 | −2.2 | 1.73 | −2.2 |
| 1.5 | 4.4 | 4.5 | 2.0 | 4.65 | 6.0 | 4.29 | −2.4 | 4.48 | 1.5 | 2.88 | 2.86 | −0.8 | 3.05 | 6.0 | 2.90 | 0.8 | 2.88 | 0.0 |
| 2.0 | 6.14 | 6.24 | 1.5 | 6.50 | 6.0 | 5.72 | −6.7 | 6.20 | 1.0 | 4.11 | 4.09 | −0.5 | 4.20 | 2.0 | 4.01 | −2.5 | 4.05 | −1.3 |
| 3.0 | 7.325 | 7.43 | 1.0 | 7.55 | 3.0 | 7.15 | −2.5 | 7.00 | −4.5 | 5.76 | 5.82 | 1.0 | 5.90 | 2.5 | 5.60 | −3.0 | 5.60 | −3.0 |
| | | Av. | +3.2 | Av. | +6.5 | Av. | −2.7 | Av. | ±2.3 | | Av. | ±1.0 | Av. | +6.3 | Av. | −3.2 | Av | −1.3 |

| | $T_r = 1.3$ | | | | | | | | | $T_r = 1.4$ | | | | | | | | |
|---|---|---|---|---|---|---|---|---|---|---|---|---|---|---|---|---|---|---|
| $P_r$ | Expt. | C.P. | % Dev. | H.W. | % Dev. | L.G.H. | % Dev. | K.T. | % Dev. | Expt. | C.P. | % Dev. | H.W. | % Dev. | L.G.H. | % Dev. | K.T. | % Dev. |
| 0.5 | 0.675 | 0.655 | −3.0 | 0.75 | 11.0 | 0.578 | 14.2 | 0.65 | −3.5 | 0.576 | 0.536 | 7.10 | 0.65 | 13.0 | 0.476 | 17.4 | 0.542 | 5.7 |
| 1.0 | 1.41 | 1.41 | 0.0 | 1.55 | 10.0 | 1.37 | 3.0 | 1.41 | 0.0 | 1.193 | 1.132 | −5.0 | 1.30 | 9.0 | 1.112 | −7.0 | 1.175 | −1.5 |
| 1.5 | 2.23 | 2.19 | −2.0 | 2.4 | 7.8 | 2.23 | 0.0 | 2.23 | 0.0 | 1.810 | 1.790 | −1.0 | 1.95 | 7.8 | 1.790 | −1.0 | 1.810 | 0.0 |
| 2.0 | 3.06 | 3.1 | 0.5 | 3.2 | 4.5 | 3.06 | 0.0 | 3.00 | 0.05 | 2.415 | 2.500 | 1.4 | 2.60 | 5.4 | 2.385 | −3.2 | 2.465 | 0.0 |
| 3.0 | 4.51 | 3.2 | 29.0 | 4.7 | 4.5 | 4.47 | −1.0 | 4.51 | 0.0 | 3.595 | 3.595 | 0.0 | 3.90 | 8.4 | 3.575 | −0.5 | 3.700 | 2.5 |
| | | Av. | ±6.8 | Av. | +7.6 | Av. | ±3.6 | Av. | −0.8 | | Av. | ±3.0 | Av. | +8.8 | Av. | +5.8 | Av. | ±2.0 |

Compound: Methane $P_c = 45.8$ atm. $T_c = 343.3°R$ $Z_c = 0.29$

| | $T_r = 1.54$ | | | | | | | $T_r = 1.893$ | | | | | | |
|---|---|---|---|---|---|---|---|---|---|---|---|---|---|---|
| $P_r$ | Expt. | L.G.H. | % Dev. | H.W. | % Dev. | K.T. | % Dev. | Expt. | L.G.H. | % Dev. | H.W. | % Dev. | K.T. | % Dev. |
| 0.297 | 0.238 | 0.28 | +17.6 | 0.32 | +34.5 | 0.22 | − 7.6 | 0.163 | 0.117 | −28.2 | 0.22 | +24.5 | – | – |
| 0.891 | 0.853 | 0.70 | −17.9 | 0.96 | +12.5 | 0.83 | 2.7 | 0.541 | 0.415 | −23.3 | 0.64 | +18.3 | 0.38 | −29.6 |
| 1.485 | 1.589 | 1.40 | −11.9 | 1.57 | + 1.2 | 1.42 | −10.6 | 0.904 | 0.750 | −17.0 | 0.99 | + 9.5 | 0.72 | −20.4 |
| 2.228 | 2.283 | 2.10 | − 8.0 | 2.40 | + 5.1 | 2.20 | − 3.6 | 1.328 | 1.150 | −13.4 | 1.45 | + 9.6 | 1.13 | −14.9 |
| 4.458 | 3.858 | 3.45 | −10.6 | 4.00 | + 3.7 | 3.80 | − 1.5 | 2.395 | 2.010 | −14.0 | 2.40 | + 0.2 | 2.2 | − 8.1 |
| | | Av. | ±13.2 | Av. | +11.4 | Av. | ± 5.2 | | Av. | −16.1 | Av. | +12.4 | Av. | −18.3 |

| | $T_r = 2.068$ | | | | | | |
|---|---|---|---|---|---|---|---|
| $P_r$ | Expt. | L.G.H. | % Dev. | H.W. | % Dev. | K.T. | % Dev. |
| 0.297 | 0.144 | 0.10 | −30.6 | 0.19 | +31.9 | – | – |
| 0.891 | 0.452 | 0.38 | −15.9 | 0.55 | +21.7 | 0.25 | 44.7 |
| 1.485 | 0.756 | 0.62 | −16.5 | 0.86 | +15.3 | 0.52 | 30.3 |
| 2.228 | 1.095 | 0.92 | −16.0 | 1.25 | +14.2 | 0.90 | 17.8 |
| 4.456 | 1.976 | 1.80 | − 8.9 | 2.00 | + 1.2 | 1.70 | 14.0 |
| | | Av. | −17.6 | Av. | +17.0 | Av. | +27.0 |

Compound: N-Pentane $P_c = 33.3$ atm. $T_c = 469.8°K$ $Z_c = 0.269$

| | $T_r = 1.088$ | | | | | | | | |
|---|---|---|---|---|---|---|---|---|---|
| $P_r$ | Expt. | C.P. | % Dev. | H.W. | % Dev. | L.G.H. | % Dev. | K.T. | % Dev. |
| 2.04 | 6.95 | 6.85 | −1.4 | 6.82 | −1.9 | 6.21 | −10.6 | 6.67 | − 2.6 |
| 3.06 | 7.85 | 7.44 | −5.2 | 7.78 | −0.9 | 7.37 | − 6.1 | 7.17 | − 8.7 |
| 4.08 | 8.19 | 7.94 | −3.1 | 8.02 | −2.1 | 7.75 | − 5.4 | 7.39 | − 9.8 |
| 6.12 | 8.47 | 8.32 | −1.8 | 8.32 | −1.8 | 8.05 | − 5.0 | 7.56 | −10.8 |
| 10.20 | 8.52 | – | – | 8.5 | −0.3 | 8.01 | − 6.0 | 7.45 | −12.5 |
| 16.32 | 8.11 | – | – | 7.41 | −8.6 | 7.42 | − 8.5 | 6.83 | −15.8 |
| | | | Av. −2.6 | | Av. −2.6 | | Av. − 7.9 | | Av. −10.3 |

Table 1 (Continued)

Compound: Ethane $P_c$ = 48.8 atm. $T_c$ = 305.2°K $Z_c$ = 0.285

| | $T_r$ = 1.075 | | | | | $T_r$ = 1.24 | | | | |
|---|---|---|---|---|---|---|---|---|---|---|
| $P_r$ | Expt. | H.W. | % Dev. | K.T. | % Dev. | Expt. | H.W. | % Dev. | K.T. | % Dev. |
| 0.143 | 0.25 | 0.29 | 16.0 | 0.26 | 4.0 | 0.17 | 0.23 | 35.3 | 0.17 | 0.0 |
| 0.285 | 0.50 | 0.60 | 20.0 | 0.55 | 10.0 | 0.35 | 0.47 | 34.3 | 0.38 | 8.6 |
| 0.570 | 1.11 | 1.3 | 17.1 | 1.17 | 5.4 | 0.76 | 0.95 | 25.0 | 0.84 | 10.5 |
| 0.854 | 1.94 | 2.2 | 13.4 | 1.96 | 1.0 | 1.22 | 1.47 | 20.5 | 1.32 | 8.2 |
| 1.14 | 3.15 | 3.5 | 11.1 | 3.24 | 2.9 | 1.68 | 2.00 | 19.1 | 1.85 | 10.1 |
| 1.43 | 4.68 | 5.4 | 15.0 | 5.10 | 9.0 | 2.22 | 2.65 | 19.4 | 2.45 | 10.4 |
| 1.78 | 6.39 | 6.7 | 4.9 | 6.40 | 0.2 | 2.94 | 3.35 | 20.1 | 2.94 | 0.0 |
| 2.14 | 6.87 | 7.4 | 7.7 | 6.90 | 0.4 | 3.67 | 4.06 | 10.6 | 3.84 | 4.6 |
| 2.49 | 7.10 | 7.6 | 7.0 | 7.15 | 0.7 | 4.33 | 4.70 | 8.6 | 4.55 | 5.1 |
| 2.85 | 7.28 | 7.9 | 7.9 | 7.29 | 0.1 | 4.88 | 5.30 | 8.6 | 4.95 | 1.4 |
| 3.55 | 7.50 | 8.1 | 8.0 | 7.46 | 0.6 | 5.52 | 6.00 | 8.7 | 5.52 | 0.0 |
| 4.28 | 7.61 | 8.3 | 9.1 | 7.56 | 0.7 | 6.87 | 6.30 | 1.4 | 5.86 | 8.3 |
| | | | Av. +11.5 | | Av. + 3.0 | | | Av. +17.6 | | Av. + 5.6 |

Compound: Isobutane $P_c$ = 36.0 atm. $T_c$ = 408.1°K $Z_c$ = 0.283

| | $T_r$ = 1.089 | | | | | | | | |
|---|---|---|---|---|---|---|---|---|---|
| $P_r$ | Expt. | C.P. | % Dev. | H.W. | % Dev. | L.G.H. | % Dev. | K.T. | % Dev. |
| 0.378 | 0.795 | 0.775 | − 2.5 | 0.80 | 0.5 | 0.62 | −22.5 | 0.74 | − 7.3 |
| 0.756 | 1.590 | 1.610 | 1.4 | 1.75 | 10.0 | 1.53 | − 3.7 | 1.60 | 0.5 |
| 1.134 | 3.880 | 2.960 | −23.8 | 3.20 | −17.5 | 2.80 | −27.8 | 3.10 | −20.0 |
| 1.512 | 4.830 | 4.665 | − 3.5 | 5.20 | 8.0 | 4.59 | − 5.0 | 4.80 | 0.5 |
| 1.890 | 6.440 | 6.220 | − 3.2 | 6.45 | 0.2 | 5.90 | − 8.3 | 6.35 | − 1.2 |
| 2.835 | 7.335 | 7.330 | 0.0 | 7.60 | 3.5 | 7.15 | − 2.5 | 7.15 | − 2.5 |
| 3.780 | 7.665 | 7.700 | 0.5 | 8.00 | 4.5 | 7.65 | 0.0 | 7.35 | − 4.0 |
| 5.670 | 7.850 | 7.830 | − 0.2 | 8.30 | 5.5 | 8.02 | 2.4 | 7.50 | − 4.3 |
| | | | Av. ± 4.4 | | Av. ± 6.2 | | Av. − 9.0 | | Av. − 5.1 |

Compound: Ammonia
$P_c$ = 111.3 atm. $T_c$ = 405.5°K $Z_c$ = 0.243

| $P_r$ | Expt.* | L.G.H. | % Dev. | H.W. | % Dev. | K.T. | % Dev. |
|---|---|---|---|---|---|---|---|
| 0.0611 | 0.198 | 0.23 | 16.0 | 0.205 | 3.5 | 0.155 | −21.7 |
| 0.0917 | 0.295 | 0.326 | 10.5 | 0.310 | 5.1 | 0.250 | −15.3 |
| 0.1222 | 0.398 | 0.46 | 15.6 | 0.415 | 4.3 | 0.352 | −11.6 |
| 0.1834 | 0.612 | 0.73 | 19.3 | 0.625 | 2.1 | 0.560 | − 8.5 |
| | | Av. | +15.4 | Av. | +3.8 | Av. | −14.3 |

*Values of H* are obtained from linear extrapolation with the information in Tables of Thermodynamic Properties of Ammonia, U.S. Bureau of Standards, Circ. 142, 1923.

Lydersen, Greenkorn and Hougen are 10-15% lower than the experimental value, while those by Hougen and Watson are 10-15% greater. For the case of ammonia, the two-parameter chart of Hougen and Watson appears to be superior. However, it should be mentioned that the enthalpy of ammonia at ideal state ($P_r = 0$) is obtained by linear extrapolation. Conceivably, this will cause certain error in the expression $\frac{H^* - H}{T_c}$, which might distort the true picture.

A question which arises in the case of methane is why a more refined method such as the one used by Lydersen, Greenkorn and Hougen does not give any better results than the simpler two-parameter method. It might be said that the experimental values used for comparison are not too accurately determined. If this is the case, some new experimental investigation should be in order. On the other hand, if the experimental values are reliable, the only conclusion would be that $Z_c$ might not be an ideal parameter to characterize the intermolecular effect, a comment which has been voiced by some current critics.

### *Conclusion*

From the comparison of this work, the present investigation makes possible the better prediction of enthalpy of gas from ideal behavior than other available methods and particularly at low temperatures. The work by Hougen and Watson appears to be superior only in the case of ammonia.

### *Nomenclature*

H = Enthalpy of real gas
H* = Enthalpy of ideal gas
P = Pressure
$P_c$ = Critical pressure
$P_r$ = Reduced pressure
R = Gas law constant
T = Temperature
$T_c$ = Critical temperature
$T_r$ = Reduced temperature
V = Volume
Z = Compressibility factor
$Z_c$ = Critical compressibility factor

### *References*


(1) Wason, L. M., and Nelson, E. F., Ind. Eng. Chem., 25, 880 (1930).
(2) Hougen, O. A., and Watson, K. M., Chemical Process Principles, Part 2, John Wiley and Sons, Inc., New York.
(3) Dodge, B. F., Ind. Eng. Chem., 24, 1353 (1952).
(4) Lydersen, A. L., Greenkorn, R. A., and Hougen, O. A., Generalized Properties of Pure Fluids, Report No. 4, Engineering Experiment Station, University of Wisconsin, October, 1955.
(5) Curl, B. F., and Pitzer, K. S., Ind. Eng. Chem., 50, 365 (1958).
(6) Nelson, L. C., and Obert, E. F., Tans. ASME, 76, 1057 (1954).
(7) Nelson, L. C., and Obert, E. F., AIChE. Journal, 1, 75 (1955).
(8) Honari, S., and Brown, G. G., Private Communication.
(9) Worthing, A. G., and Geffner, J, Treatment of Experimental Data, John Wiley and Sons, Inc., New York, 1943.
(10) Sage, B. H., Olds, R. H., and Lacey, W. N., California Oil World, (1946).
(11) Tables of Thermodynamic Properties of Ammonia, U.S. Bur. Standards Circ. 142, 1923.


★ ★ ★